Report No. CG-D-05-95

OBJECTIVE ANALYSIS OF OCEANIC DATA FOR COAST GUARD TRAJECTORY MODELS

Applied Mathematics, Inc.
1622 Route 12, P.O. Box 637
Gales Ferry, CT 06335

and

U.S. Coast Guard
Research and Development Center
1082 Shennecossett Road
Groton, CT 06340-6096

FINAL REPORT
MARCH 1994

Prepared for:

U.S. Department Of Transportation
United States Coast Guard
Office of Engineering, Logistics, and Development
Washington, DC 20593-0001

NOTICE

This document is disseminated under the sponsorship of the Department of Transportation in the interest of information exchange. The United States Government assumes no liability for its contents or use thereof.

The United States Government does not endorse products or manufacturers. Trade or manufacturers' names appear herein solely because they are considered essential to the object of this report.

The contents of this report reflect the views of the Coast Guard Research & Development Center. This report does not constitute a standard, specification, or regulation.

W. E. Colburn, Jr.
Technical Director, Acting
United States Coast Guard
Research & Development Center
1082 Shennecossett Road
Groton, CT 06340-6096

Technical Report Documentation Page

1. Report No.	2. Government Accession No.	3. Recipient's Catalog No.
CG-D-05-95		

4. Title and Subtitle	5. Report Date
Objective Analysis of Oceanic Data for Coast Guard Trajectory Models	March 1994
	6. Performing Organization Code
7. Author(s)	8. Performing Organization Report No.
Applied Mathematics, Inc.	R&DC 17/94

9. Performing Organization Name and Address		10. Work Unit No. (TRAIS)
U.S. Coast Guard Research and Development Center 1082 Shennecossett Road Groton, Connecticut 06340-6096	Applied Mathematics, Inc. 1622 Route 12, P.O. Box 637 Gales Ferry, CT 06335	11. Contract or Grant No. DTRS-57-93-C-00133
12. Sponsoring Agency Name and Address Department of Transportation U.S. Coast Guard Office of Engineering, Logistics, and Development Washington, D.C. 20593-0001		13. Type of Report and Period Covered DOT Program SBIR - 1993, Phase I Final Report
		14. Sponsoring Agency Code

15. Supplementary Notes

This report documents research conducted to study the feasibility of adapting objective analysis techniques for use with Coast Guard data. This is the final report for this SBIR Phase I project and is the twelfth in a series that documents the Improvement of Search and Rescue Capabilities (ISARC) Project at the USCG R&D Center. Coast Guard R&D Center COTR: LCDR B. Perkins, 203-441-2618.

16. Abstract

The Coast Guard uses ocean surface velocity fields as input to trajectory models in search planning to determine search area movement. Statistical techniques, called objective analysis, are used by meteorologists and oceanographers to combine observed data, which are irregularly distributed in space and time, to make conclusions about the total variation of the variables within a region of interest. The purpose of the Phase I research was to study the feasibility of adapting objective analysis techniques for use with Coast Guard data. The following research was completed. Objective analysis techniques were used to combine irregularly spaced and temporally observed ocean current velocity data in order to determine an optimally estimated velocity field and associated error field. The technique was applied to a drifting buoy data set collected by the Coast Guard. A numerical experiment was also conducted to examine the number of buoys required to determine the velocity field in a typical Search and Rescue domain. Techniques for combining two velocity fields were also investigated.

The research findings were that objective analysis techniques can be used to provide the Coast Guard with accurate estimates, in real time, of ocean surface velocity and associated error.

Potential applications of this research are in support of Coast Guard Search and Rescue, Ice Patrol and Environmental Protection missions.

17. Key Words	18. Distribution Statement
CASP, search, search planning, surface velocity, objective analysis, combining, velocity field, Monte Carlo	Document is available to the public through the National Technical Information Service, Springfield, Virginia 22161

19. Security Classif. (of this report)	20. SECURITY CLASSIF. (of this page)	21. No. of Pages	22. Price
UNCLASSIFIED	UNCLASSIFIED		

Form DOT F 1700.7 (8/72) Reproduction of form and completed page is authorized

METRIC CONVERSION FACTORS

Approximate Conversions to Metric Measures

Symbol	When You Know	Multiply By	To Find	Symbol
	LENGTH			
in	inches	* 2.5	centimeters	cm
ft	feet	30	centimeters	cm
yd	yards	0.9	meters	m
mi	miles	1.6	kilometers	km
	AREA			
in^2	square inches	6.5	square centimeters	cm^2
ft^2	square feet	0.09	square meters	m^2
yd^2	square yards	0.8	square meters	m^2
mi^2	square miles	2.6	square kilometers	km^2
	acres	0.4	hectares	ha
	MASS (WEIGHT)			
oz	ounces	28	grams	g
lb	pounds	0.45	kilograms	kg
	short tons (2000 lb)	0.9	tonnes	t
	VOLUME			
tsp	teaspoons	5	milliliters	ml
tbsp	tablespoons	15	milliliters	ml
fl oz	fluid ounces	30	milliliters	ml
c	cups	0.24	liters	l
pt	pints	0.47	liters	l
qt	quarts	0.95	liters	l
gal	gallons	3.8	liters	l
ft^3	cubic feet	0.03	cubic meters	m^3
yd^3	cubic yards	0.76	cubic meters	m^3
	TEMPERATURE (EXACT)			
°F	Fahrenheit temperature	5/9 (after subtracting 32)	Celsius temperature	°C

*1 in = 2.54 (exactly).

Approximate Conversions from Metric Measures

Symbol	When You Know	Multiply By	To Find	Symbol
	LENGTH			
mm	millimeters	0.04	inches	in
cm	centimeters	0.4	inches	in
m	meters	3.3	feet	ft
m	meters	1.1	yards	yd
km	kilometers	0.6	miles	mi
	AREA			
cm^2	square centimeters	0.16	square inches	in^2
m^2	square meters	1.2	square yards	yd^2
km^2	square kilometers	0.4	square miles	mi^2
ha	hectares (10,000 m^2)	2.5	acres	
	MASS (WEIGHT)			
g	grams	0.035	ounces	oz
kg	kilograms	2.2	pounds	lb
t	tonnes (1000 kg)	1.1	short tons	
	VOLUME			
ml	milliliters	0.03	fluid ounces	fl oz
l	liters	0.125	cups	c
l	liters	2.1	pints	pt
l	liters	1.06	quarts	qt
l	liters	0.26	gallons	gal
m^3	cubic meters	35	cubic feet	ft^3
m^3	cubic meters	1.3	cubic yards	yd^3
	TEMPERATURE (EXACT)			
°C	Celsius temperature	9/5 (then add 32)	Fahrenheit temperature	°F

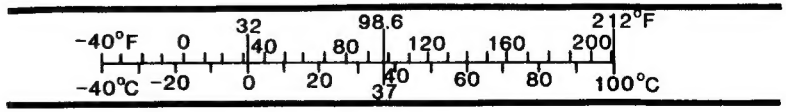

ACKNOWLEDGMENT

We would like to acknowledge the splendid cooperation and direction we received from the Project Officer, LT Brian D. Perkins, Coast Guard Research & Development Center. Discussions with LT Perkins, Art Allen and their colleagues at the Coast Guard Research & Development Center were very helpful throughout the project. The dataset provided by Art Allen was especially useful.

The project team consisted of Dr. William J. Browning, Dr. Byron D. Biggs, Dr. J. Robert Buchanan, Karen L. King, Dr. Christopher P. Thron, and Dr. Joseph T. Wissmann, Applied Mathematics; Dr. Allan R. Robinson, Dr. Avijit Gangopadhyay, Harvard University.

TABLE OF CONTENTS

1.0 INTRODUCTION

The Coast Guard uses ocean surface velocity fields from various ocean circulation models to provide input into trajectory models which are used in search planning to determine search area movement. Numerical techniques, called objective analysis, are used by oceanographers to combine observed data, irregularly distributed in space and time, to determine the total variation of the variables in the region of interest.

The purpose of this project is to study the feasibility of adapting objective analysis techniques for use with Coast Guard observation data in order to provide a significant improvement in Coast Guard search effectiveness in a variety of mission areas.

The following tasks were completed:

> Use objective analysis techniques to combine irregularly spaced and temporally observed ocean current velocity data in order to determine an optimally estimated velocity field, and
>
> Develop techniques to combine the regularly gridded velocity data output from two or more ocean circulation models to obtain a single optimally estimated velocity field.

In this report, we present the results of the Phase I effort.

Organization of Report. The report is organized in the following manner.

Coast Guard applications of ocean surface velocity fields are discussed in Section 2. A description of the mathematical theory underlying Objective Analysis (OA) is given in Section 3. A computer implementation of the OA algorithm to estimate ocean surface velocity fields is described in Section 4.

The Dataset used to illustrate the application of Objective Analysis is described in Section 5. Examples of an Objective Analysis derived velocity field are given in Section 6. A method to combine velocity fields from two or more models is given in Section 7. An illustration of the projection of an area of uncertainty using an OA velocity field is given in Section 8. Conclusions are presented in Section 9.

2.0 COAST GUARD APPLICATIONS OF OCEAN SURFACE VELOCITY FIELDS

The Coast Guard is the primary federal agency with maritime authority for the United States. The Coast Guard's four main missions are maritime law enforcement, maritime safety, environmental protection and national security.

Specific Coast Guard missions that will benefit from this research are Search and Rescue, Ice Patrol, and Environmental Protection. Central to the Coast Guard's research efforts in support of these missions is the need to model accurately the ocean current in order to calculate the movement of search areas.

Search and Rescue (SAR). The Coast Guard operates the world's largest SAR organization consisting of a nationwide system of boats, aircraft, cutters, and rescue coordination centers on 24-hour alert ready to rescue persons in peril at sea. The objective of the Coast Guard SAR program is to minimize loss of life, personal injury and property damage on the high seas and in all U.S. waters.

In 1992, a total of 52,645 SAR cases were conducted with 5,547 lives saved and $538M in property loss prevented.

Ice Patrol. The Coast Guard conducts the International Ice Patrol to observe and chart the position and movements of icebergs.

Environmental Protection. The Coast Guard is the lead agency to respond to the threat of pollution in the coastal zone. Their mission is to minimize damage caused by spills of oil or hazardous substances and to assist in pollution response planning efforts. In 1992, the Coast Guard responded to 8,700 oil pollution incidents.

3.0 OBJECTIVE ANALYSIS

3.1 INTRODUCTION

Objective Analysis is a numerical procedure for combining a number of atmospheric or oceanographic observations, which may be irregularly distributed in space and time, in order to draw conclusions about the total variation of meteorological or oceanographic variables in a specific region (Reference [a]).

Numerical procedures that have been used for objective analysis include polynomial interpolation, statistical interpolation, successive correction methods, variational methods, and spectral analysis methods. A study conducted by Gandin, discussed in Reference [a], indicated that when the data available are dense, these techniques all give similar results. When the data are sparse, the statistical interpolation method provided the best performance. The objective analysis technique used in this report is a statistical interpolation procedure which provides a minimum variance estimate.

The description of objective analysis in this section is taken from References [a] and [b]. The mathematical theory for objective analysis of a scalar field (i.e., a single variable specified at each space-time location) is given in Section 3.2.1. These results are extended in Section 3.2.2 to apply to a vector field with several variables specified at each space-time point, and where different field variables may be cross-correlated.

3.2 MATHEMATICAL THEORY

3.2.1 Scalar Objective Analysis

To explain the theory behind objective analysis, we introduce the following notation and statistical concepts.

The quantity under observation will be referred to as "the field", and denoted by the symbol f. In addition, let

f_{it} denote the true field value at position i and time t, (1a)

f_{it}^{obs}, the observed field value at position i and time t, and (1b)

e_{it}, the observational error at position i and time t. (1c)

These quantities are related by the equation

$$f_{it}^{obs} = f_{it} + e_{it}. \tag{2}$$

For a continuous variable, a mean value over time will be denoted

$$\langle f_i \rangle = \frac{1}{T}\int_T f_{it} dt. \tag{3a}$$

For a discrete variable, the mean value over n observations will be denoted

$$\langle f_{it} \rangle = \frac{\sum_{j=1} f_{it_j}}{n}. \tag{3b}$$

The deviation of a field from its mean (sometimes referred to as an anomaly) will be represented by

$$f'_{it} = f_{it} - \langle f_{it} \rangle. \tag{4}$$

The mean value over time of the square of the deviation from the mean is known as the variance, σ_i^2. Its square root is called the standard deviation, σ_i. The covariance between the field at position i and position j is denoted by

$$\begin{aligned} m_{ij} &= \langle (f_{it} - \langle f_{it} \rangle)(f_{jt} - \langle f_{jt} \rangle) \rangle \\ &= \langle f_{it}' f_{jt}' \rangle. \end{aligned} \tag{5}$$

Because the true field value is usually not known, the concept of the anomaly must be generalized by allowing it to be the deviation of an observation from a preliminary estimate of the true field value. A convenient preliminary estimate is the weighted mean value of temporally and spatially nearby points. The symbol f_{it}^p will denote the preliminary field value which is given by

$$f_{it}^p = \frac{\sum_{j=1} \frac{f_{jt}^{obs}}{l_{ij}}}{\sum \frac{1}{l_{ij}}}. \tag{6}$$

The weights, l_{ij}, in Equation (6) typically depend on the spatial and temporal distance of the observations from the point of interest and may include a dependence on the amount of measurement error associated with an observation.

In the following, the field anomalies and covariances will be taken with respect to the preliminary estimate of the field, rather than its mean value over time. Thus, Equations (4) and (5) are replaced by

$$f_{it}' = f_{it} - f_{it}^{p}, \text{ and} \tag{7}$$

$$\begin{aligned} m_{ij} &= \langle (f_{it} - f_{it}^{p})\,(f_{jt} - f_{jt}^{p}) \rangle \\ &= \langle f_{it}' f_{jt}' \rangle . \end{aligned} \tag{8}$$

It is assumed that f_{it}' has mean 0, that is, $\langle f_{it}' \rangle = 0$.

After the preliminary field value is determined, a minimum variance estimate of the field at a point can be calculated. A minimum variance estimate is one whose value will on average deviate least from the true value. The objective analysis estimated value, $\hat{f}_{gt}$, at point g and time t computed using n nearby observations, f_{it}^{obs} $(i = 1, 2, \ldots, n)$, is a linear combination of the preliminary field estimate and the deviations of the observations from the preliminary field estimate:

$$\hat{f}_{gt} = f_{gt}^{p} + \sum_{i=1}^{n} \alpha_i (f_{it}^{obs} - f_{it}^{p}) . \tag{9}$$

The linear coefficients, α_i $(i = 1, 2, \ldots, n)$, are chosen so as to minimize the variance of the field estimate $\hat{f}_{gt}$:

$$V_{gt} = \langle (f_{gt} - \hat{f}_{gt})^2 \rangle \tag{10}$$

$$\begin{aligned} &= \langle (f'_{gt})^2 \rangle + \sum_{i=1}^{n} \sum_{j=1}^{n} \alpha_i \alpha_j (\langle f'_{it} f'_{jt} \rangle + \langle e_{it} f'_{jt} \rangle + \langle f'_{it} e_{jt} \rangle + \langle e_{it} e_{jt} \rangle) - \\ &\quad 2 \sum_{i=1}^{n} \alpha_i (\langle f'_{gt} f'_{it} \rangle + \langle f'_{gt} e_{it} \rangle) . \end{aligned}$$

Under the assumption that the observational errors e_{it} and the deviations f_{it}' are uncorrelated, the variance reduces to

$$V_{gt} = \langle (f'_{gt})^2 \rangle + \sum_{i=1}^{n} \sum_{j=1}^{n} \alpha_i \alpha_j (\langle f'_{it} f'_{jt} \rangle + \langle e_{it} e_{jt} \rangle) - 2 \sum_{i=1}^{n} \alpha_i \langle f'_{gt} f'_{it} \rangle . \tag{11}$$

For purposes of brevity, the symbol $d_{ij} = \langle e_{it} e_{jt} \rangle$ will be introduced, so Equation (11) can be rewritten as

$$V_{gt} = m_{gg} + \sum_{i=1}^{n} \sum_{j=1}^{n} \alpha_i \alpha_j (m_{ij} + d_{ij}) - 2 \sum_{i=1}^{n} \alpha_i m_{gi}. \tag{12}$$

A necessary condition for minimizing V_{gt} with respect to the weights α_k is that for $k = 1, 2, \ldots, n$

$$\frac{\partial V_{gt}}{\partial \alpha_k} = 2 \left[\sum_{i=1}^{n} \alpha_i (m_{ik} + d_{ik}) - m_{gk} \right] = 0, \text{ or} \tag{13}$$

$$\sum_{i=1}^{n} \alpha_i (m_{ik} + d_{ik}) = m_{gk}. \tag{14}$$

In order to solve the linear system (14), the covariances, m_{ik}, m_{gk}, and d_{ik} must be known for $i, k = 1, 2, \ldots, n$. The computer code described in Section 4 assumes that the covariances m_{ik} are functions of the form

$$C = \sigma_p^2 (1 - a_2) e^{b_2} \tag{15}$$

where $a_2 > 0$ and $b_2 < 0$. The parameter σ_p^2 is an a priori estimate of the variance of the preliminary field estimate, while the parameters a_2 and b_2 depend on the spatial and temporal separation between points of interest. One choice of parameters is

$$a_2 = \left(\frac{\Delta x_{ij}}{x_0} \right)^2 + \left(\frac{\Delta y_{ij}}{y_0} \right)^2 \tag{16}$$

and

$$b_2 = -\frac{1}{2} \left(\left(\frac{\Delta x_{ij}}{x_d} \right)^2 + \left(\frac{\Delta y_{ij}}{y_d} \right)^2 + \left(\frac{\Delta t_{ij}}{t_d} \right)^2 \right). \tag{17}$$

The quantities Δx_{ij}, Δy_{ij}, and Δt_{ij} are the x, y and t components, respectively, of the distance between positions corresponding to field values f_i and f_j. The parameters x_0 and y_0 determine the zero crossing of the correlation function. The parameters x_d, y_d, and t_d are the decay scales for the correlation function.

The variance of the objective analysis field estimate, which is, in fact, the minimum variance, may be found by substituting Equation (14) into Equation (12):

$$V_{gt}^{(min)} = m_{gg} - \sum_{i=1}^{n} \alpha_i m_{gi}. \tag{18}$$

Equations (9), (14) and (18) can be conveniently expressed in vector-matrix notation, following Reference [b]. Let

$$\Delta f = (f_{it}^{obs} - f_{it}^{p}, \ldots, f_{nt}^{obs} - f_{nt}^{p}), \tag{19}$$

$$a = (\alpha_1, \ldots, \alpha_n), \tag{20}$$

$$C_f = \begin{pmatrix} m_{11} + d_{11} & \cdots & m_{1n} + d_{1n} \\ \cdot & & \cdot \\ \cdot & & \cdot \\ m_{n1} + d_{n1} & \cdots & m_{nn} + d_{nn} \end{pmatrix}, \tag{21}$$

$$C_{gf} = (m_{g1}, \ldots, m_{gn}), \tag{22}$$

Then Equations (9), (14) and (18) become

$$\hat{f}_{gt} = f_{gt}^{p} + (a \cdot \Delta f), \tag{23}$$

$$a = C_{gf} C_f^{-1}, \text{ and} \tag{24}$$

$$V_{gt} = \text{Var}(\hat{f}_{gt}) = m_{gg} - C_{gf} C_f^{-1} C_{gf}^{\mathrm{T}}. \tag{25}$$

Note that the subscript g refers to the particular grid point at which the field is being estimated, while the subscript f refers to the field being estimated.

3.2.2 Vector Objective Analysis

Objective analysis can also be used to estimate vector fields such as velocity, for which the different components of the field are cross-correlated.

In vector objective analysis, the definitions given by expressions (19) - (22) must be replaced by analogous versions, in which vector and matrix entries are replaced by matrices. Equations (23), (24) and (25) remain essentially the same.

In vector objective analysis, the definitions given by expressions (19) - (22) must be replaced by analogous versions, in which vector and matrix entries are replaced by matrices. Equations (23), (24) and (25) remain essentially the same.

For purposes of illustration, the equations for a 2-component field, $U = \begin{pmatrix} u \\ v \end{pmatrix}$, will now be given. Let

$$U_{it} = \begin{pmatrix} u_{it} \\ v_{it} \end{pmatrix} = \text{the true vector field value at position } i \text{ at time t,} \tag{26}$$

$$\mathrm{U}_{it}^{obs} = \begin{pmatrix} u_{it}^{obs} \\ v_{it}^{obs} \end{pmatrix} = \text{the observed vector field value at position } i \text{ at time t,} \tag{27}$$

$$\mathrm{E}_{it} = \begin{pmatrix} \mu_{it} \\ \nu_{it} \end{pmatrix} = \text{observational error vector at position } i \text{ and time t, and} \tag{28}$$

$$\mathrm{U}_{it}^{p} = \begin{pmatrix} u_{it}^{p} \\ v_{it}^{p} \end{pmatrix} = \text{the preliminary field estimate, where}$$

$$u_{it}^{p} = \left[\sum_{j=1}^{n} u_{jt}^{obs} / l_{ij} \right] / \sum_{j=1}^{n} l_{ij} \tag{29}$$

and

$$v_{it}^{p} = \left[\sum_{j=1}^{n} v_{jt}^{obs} / l_{ij} \right] / \sum_{j=1}^{n} l_{ij}. \tag{30}$$

The $\{l_{ij}\}$ in Equations (29) and (30) are weights as in Equation (6). Using the above definitions, the vector equations corresponding to Equations (19) through (22) may be given as:

$$\mathrm{D}\boldsymbol{U} = (U_{1t}^{obs} - U_{1t}^{p}, \ldots, U_{nt}^{obs} - U_{nt}^{p}), \tag{31}$$

$$\boldsymbol{A} = (A_1, \ldots, A_n), \text{ where} \tag{32}$$

$$C_U = \begin{pmatrix} M_{11}+D_{11} & \cdots & M_{1n}D_{1n} \\ \cdot & & \cdot \\ \cdot & & \cdot \\ M_{n1}+D_{n1} & \cdots & M_{nn}+D_{nn} \end{pmatrix}, \quad \text{where} \tag{33}$$

$$M_{ij} = \begin{pmatrix} \langle u_{it}u_{jt}\rangle & \langle u_{it}v_{jt}\rangle \\ \langle v_{it}u_{jt}\rangle & \langle v_{it}v_{jt}\rangle \end{pmatrix} \quad \text{and} \tag{34}$$

$$D_{ij} = \begin{pmatrix} \langle \mu_{it}\mu_{jt}\rangle & \langle \mu_{it}\nu_{jt}\rangle \\ \langle \nu_{it}\mu_{jt}\rangle & \langle \nu_{it}\nu_{jt}\rangle \end{pmatrix}, \quad \text{and} \tag{35}$$

$$C_{gU} = (M_{g1}, \ldots, M_{gn}) . \tag{36}$$

Now the vector equations analogous to Equations (23), (24) and (25) become

$$\hat{U}_{gt} = \begin{pmatrix} \hat{u}_{gt} \\ \hat{v}_{gt} \end{pmatrix} = \text{the objective analysis field estimate,}$$

$$= U^p_{gt} + A \cdot \Delta U, \tag{37}$$

$$A = C_{gU}C_U^{-1}, \tag{38}$$

$$V_{gt} = \text{covariance matrix for } \hat{U}_{gt}$$

$$= \begin{pmatrix} \langle (\hat{u}_{gt}-u_{gt})^2\rangle & \langle (\hat{u}_{gt}-u_{gt})\,(\hat{v}_{gt}-v_{gt})\rangle \\ \langle (\hat{u}_{gt}-u_{gt})\,(\hat{v}_{gt}-v_{gt})\rangle & \langle (\hat{v}_{gt}-v_{gt})^2\rangle \end{pmatrix}$$

$$= M_{gg} - C_{gU}C_U^{-1}C_{gU}^{\mathrm{T}}. \tag{39}$$

Equations (26) through (39) specify the vector objective analysis estimates for the field components and their covariances.

For the purposes of computer coding, it is more convenient to re-express Equations (37) and (38) so that the field components u and v are separated. Given the definitions

$$\mathrm{M}_{ij} = \begin{pmatrix} m_{ij}^{(1)} & m_{ij}^{(2)} \\ m_{ij}^{(3)} & m_{ij}^{(4)} \end{pmatrix},$$

$$D_{ij} = \begin{pmatrix} d_{ij}^{(1)} & d_{ij}^{(2)} \\ d_{ij}^{(3)} & d_{ij}^{(4)} \end{pmatrix},$$

then it follows that:

$$\begin{pmatrix} \hat{u}_{gt} \\ \hat{v}_{gt} \end{pmatrix} = \begin{pmatrix} u_{gt}^{p} \\ v_{gt}^{p} \end{pmatrix} + \begin{pmatrix} a_{11}\ldots a_{1n} & a_{21}\ldots a_{2n} \\ a_{31}\ldots a_{3n} & a_{41}\ldots a_{4n} \end{pmatrix} \begin{pmatrix} \Delta u_1 \\ \vdots \\ \Delta u_n \\ \\ \Delta v_1 \\ \vdots \\ \Delta v_n \end{pmatrix}, \text{ where}$$

$$\begin{pmatrix} a_{11}\ldots a_{1n} & a_{21}\ldots a_{2n} \\ a_{31}\ldots a_{3n} & a_{41}\ldots a_{4n} \end{pmatrix} = \tilde{C}_{gU}\tilde{C}_{U}^{-1}, \text{ and}$$

$$\tilde{C}_{gU} = \begin{pmatrix} m_{g1}^{(1)}\ldots m_{gn}^{(1)} & m_{g1}^{(2)}\ldots m_{gn}^{(2)} \\ m_{g1}^{(3)}\ldots m_{gn}^{(3)} & m_{g1}^{(4)}\ldots m_{gn}^{(4)} \end{pmatrix},$$

$$\tilde{C}_{U} = \left(\begin{array}{c|c} m_{11}^{(1)} + d_{11}^{(1)}\ldots m_{1n}^{(1)} + d_{1n}^{(1)} & m_{11}^{(2)} + d_{11}^{(2)}\ldots m_{1n}^{(2)} + d_{1n}^{(2)} \\ \vdots & \vdots \\ m_{n1}^{(1)} + d_{n1}^{(1)}\ldots m_{nn}^{(1)} + d_{nn}^{(1)} & m_{n1}^{(2)} + d_{n1}^{(2)}\ldots m_{nn}^{(2)} + d_{nn}^{(2)} \\ \hline m_{11}^{(3)} + d_{11}^{(3)}\ldots m_{1n}^{(3)} + d_{1n}^{(3)} & m_{11}^{(4)} + d_{11}^{(4)}\ldots m_{1n}^{(4)} + d_{1n}^{(4)} \\ \vdots & \vdots \\ m_{n1}^{(3)} + d_{n1}^{(3)}\ldots m_{nn}^{(3)} + d_{nn}^{(3)} & m_{n1}^{(4)} + d_{n1}^{(4)}\ldots m_{nn}^{(4)} + d_{nn}^{(4)} \end{array}\right),$$

and

$$V_{gt} = M_{gg} - \tilde{C}_{gU}\tilde{C}_{U}^{-1}\tilde{C}_{gU}^{\mathrm{T}}.$$

4.0 COMPUTER IMPLEMENTATION OF OA ALGORITHM

In this section, we describe a computer implementation in FORTRAN of the vector OA algorithms presented in Section 3.

A scalar version of the OA algorithm in FORTRAN is contained in the Harvard University GULFCAST system. The code was modified in this project to accept vector components.

Program Input. The velocity observation data is shown in Table 4-1. The OA program is controlled by the parameters which are shown in Table 4-2.

Table 4-1. Velocity Observation Data

Program Parameter	Description
DEPTH	Depth at which the observation was made.
TIM	Time at which the observation was made.
LON	Longitude at which the observation was made.
LAT	Latitude at which the observation was made.
U	Zonal component of velocity.
V	Meridional component of velocity.
UVAR	Variance of the zonal component of velocity.
VVAR	Variance of the meridional component of velocity.

Program Flow. The vector objective analysis program begins by reading an input file containing the parameters listed in the Table 4-2. The last line of the parameter file contains the name of the file containing the observation data.

The observation data file is read, and the data is stored in arrays. Next the positions of the grid points in the interpolation region are calculated. The following steps are then repeated for each grid point.

Table 4-2. OA Parameters

Program Parameter	Description
IM	Number of grid points in the zonal direction.
JM	Number of grid points in the meridional direction.
DX	Zonal grid spacing.
DY	Meridional grid spacing.
CLNG	Domain centroid longitude (west values are negative).
CLAT	Domain centroid latitude (south values are negative).
XOFF	Zonal offset for the domain centroid.
YOFF	Meridional offset for the domain centroid.
THETAD	Domain rotation (counterclockwise from east).
NNCE	Maximum number of influential observations used in estimating the field at a point of interest.
RNCE	Spatial radius of influence of observations.
TNCE	Temporal radius of influence.
XZERO	Zero crossing in the zonal direction of the analytical correlation function (corresponding to x_0 in Equation (16)).
YZERO	Zero crossing in the meridional direction of the analytical correlation function (corresponding to y_0 in Equation (16)).
XDCAY	Zonal decorrelation scale of the analytical correlation function (corresponding to x_d in Equation (17)).
YDCAY	Meridional decorrelation scale of the analytical correlation function (corresponding to y_d in Equation (17)).
TDCAY	Temporal decorrelation scale of the analytical correlation function (corresponding to t_d in Equation (17)).
UPHSE	Zonal phase speed.
VPHSE	Meridional phase speed.
OADAY	Time for which the field is estimated.

A subroutine, SELECT, searches the arrays of input data to identify observations within the influential spatial radius (parameter RNCE) and within the influential temporal radius (parameter TNCE) of the grid point of interest. If more than the user specified maximum number of influential observations (parameter NNCE) are found, the NNCE observations that are most highly correlated with the point of interest are used.

A subroutine, REMAV, calculates the mean and variance of the velocity components of the influential points as determined by subroutine SELECT. Subroutine REMAV also subtracts the mean from the velocity components, thus producing the vector of deviations from the mean which will be weighted to produce the estimated velocity components at the point of interest.

The objective analysis calculations are performed in subroutine OBJAN. This subroutine solves a linear system for the weights to be applied to the deviations calculated by REMAV. Subroutine OBJAN calls subroutine SETA which calculates the correlation matrix of observations. The correlation matrix is normalized by the variances of the velocity components of the influential observation. This matrix is block diagonal and symmetric. The upper left block represents the correlation between the first components of velocity while the lower right block represents the correlation between the second components of velocity. The remaining off diagonal blocks are zero because of the assumption that the zonal and meridional components of velocity are uncorrelated. Before returning control to OBJAN, SETA inverts the correlation matrix and checks for ill-conditioning. Subroutine OBJAN multiplies the inverted correlation matrix by the vector of correlations between the point of interest and the observation points. The resulting vector of weights is multiplied elementwise by the vector of deviations from the mean calculated previously by REMAV. Once the previously removed velocity mean is added back, the estimation of the velocity components at the point of interest is complete. The algorithm then proceeds to the calculation of the velocity field at the next grid point.

Program Output. The OA program is run for the specified solution time. At each grid point, a velocity field and associated uncertainties are calculated. The uncertainty in each velocity component at a grid point is calculated as a relative quantity with respect to the sample variance of the input values determined by the subroutine SELECT. These relative variances are converted to absolute error values. The velocity field is smoothed using a Shapiro filter as described in References [c] and [d]. This filtering smooths regions of discontinuity which arise as the influential points change during the OA analysis. The latitude, longitude, x component of velocity and variance, and y component of velocity and variance are stored for each of the specified grid points. These values determine the velocity and error fields shown, for example, in Figure 6-3.

5.0 DATASET

The United States Coast Guard Research and Development Center provided a dataset of drifting buoy positions versus time (Reference [e]) for use in this project. Arthur Allen of the USCG R&D Center directed the deployment of several different types of drifter buoys from the Canadian Coast Guard Ship Sir Humphrey Gilbert. The test was conducted in November and December, 1993, off the east coast of the Avalon Peninsula near St. John's, Newfoundland. The test area, approximately 100 nm on a side, is shown in Figure 5-1.

5.1 DESCRIPTION

A MINIMET buoy was moored during the test. This buoy was equipped with sensors for air and water temperature, wind speed and direction, air pressure, wave height and period, and current. The meteorological instruments were mounted on a mast three meters above the sea surface. The MINIMET buoy was anchored in water approximately 600 feet deep on a 1900 foot line (which allowed the buoy to drift in a circle around the anchor point). Thirty feet below the buoy was a rectangular window shade drogue (2m by 10m). A S4 current meter was suspended at 1m depth from a float 70 feet from the main MINIMET buoy. The MINIMET buoy served as a reference point for the deployment of the drifter buoys. The MINIMET buoy position was determined every half hour using GPS. The buoy also recorded all collected data on-board in EPROM which was read when the buoy was recovered.

In addition to the MINIMET buoy, ten freely drifting buoys were deployed at various locations and times during the test. The positions of these buoys were collected and reported by the Argos satellite system. The initial position of each drifter buoy was taken to be the deploying ship's GPS position. After deployment, the drifter buoys' positions were calculated and recorded by the Argos system. The Argos system uses the Doppler shift of radio waves broadcast at frequency 401.65 MHz to measure the position of transmitters in the drifting buoys.

Service Argos provides a discrete measure of positional accuracy called the "fix quality". The qualities are given in Table 5-1.

Table 5-1. Argos Position Error

Fix Quality	Positional Error
3	< 150m
2	< 350m
1	< 1000m
0	> 1000m

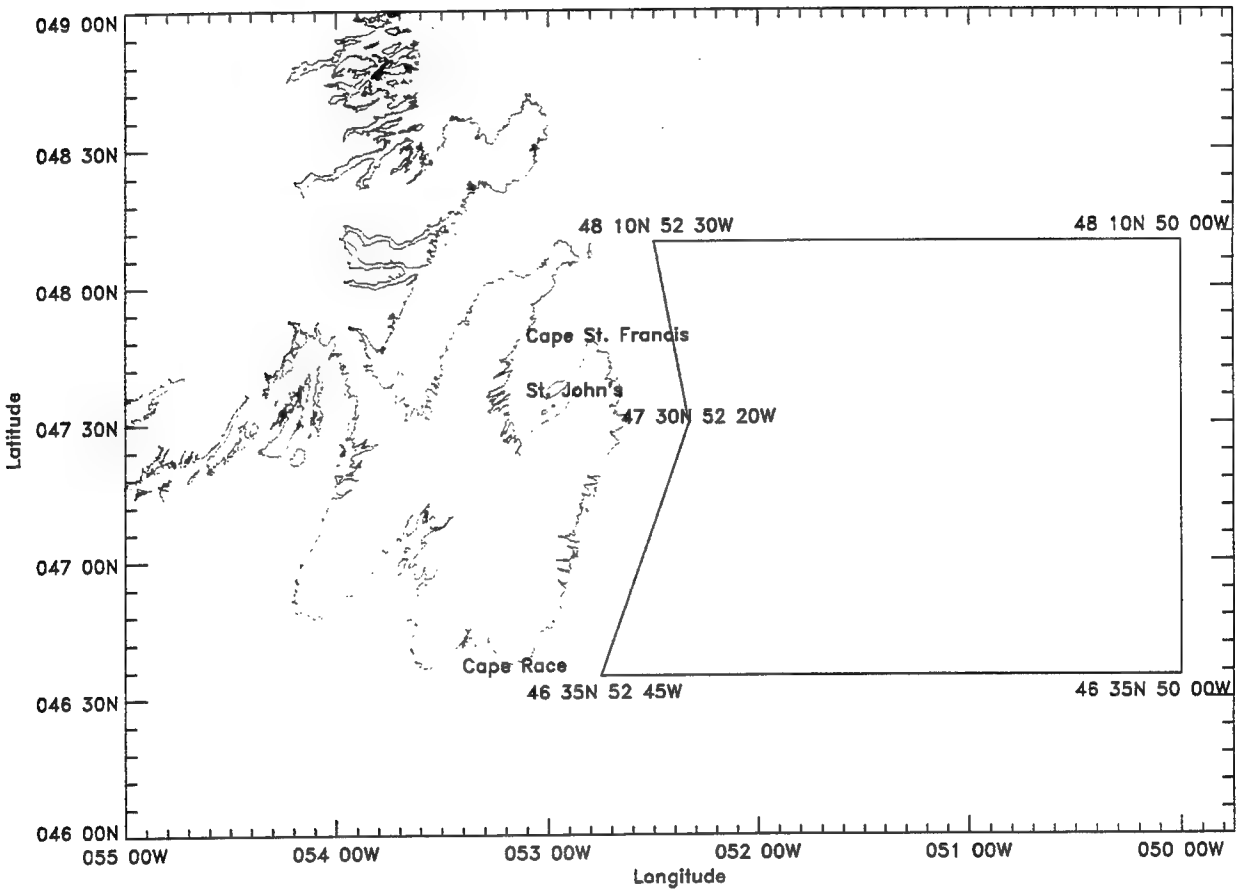

Figure 5-1. Test Area

The errors given in Table 5-1 are one standard deviation values For example, 68% of positions reported with fix quality 3 are assumed to be within 150m of the true position. The GPS positions are considered accurate to within 100m. Any GPS positions recorded in the data were indicated with a fix quality of 9.

Figure 5-2 shows the time periods in which the buoys were deployed. Table 5-2 lists the times, buoy ID number and fix qualities for each reported position. Figure 5-3 presents a histogram of the buoy fix qualities.

Three different types of drifter buoys were deployed: three self locating datum marker buoys (SL-DMB) manufactured by Seimac Limited (ID numbers 2619, 4521, 4529), five Davis/CODE drifters (ID # 4531 and 4532 manufactured by Clearwater Instruments and ID # 4533, 4534, 4535 manufactured by Technoceans), and two WOCE drifter buoys (ID # 2590 and 2591 manufactured by Clearwater Instruments).

Three of the drifting buoys (2591, 4521, 4529) were deployed at the location of the MINIMET buoy. Because the MINIMET moved several miles south before the end of the test, not all of these buoys were deployed at the same location.

The drift paths are shown in Figure 5-4 through 5-6 separately for each type of buoy deployed. The green asterisk denotes the buoy initial points; the red asterisk indicates the buoy final points. No quality zero fix positions are plotted.

5.2 DETERMINATION OF BUOY VELOCITY

The velocities of the buoys were calculated using the position, time, and fix quality information provided in the dataset. The buoys were assumed to move on a constant course and speed track between observation points. The positional data were filtered to remove all observations with fix quality 0, and the great circle distances and bearings between successive positions were calculated. The average velocities of the buoys were determined from these distances and elapsed times. These average velocities were resolved into perpendicular components using the bearing angles. The position and time of the first observation in each pair were used as the position and time of each derived velocity.

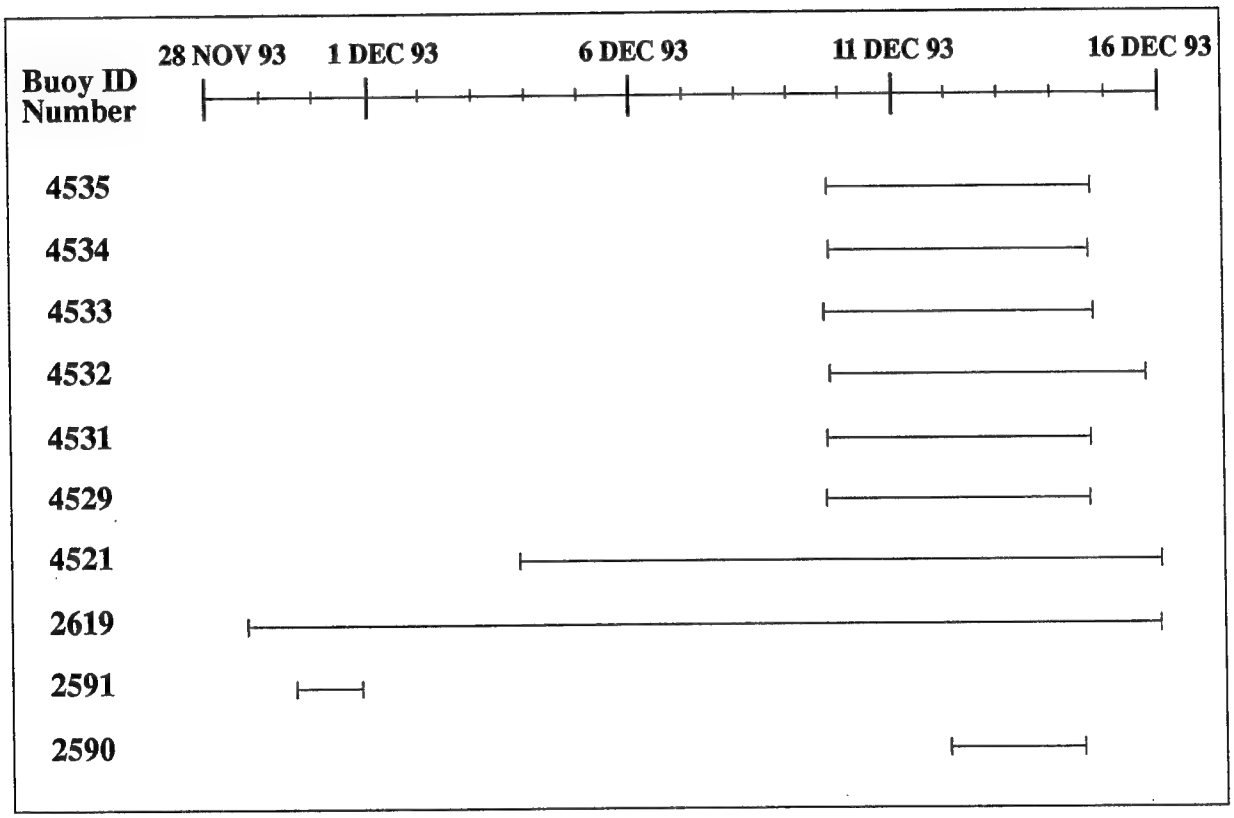

Figure 5-2. Buoy Deployment Time Line

Table 5-2. Buoy Position Time, ID Number and Fix Quality

DTG	Buoy ID #	Fix Quality
NOV 93		
281725Z	2619	9
291431Z	2591	9
2159Z	2619	0
2341Z	2591	2
300931Z	2619	0
1013Z	2619	0
1332Z	2619	0
1741Z	2591	1
1920Z	2591	1
1920Z	2619	2
2036Z	2591	9
2100Z	2619	0
2137Z	2619	3
2318Z	2619	0
DEC 93		
010953Z	2619	0
1309Z	2619	0
1726Z	2619	0
2048Z	2619	0
2256Z	2619	1
020729Z	2619	0
0911Z	2619	0
1247Z	2619	0
1854Z	2619	1
2057Z	2619	0
2235Z	2619	2
030713Z	2619	1
0854Z	2619	1
1047Z	2619	2
1227Z	2619	0
1844Z	2619	1
2015Z	4521	9
2025Z	2619	0
2034Z	2619	0
2355Z	2619	0
040703Z	4521	0
0844Z	2619	0
0844Z	4521	1
1020Z	2619	0
1022Z	4521	0
1024Z	2619	0

DTG	Buoy ID #	Fix Quality
DEC 93		
041030Z	4521	0
1208Z	4521	1
1210Z	2619	2
1347Z	4521	1
1652Z	4521	0
1831Z	2619	1
1831Z	4521	2
2009Z	2619	0
2011Z	4521	3
2015Z	4521	0
2151Z	4521	2
2331Z	2619	3
2332Z	4521	3
050647Z	2619	0
0648Z	4521	2
1006Z	2619	0
1010Z	2619	0
1010Z	4521	1
1145Z	2619	0
1147Z	4521	2
1324Z	2619	0
1326Z	4521	0
1639Z	2619	0
1639Z	4521	0
1817Z	2619	1
1817Z	4521	2
1958Z	2619	1
1959Z	4521	2
2130Z	4521	2
2131Z	2619	2
2309Z	4521	3
2312Z	2619	1
060812Z	4521	0
0819Z	2619	0
0940Z	2619	0
0941Z	4521	0
0957Z	2619	0
1000Z	4521	3
1128Z	2619	0
1303Z	2619	0
1306Z	4521	1

DTG	Buoy ID #	Fix Quality
DEC 93		
061807Z	2619	1
1807Z	4521	1
1945Z	4521	2
1946Z	2619	1
2108Z	2619	1
2108Z	4521	1
2249Z	2619	2
2249Z	4521	1
070623Z	4521	0
0805Z	4521	2
0947Z	4521	2
1100Z	2619	1
1240Z	2619	0
1244Z	4521	2
1754Z	4521	0
1755Z	2619	0
1933Z	2619	0
1933Z	4521	1
2048Z	2619	0
2048Z	4521	0
2229Z	4521	0
080752Z	2619	1
0933Z	2619	0
0933Z	4521	1
1040Z	2619	1
1040Z	4521	3
1221Z	2619	0
1221Z	4521	1
1741Z	2619	0
1741Z	4521	1
1923Z	4521	1
2025Z	4521	0
2204Z	2619	1
2204Z	4521	1
2345Z	2619	0
090739Z	2619	3
0740Z	4521	2
** 0920Z	2619	1
0924Z	4521	3
1020Z	2619	2
1020Z	4521	1

Table 5-2. Buoy Position Time, ID Number and Fix Quality (Continued)

DTG	Buoy ID #	Fix Quality
DEC 93		
091202Z	2619	0
1202Z	4521	1
1339Z	2619	0
1616Z	4533	9
1647Z	4531	9
1711Z	4529	9
1731Z	4521	0
1732Z	4534	9
1804Z	4535	9
1840Z	4532	9
* 2005Z	4532	2
* 2006Z	4531	2
2049Z	2619	0
2049Z	4534	2
2051Z	4529	0
2051Z	4531	2
2051Z	4532	3
2052Z	4521	0
2052Z	4533	2
2144Z	4521	2
2144Z	4529	1
2144Z	4531	2
2144Z	4532	2
2144Z	4533	2
2144Z	4535	2
2146Z	4534	2
2148Z	2619	0
2324Z	4529	2
2324Z	4531	3
2325Z	4521	0
2325Z	4532	2
2325Z	4533	3
2326Z	4535	2
100726Z	4535	2
0727Z	4529	2
0727Z	4533	2
0729Z	2619	0
0729Z	4531	3
0729Z	4532	3
0729Z	4534	2
0908Z	2619	0

DTG	Buoy ID #	Fix Quality
DEC 93		
100908Z	4535	2
0910Z	4521	0
0910Z	4529	1
* 0911Z	4531	2
0911Z	4532	3
0911Z	4533	2
0911Z	4534	2
* 0957Z	4532	3
0959Z	4529	0
0959Z	4531	3
1047Z	4531	2
1135Z	4521	0
1316Z	2619	0
1316Z	4521	0
1316Z	4531	2
1316Z	4534	3
1317Z	4532	3
1319Z	4529	0
1716Z	4529	0
1719Z	4531	2
1719Z	4532	3
1857Z	4531	2
1857Z	4534	2
1857Z	4535	2
1901Z	2619	0
2038Z	4529	1
2038Z	4531	2
2039Z	4534	3
2041Z	4532	2
2123Z	4532	2
2124Z	4531	2
2124Z	4535	2
2300Z	2619	0
2302Z	4531	3
2302Z	4532	2
2302Z	4535	2
2303Z	4533	2
2305Z	4534	2
110714Z	4532	3
0716Z	4529	0
0716Z	4531	2

DTG	Buoy ID #	Fix Quality
DEC 93		
110857Z	2619	0
0858Z	4529	2
0858Z	4531	2
0858Z	4532	3
0858Z	4533	2
0858Z	4534	2
0858Z	4535	3
1036Z	4531	2
1036Z	4532	2
1112Z	4529	0
1116Z	4531	2
1116Z	4532	2
1116Z	4535	2
1118Z	4533	2
** 1118Z	4534	2
1256Z	4534	3
1256Z	4535	2
1257Z	4531	2
1257Z	4532	3
1705Z	4529	0
1706Z	4531	2
1706Z	4532	2
1841Z	4529	0
1844Z	4535	2
1846Z	2619	0
1846Z	4531	2
1846Z	4532	2
1846Z	4533	2
1846Z	4534	2
2025Z	4529	0
2025Z	4531	2
2025Z	4532	2
2025Z	4533	2
2028Z	4535	2
2101Z	4529	0
2101Z	4531	3
2101Z	4533	3
2101Z	4534	3
2101Z	4535	2
2102Z	4532	2
2239Z	4529	2

Table 5-2. Buoy Position Time, ID Number and Fix Quality (Continued)

DTG	Buoy ID #	Fix Quality
DEC 93		
112239Z	4531	2
2239Z	4533	2
2239Z	4534	2
2240Z	4532	2
2243Z	4535	2
120015Z	2590	9
0023Z	4531	2
0024Z	4529	0
0703Z	4532	3
0703Z	4533	2
0704Z	2590	1
0704Z	4531	2
0847Z	2590	2
0847Z	4533	2
0848Z	4531	2
0848Z	4532	2
* 1023Z	4532	2
* 1023Z	4533	2
1024Z	4529	0
* 1024Z	4531	2
1052Z	4529	0
1053Z	2619	0
1055Z	4531	2
1055Z	4532	2
1055Z	4534	2
1058Z	4533	2
1234Z	4531	2
1234Z	4533	2
1235Z	4534	2
1237Z	4529	3
1237Z	4532	2
1653Z	4529	0
1834Z	2590	2
1834Z	4531	2
1834Z	4532	2
1834Z	4533	2
1834Z	4534	2
2015Z	4529	0
2015Z	4534	2
2041Z	2590	1
2041Z	4529	0

DTG	Buoy ID #	Fix Quality
DEC 93		
122041Z	4531	3
2041Z	4532	3
2041Z	4533	2
130000Z	4532	2
0001Z	4529	0
0001Z	4531	2
0653Z	4532	3
1012Z	4531	2
1013Z	2590	1
1030Z	4529	0
1033Z	4532	3
1033Z	4534	2
1212Z	4533	2
1212Z	4534	3
1214Z	2590	1
1214Z	4532	2
1215Z	4531	2
1352Z	4531	2
1821Z	2590	1
1823Z	4531	3
2000Z	4531	2
2002Z	2590	2
2157Z	4531	2
2157Z	4535	2
2336Z	4535	2
2338Z	4534	2
2339Z	4531	2
2339Z	4532	2
140638Z	4529	0
0638Z	4535	2
0640Z	4533	3
1000Z	4531	3
1000Z	4535	2
1001Z	4529	0
1010Z	4529	3
1010Z	4532	3
1010Z	4533	3
1010Z	4534	3
1013Z	2590	1
1151Z	4535	2
1154Z	4529	1

DTG	Buoy ID #	Fix Quality
DEC 93		
141154Z	4531	2
1154Z	4533	2
1155Z	4532	2
1330Z	4531	2
1339Z	2590	9
1635Z	4534	9
1702Z	4529	9
1804Z	4531	9
1810Z	4535	2
1834Z	4533	9
1913Z	4535	9
150947Z	4521	0
1900Z	4532	9
2255Z	2619	0
182328Z	2619	0
202243Z	4521	0
240937Z	2619	0
1932Z	2619	0

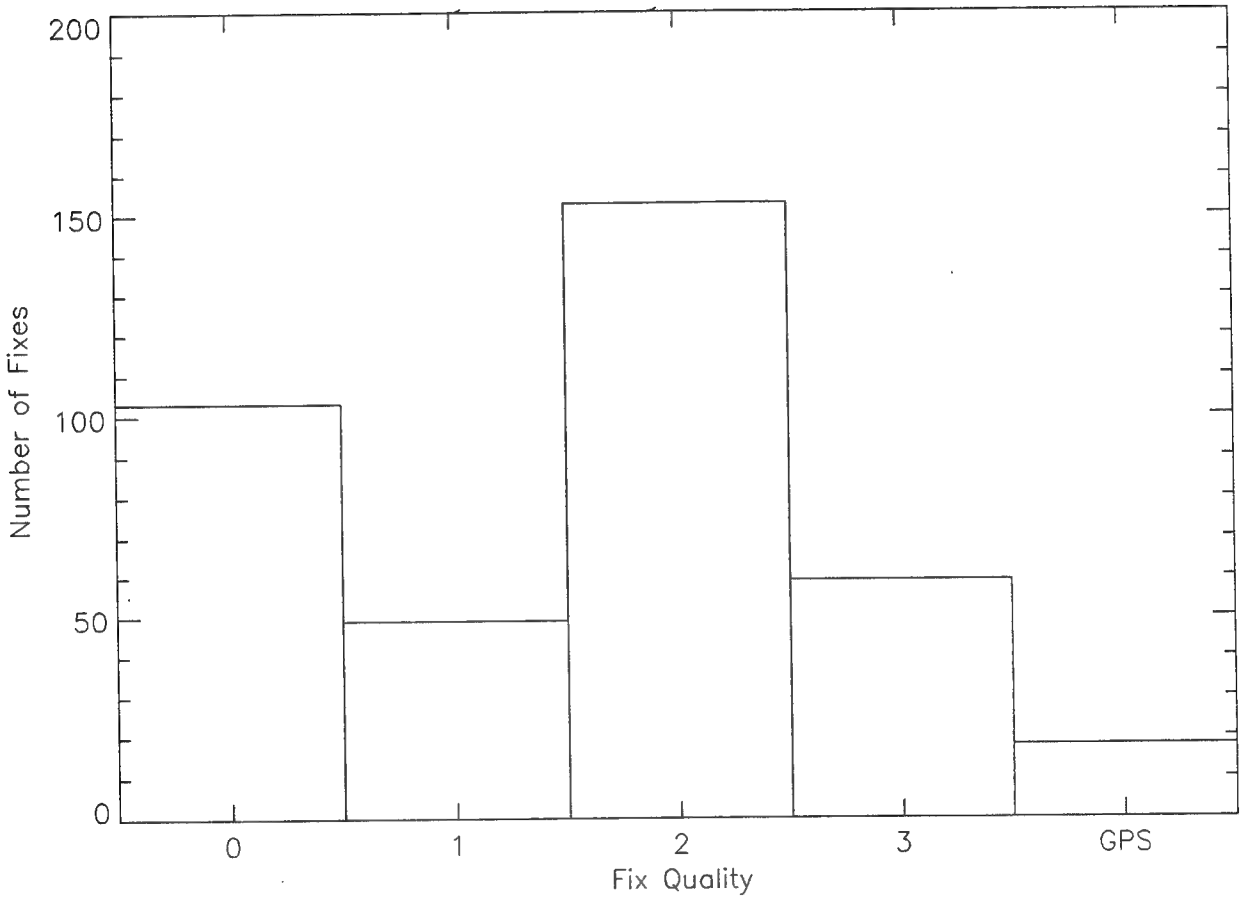

Note: Total = 382

Figure 5-3. Histogram of Buoy Fix Quality

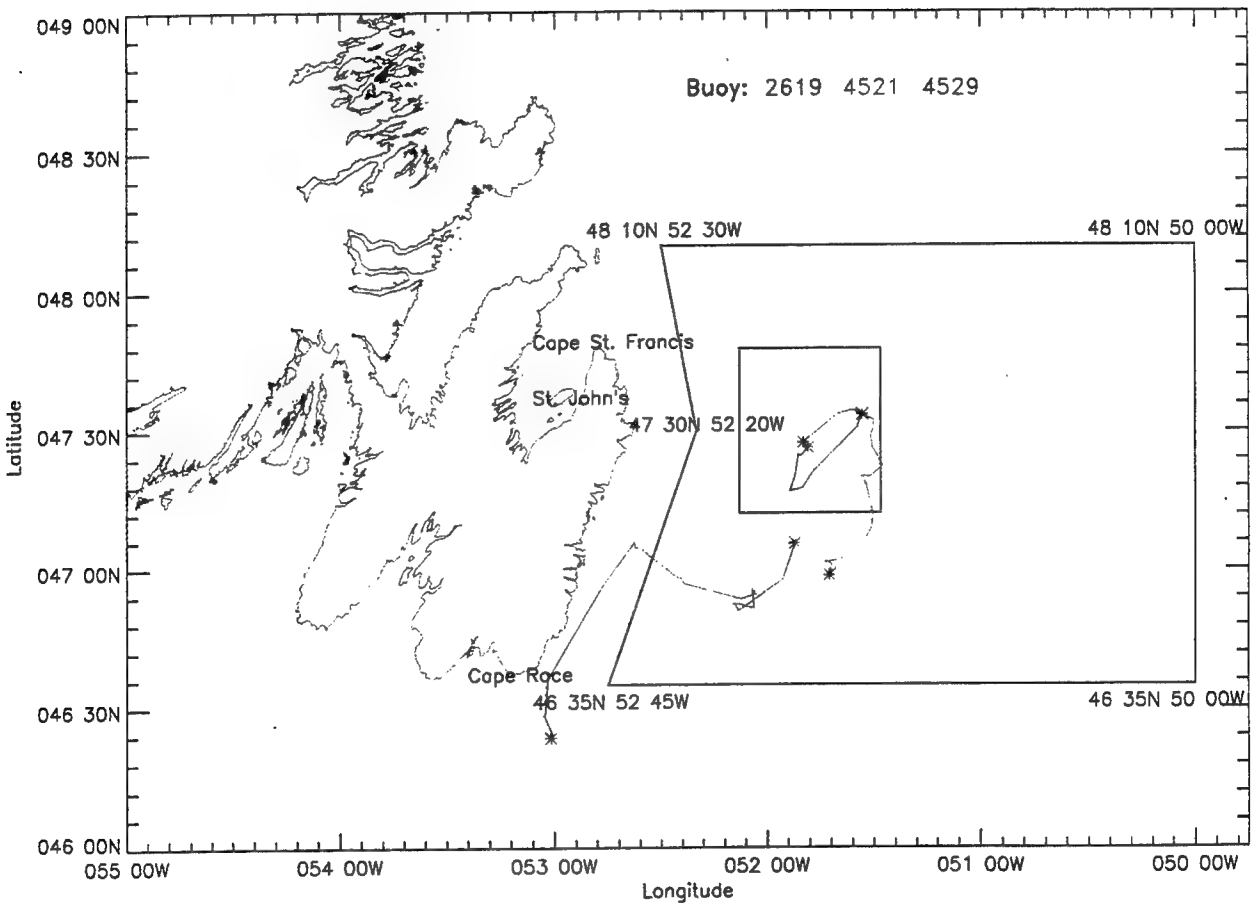

Figure 5-4. SL-DMB Buoy Tracks

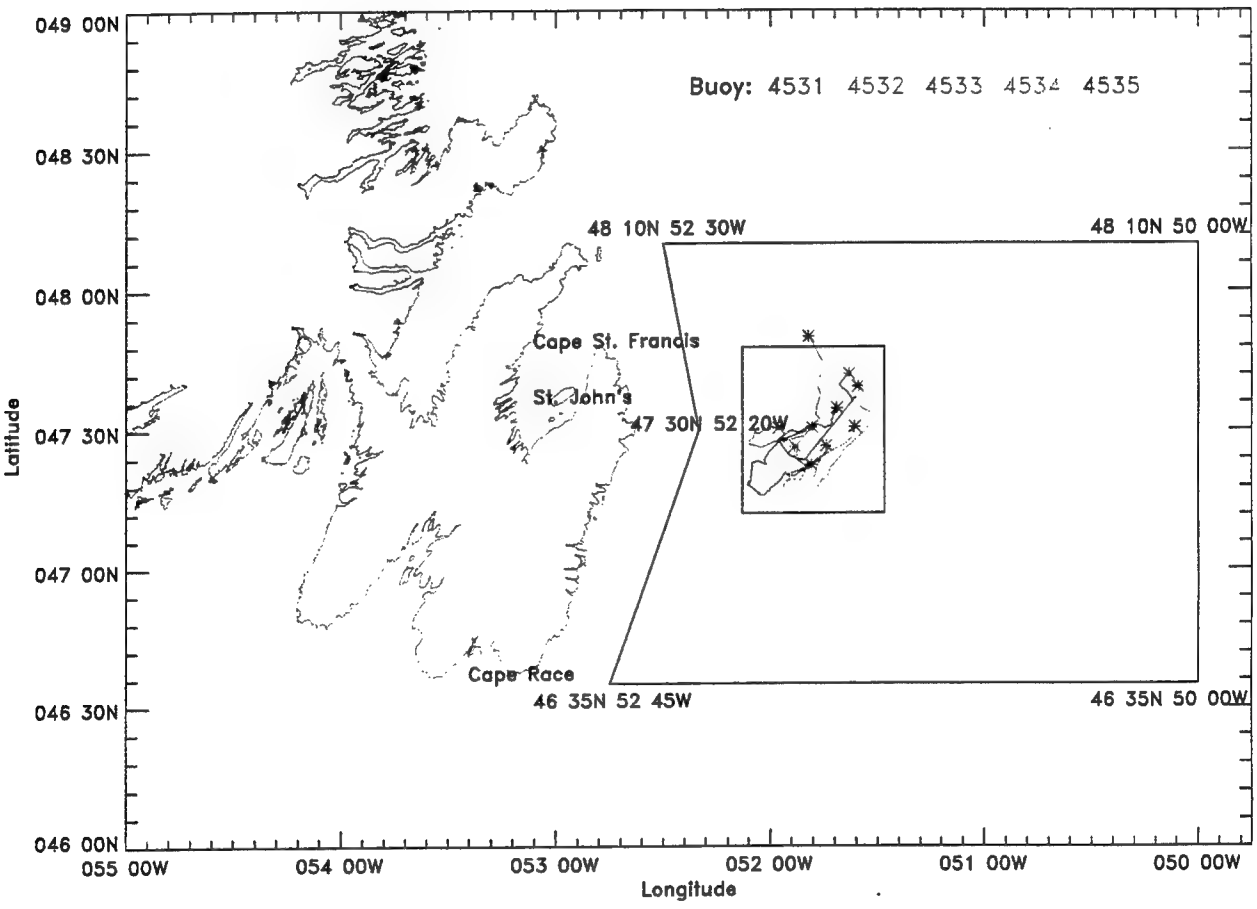

Figure 5-5. Davis/CODE Buoy Tracks

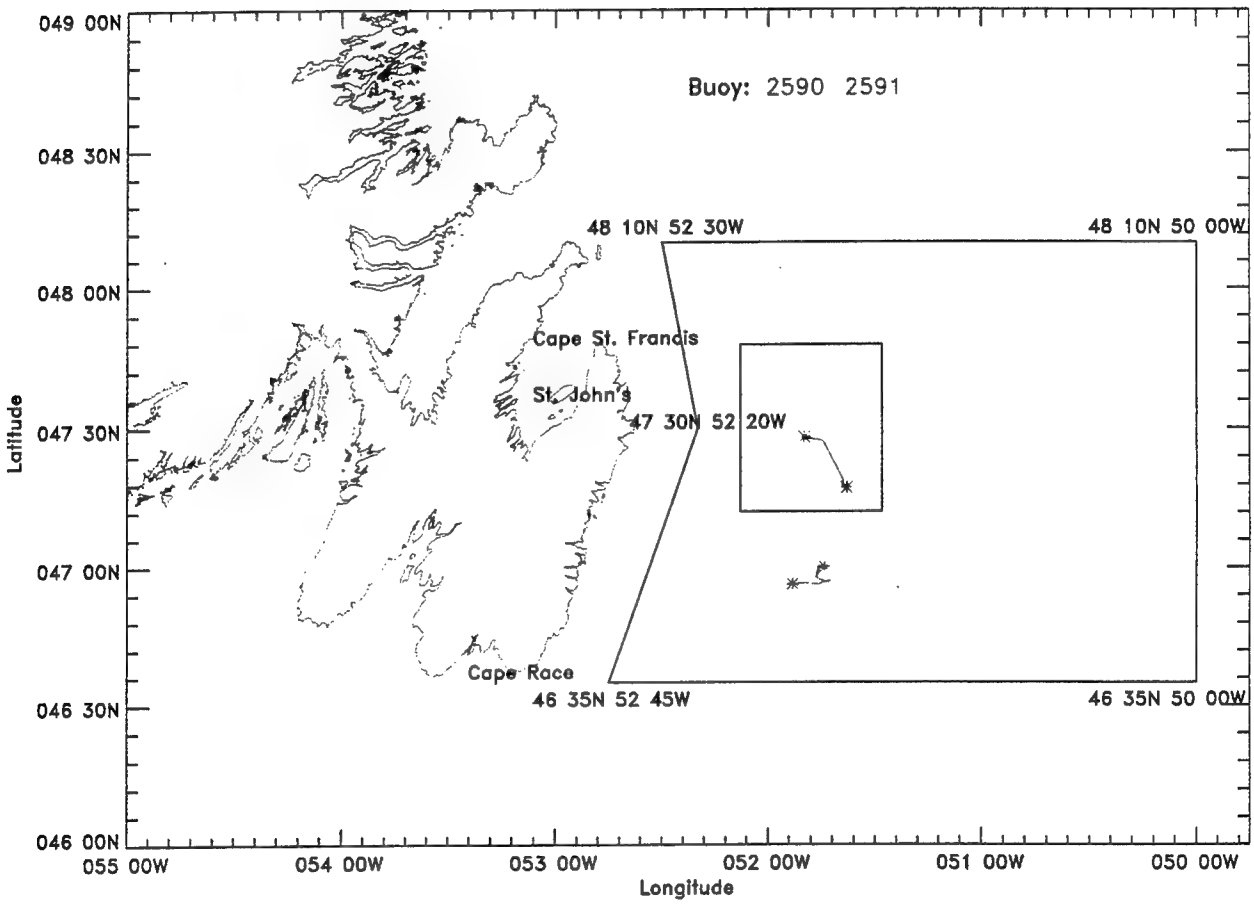

Figure 5-6. WOCE Buoy Tracks

5.3 VELOCITY ERROR MODEL

The velocity variance used as an input parameter in the objective analysis was estimated using the Argos fix position and the associated fix quality.

An Argos fix determines a buoy's position at a specified time with a standard deviation given by the fix quality. Two successive Argos fixes of a buoy determine a mean velocity with error as follows.

Assume that two successive Argos fixes are defined by

$$(t_1, x_1, y_1) \text{ and } (t_2, x_2, y_2).$$

Each fix has an associated fix quality σ_i, $i = 1, 2$. The uncertainty in position (x_i, y_i) at time t_i is assumed to be a circular normal distribution with standard deviation $\sigma_i = \sigma_{x_i} = \sigma_{y_i}$, $i = 1, 2$. An example of a circular normal probability distribution with $\sigma = 1$ is shown in Figure 5-7.

The buoy's mean velocity from time t_1 to t_2 is

$$\begin{pmatrix} \dot{x} \\ \dot{y} \end{pmatrix} = \frac{1}{t_2 - t_1} \begin{pmatrix} x_2 - x_1 \\ y_2 - y_1 \end{pmatrix}.$$

We assume that the Argos fixes are independent. The uncertainties of the components of velocity are then given by

$$\sigma_{\dot{x}} = \sigma_{\dot{y}} = \frac{1}{t_2 - t_1} \sqrt{\sigma_1^2 + \sigma_2^2}.$$

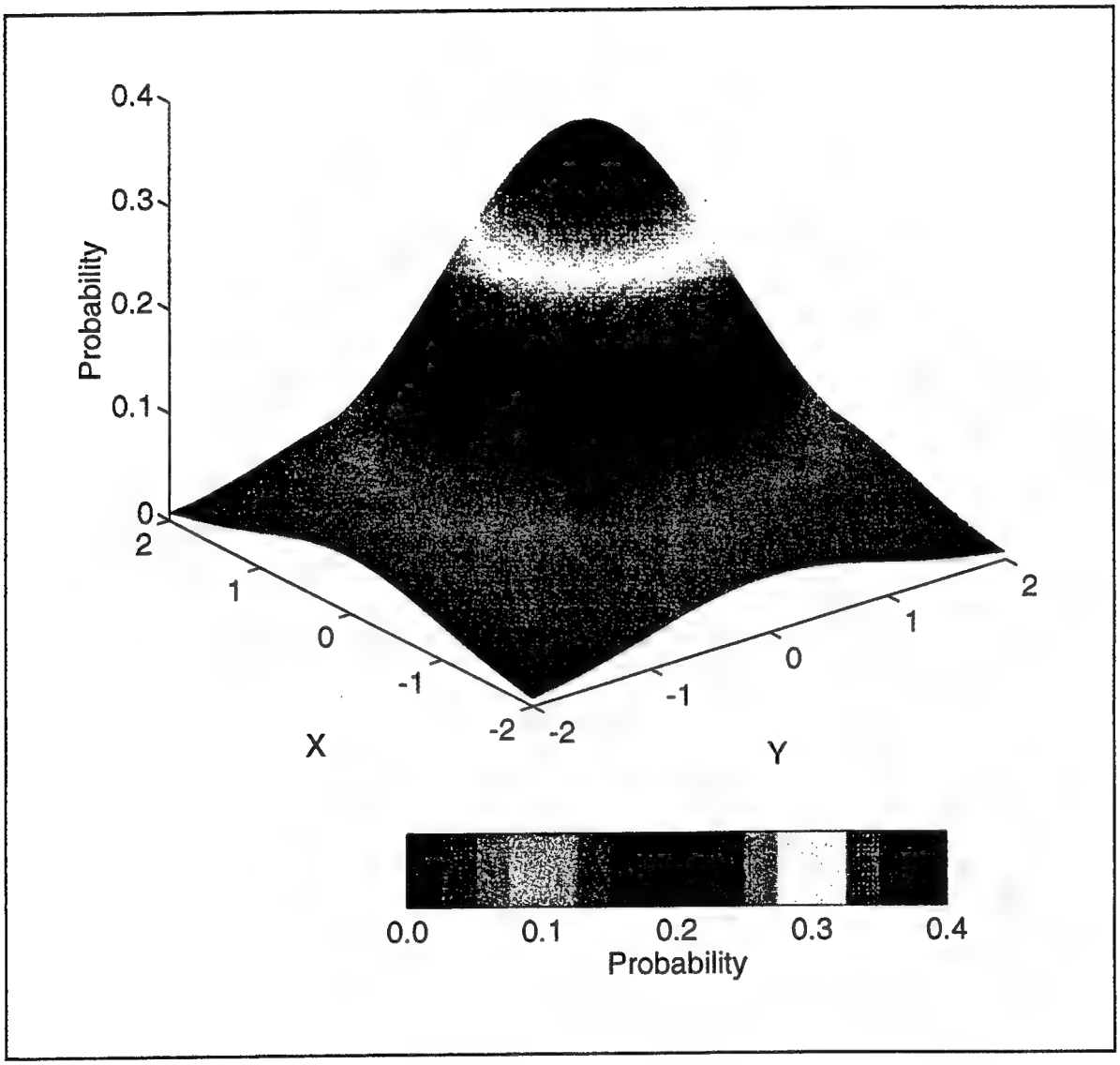

Figure 5-7. Circular Normal Probability Distribution for $\sigma = 1$

6.0 OA DERIVED VELOCITY FIELD

The objective analysis computer code discussed in Section 4 was used to generate surface current velocity field estimates for the dataset described in Section 5. The OA inputs used and the results are presented in Section 6.1

A numerical subsampling experiment conducted to examine the number of measurements required to represent the flow field in a typical SAR domain is described in Section 6.2.

6.1 OA USING COAST GUARD BUOY DATA

Input Parameters. The OA input parameters used with this dataset are presented in Table 6-1.

Table 6-1. OA Input Values

Program Parameter	Value	Description
IM	23	Number of grid points in the zonal direction
JM	23	Number of grid points in the meridional direction
DX	2.25 km	Zonal grid spacing (km)
DY	3.0 km	Meridional grid spacing (km)
CLNG	051 48W	Domain center longitude (dd.dd)
CLAT	47 30N	Domain center latitude (dd.dd)
XOFF	0.0 km	Zonal offset for the domain centroid
YOFF	0.0 km	Meridional offset for the domain centroid
THETAD	0.0 degrees	Domain rotation (counterclockwise from east)
NNCE	10	Number of influential points
RNCE	100.0 km	Radius of influence (km)
TNCE	1.0-3.0 days	Influential time window (days)
XZERO	80.0 km	Correlation, zonal zero crossing (km)
YZERO	80.0 km	Correlation, meridional zero crossing (km)
XDCAY	40.0 km	Zonal decorrelation (decay) scale (km)
YDCAY	40.0 km	Meridional decorrelation (decay) scale (km)
TDCAY	3.0 days	Temporal decorrelation (decay) scale (km)
UPHSE	0.0 m/s	Zonal phase speed
VPHSE	0.0 m/s	Meridional phase speed
OADAY	343.977083 344.961806 345.946528 346.861806	Solution time: 09 DEC 93, 23:27 10 DEC 93, 23:05 11 DEC 93, 22:43 12 DEC 93, 20:41

The domain centroid position was chosen to be near the center of the ocean region where most of the buoys drifted. The OA grid dimensions and spacing were also chosen to contain the region which was dense with the input data from the drifting buoys. The buoy track density is shown in Figure 6-1. Data with fix quality 0 are excluded from Figure 6-1. The grid covers an area of 3267 km^2. The OA region is a rectangle with center at 47 30N, 051 48W. The northern and southern edges are parallel to the equator; the offset point and domain rotation angle are all zero. Choice of the maximum number of influential points is determined by balancing the amount of computation required with the desired quality of output. Carter and Robinson (Reference [f]) state that using ten influential points is usually sufficient. The radius of influence was set to 100 km so that observations from the entire input dataset would be eligible to contribute to the velocity estimate at each grid point. This maximizes the amount of data available for use in computing the flow field. The influential time window was varied between one and three days to demonstrate the effect of accumulation of input data.

The zero crossing and decorrelation scales are chosen based on prior knowledge of the specific ocean region. They are related to a quantity known as the Rossby radius. The Rossby radius varies with location and, in general, is the distance at which the earth's gravitational forces balance with its rotational forces. For the North Atlantic ocean near the location of the objective analysis region, the Rossby radius is 40 km. The zero crossing distance was chosen to be two Rossby radii. The temporal decay scale was chosen by examining the current meter dataset from the MINIMET buoy. The dominant time scale of current activity was estimated to be between one and three days; thus, the temporal decay scale was chosen to be three days. Examining the derived velocities of the drifting buoys, no long term prevalent motion of the buoys was seen; accordingly, the phase velocities of the region were set to zero.

Times for which the velocity fields were computed was varied from Julian days 343 to 346 (corresponding to 09-12 DEC 1993) to correspond with the time period in which buoys were deployed.

Those fixes with an Argos fix quality equal to zero were not used. Additional data with fix quality greater than zero was omitted if there were multiple fixes of a buoy obtained during a single Argos pass, or if the Argos fix was inconsistent with the surrounding fixes. Data not used in the OA is noted in Table 5-1, with "*" indicating a multiple fix and "**" indicating inconsistent data.

Figure 6-2 presents a graph of the correlation function using the appropriate values from Table 6-1.

OA Output. Time dependent OA estimates were performed for the four day period 09 - 12 DEC during which six buoys were simultaneously deployed in a 27.0 nm x 35.6 nm region.

The nature of the prevalent flow fluctuated throughout this time period. We accordingly examined sensitivity to the influential time window by performing OA estimates with an influential time window of one, two, and three days. The solution time used for each estimate was the latest ARGOS fix time of all buoys on the given day. All data from time 090000Z DEC 93 to the solution time was available for an OA estimate. The actual amount of data considered was determined by the influential time window. The solution times are given in Table 6-2.

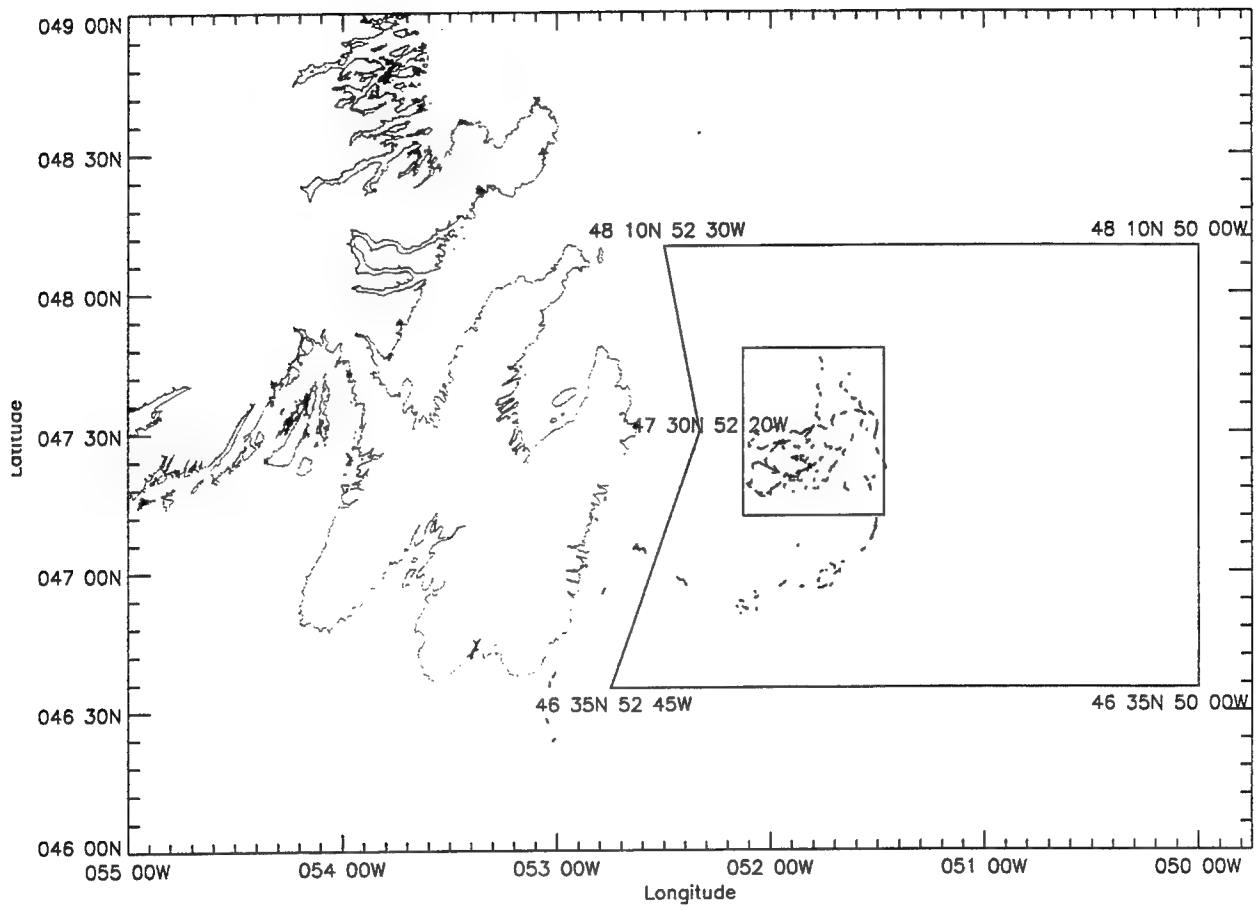

Figure 6-1. Buoy Track Density

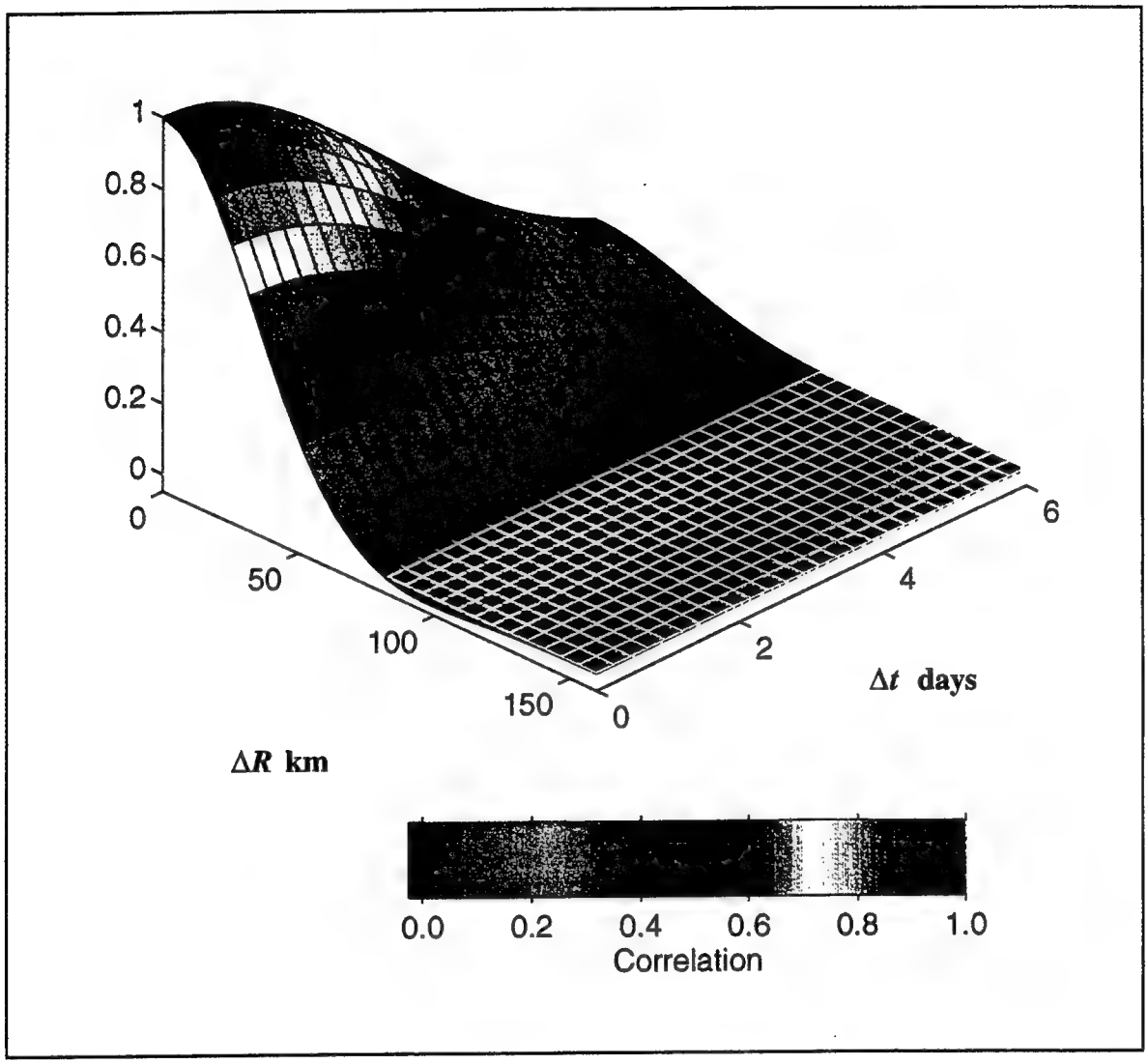

Figure 6-2. Correlation Function for Example OA

Table 6-2. OA Solution Times

Day	Solution Time (hh:mm)
09 DEC 93	23:27
10 DEC 93	23:05
11 DEC 93	22:43
12 DEC 93	20:41

Because no buoy data prior to 09 DEC 93 was used, we did not calculate an OA estimate with the two day influential time window on day 09 DEC. Similarly, we did not calculate an OA estimate with the three day influential time window on the days 09 DEC and 10 DEC.

Figures 6-3 through 6-20 are plots of the OA velocity field estimates. Each estimate is displayed in two plots. The first type of plot (e.g. Figure 6-3) is the velocity field overlaid on the absolute velocity error field which is shown in color. This plot includes the last position of each buoy, plotted as red asterisks, prior to the solution time.

The second type of plot (e.g. Figure 6-4) presents the same velocity field without the error field and the last velocity estimate for each buoy prior to the solution time. These velocities are plotted as either red or blue vectors. The vector is red if the velocity observation is within four hours of the solution time, otherwise it is blue. The MINIMET S4 current data was available for the days 09 DEC 93 and 10 DEC 93. The MINIMET current estimate is plotted as a green vector for those days when it was available. This estimate is an average of the MINIMET current readings immediately prior to and after the solution time.

A buoy velocity estimate requires using two Argos fixes. The buoy data plotted in Figures 6-3 through 6-20 are based on the last two fixes before the solution time. The distance between these fix positions and the time between them determine a mean velocity during this period. The first plot, described above, displays the buoy position at the last fix. This is the last geographical position of the buoy prior to the solution time. The second plot displays the buoy velocity at the next-to-last fix and is the last velocity used in the OA.

The buoy positions prior to the solution time plotted in the figures indicate where the latest data is located that was used for the OA estimate. The OA estimates show lower uncertainty in the vicinity of this data and higher uncertainty in regions away from the data. The influence of an observation decays with distance and larger uncertainty occurs as estimates are extrapolated from the observed data.

The last velocity estimate of each buoy prior to the solution time plotted in the figures indicates the latest velocity which was used in the OA estimate. The influence of an observation decays in time, and the older data plotted in blue will have less influence than those plotted in red. Some

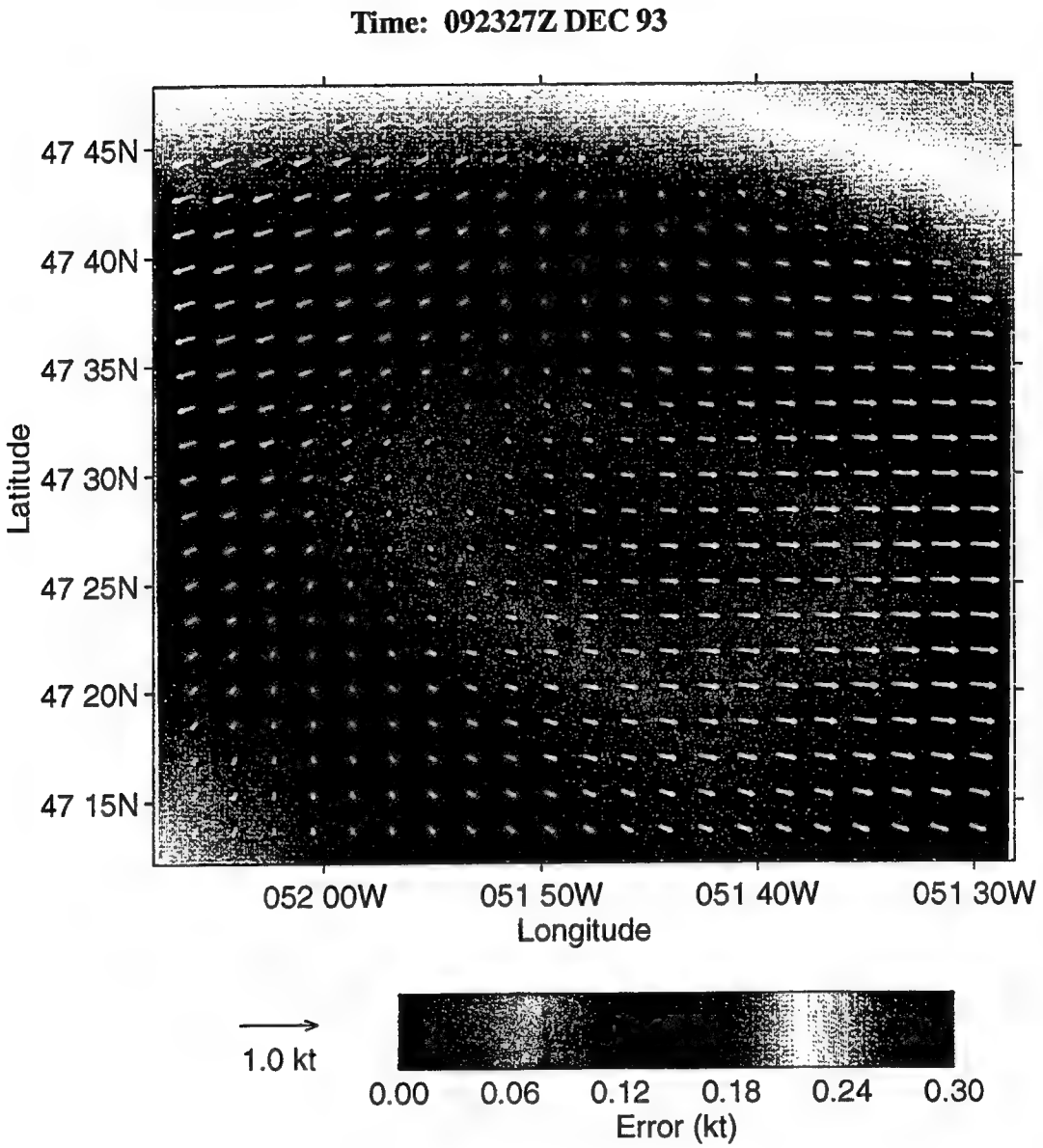

Figure 6-3. OA Velocity Field and Error Field Using a 1 Day Influential Time Window

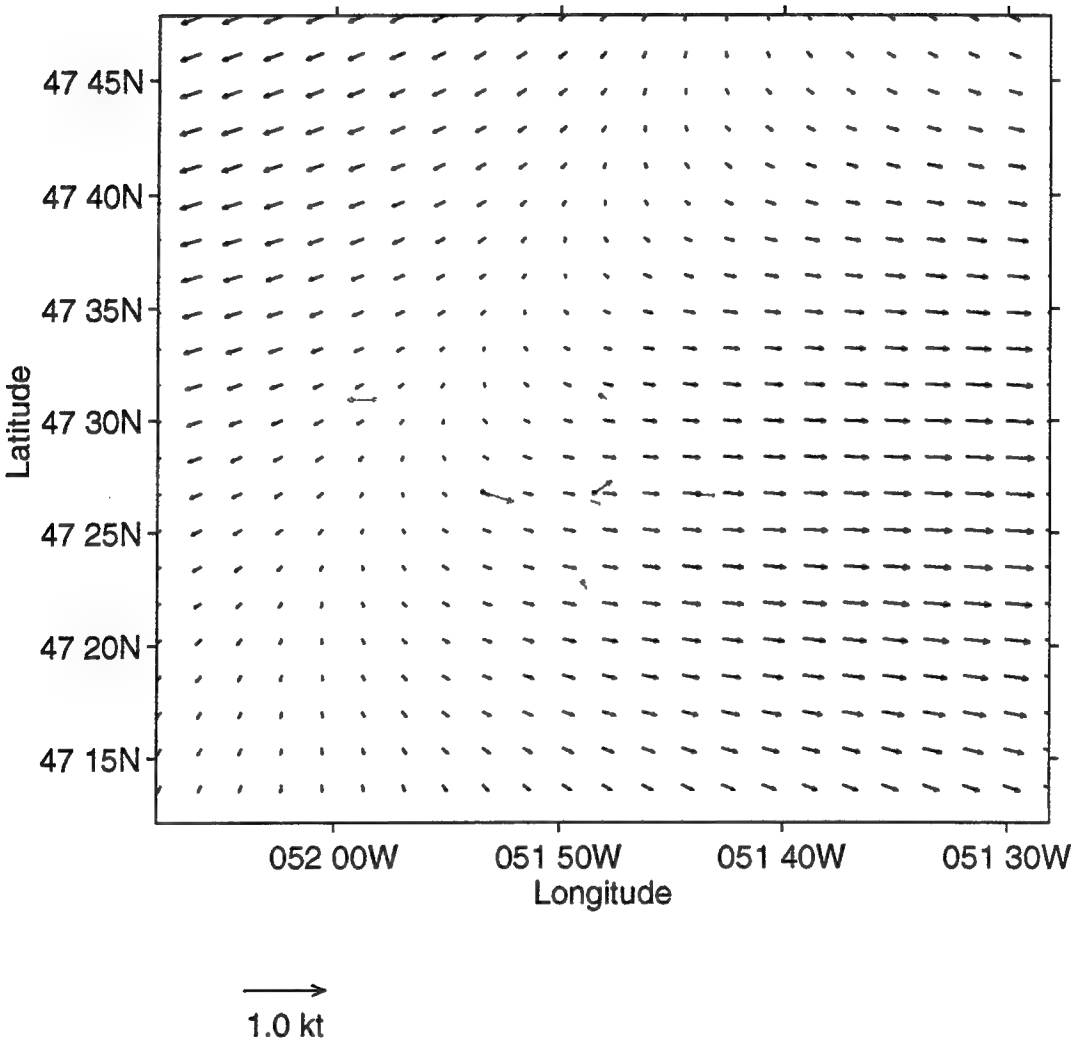

Figure 6-4. OA Velocity Field Using a 1 Day Influential Time Window

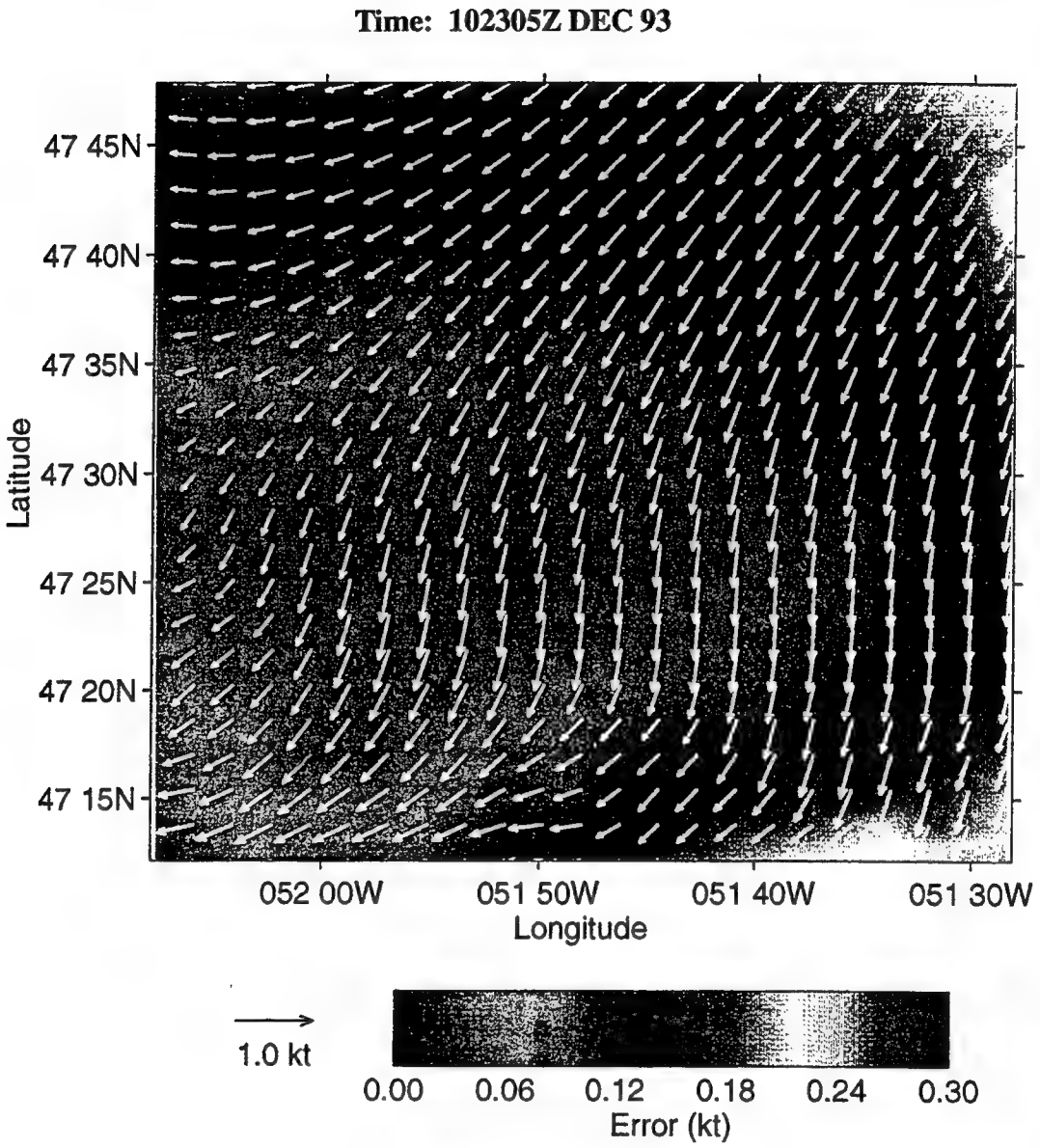

Figure 6-5. OA Velocity Field and Error Field Using a 1 Day Influential Time Window

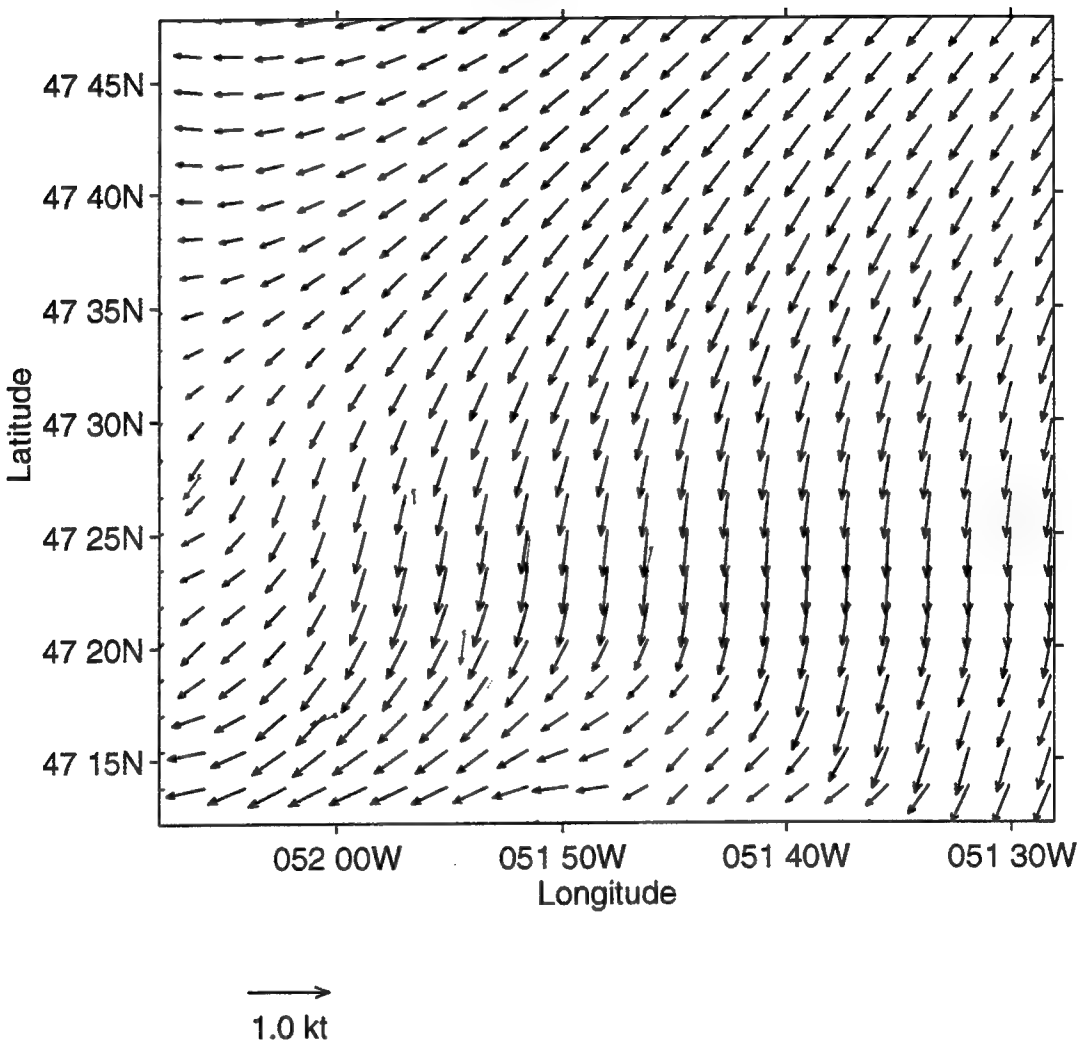

Figure 6-6. OA Velocity Field Using a 1 Day Influential Time Window

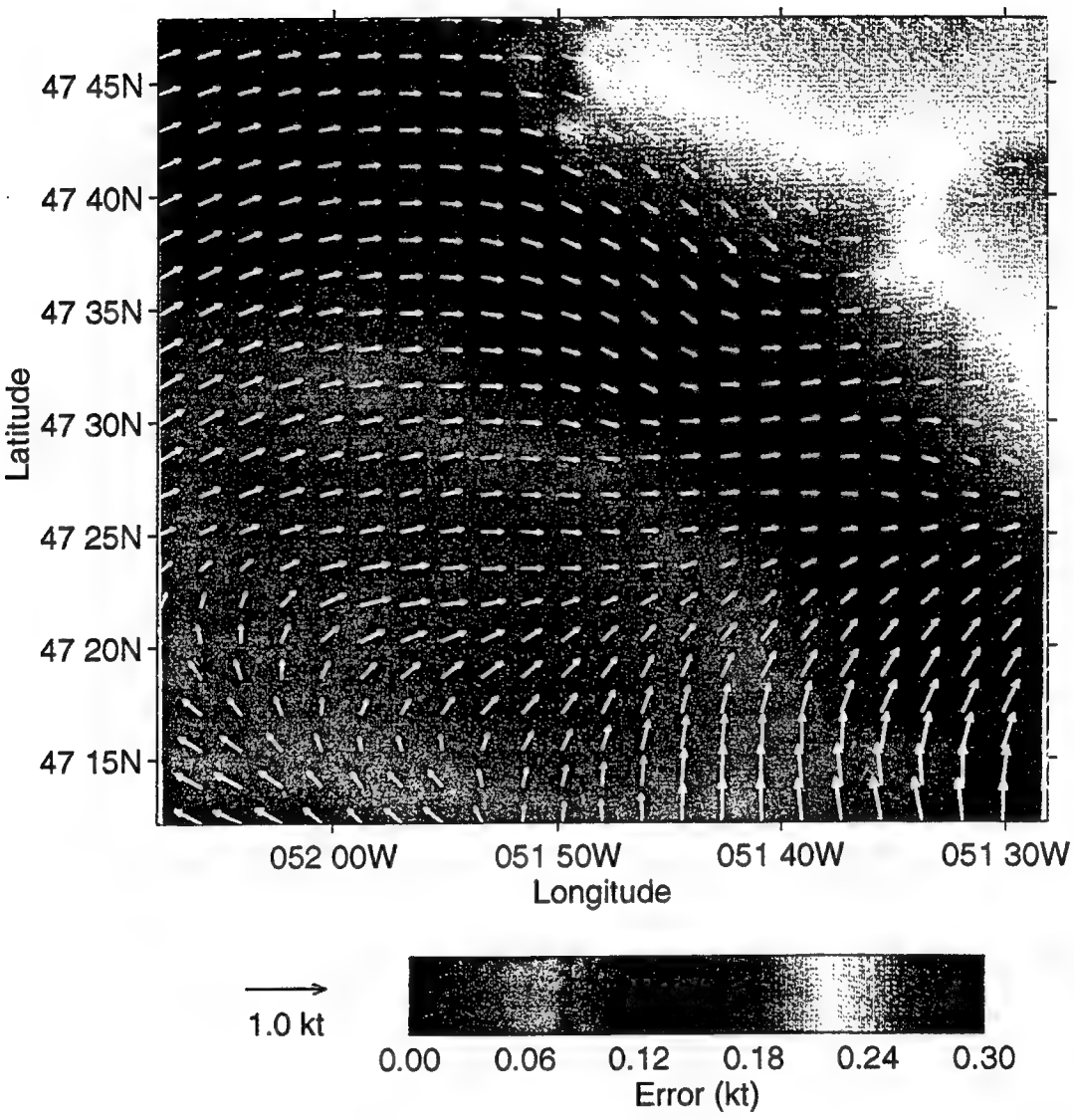

Figure 6-7. OA Velocity Field and Error Field Using a 1 Day Influential Time Window

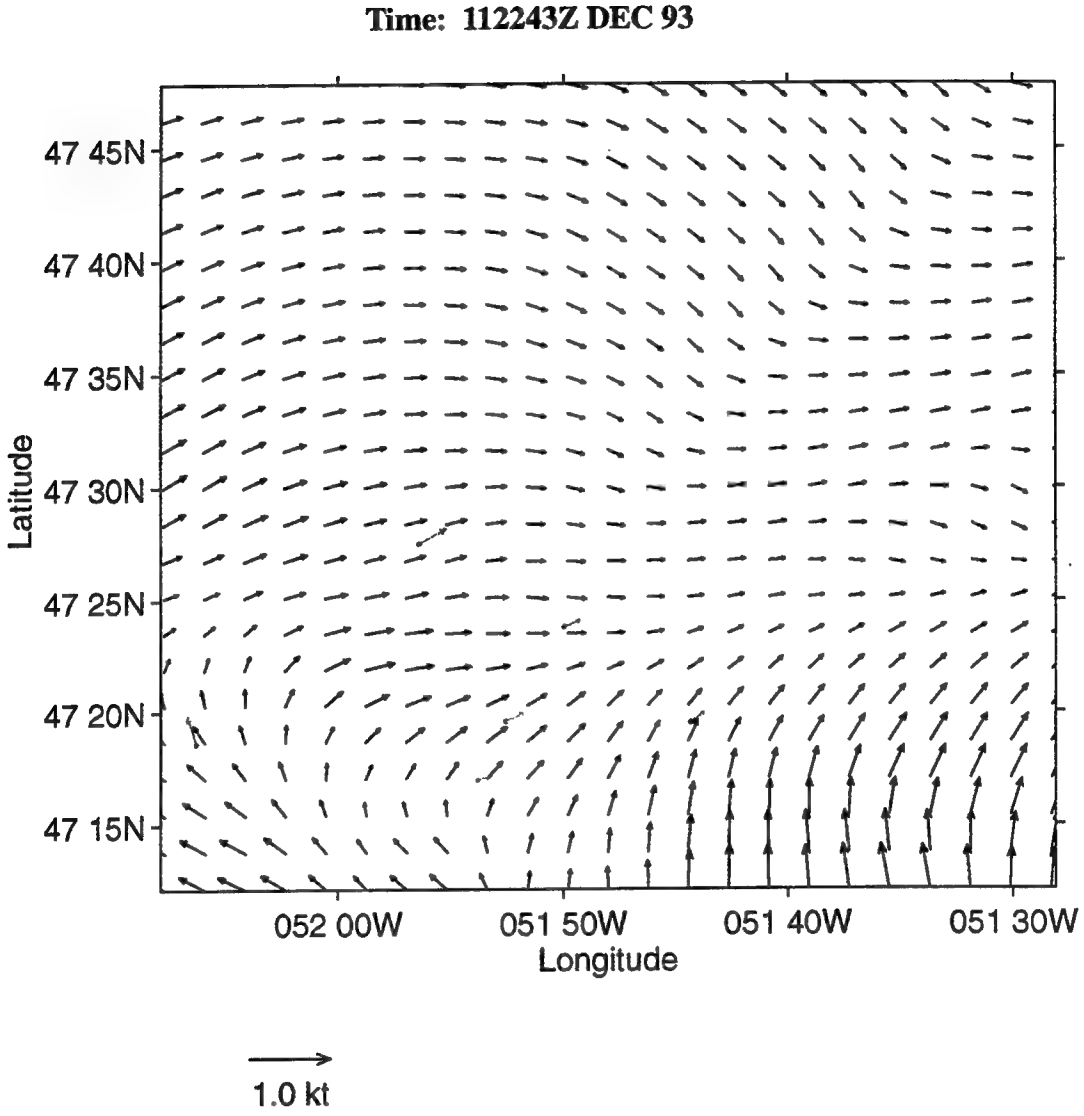

Figure 6-8. OA Velocity Field Using a 1 Day Influential Time Window

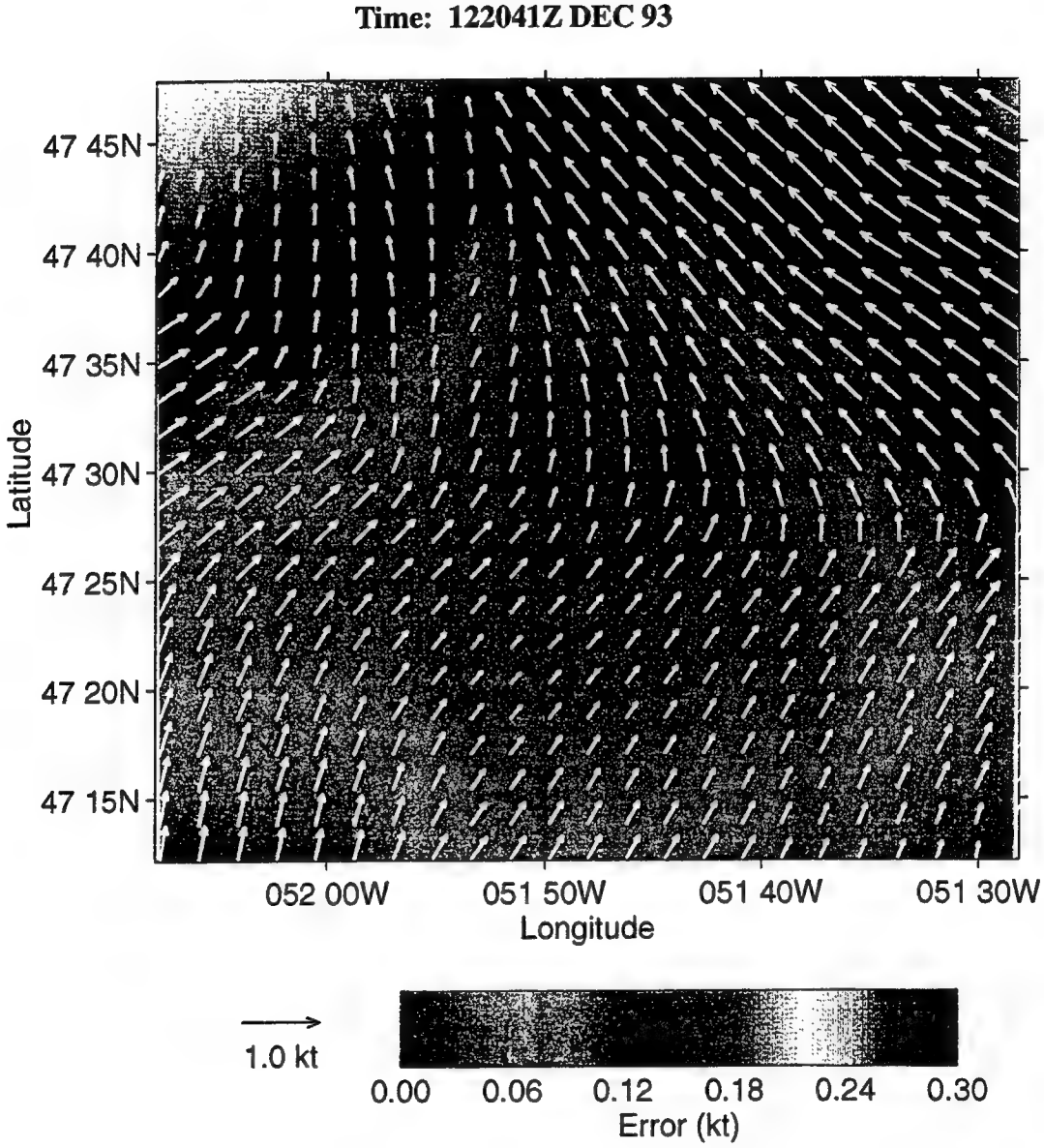

Figure 6-9. OA Velocity Field and Error Field Using a 1 Day Influential Time Window

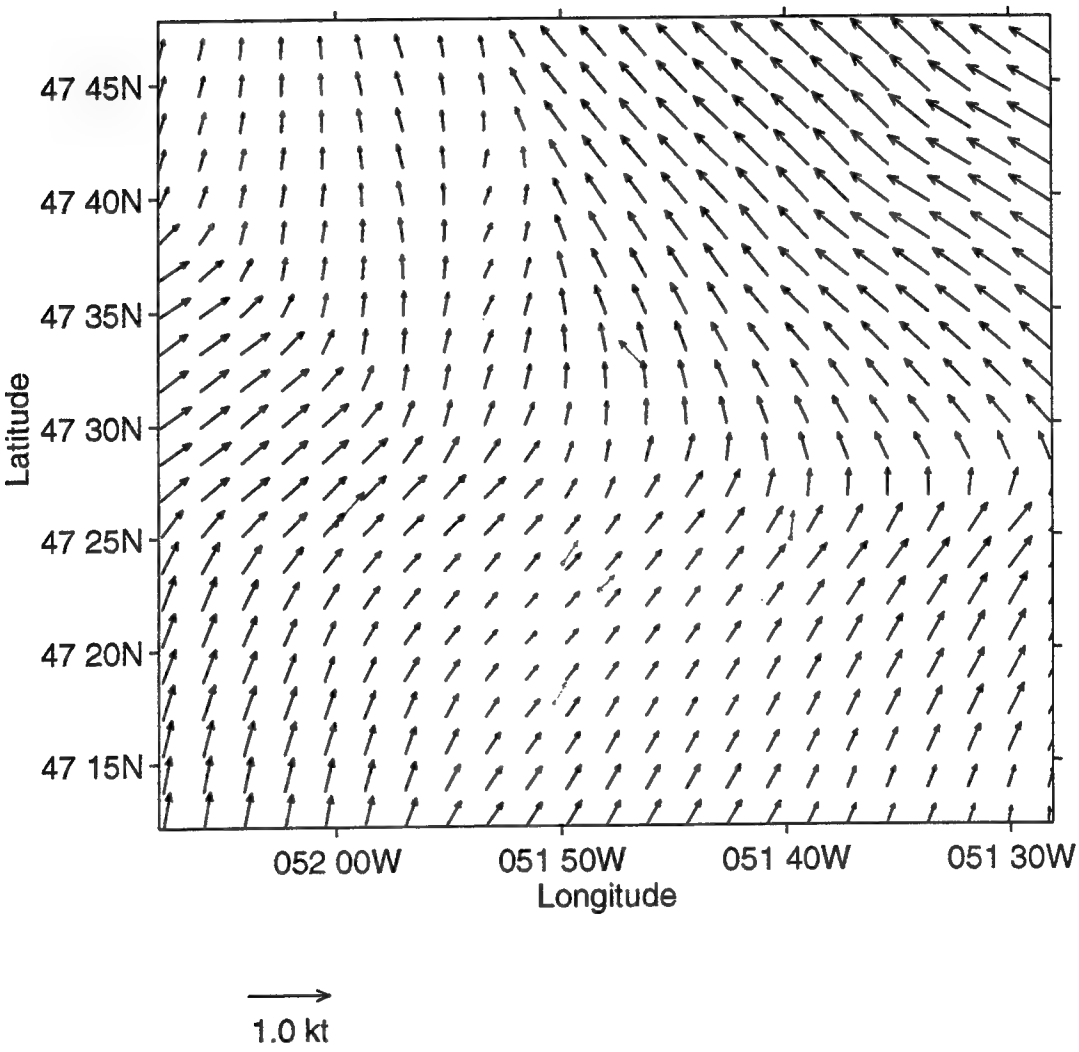

Figure 6-10. OA Velocity Field Using a 1 Day Influential Time Window

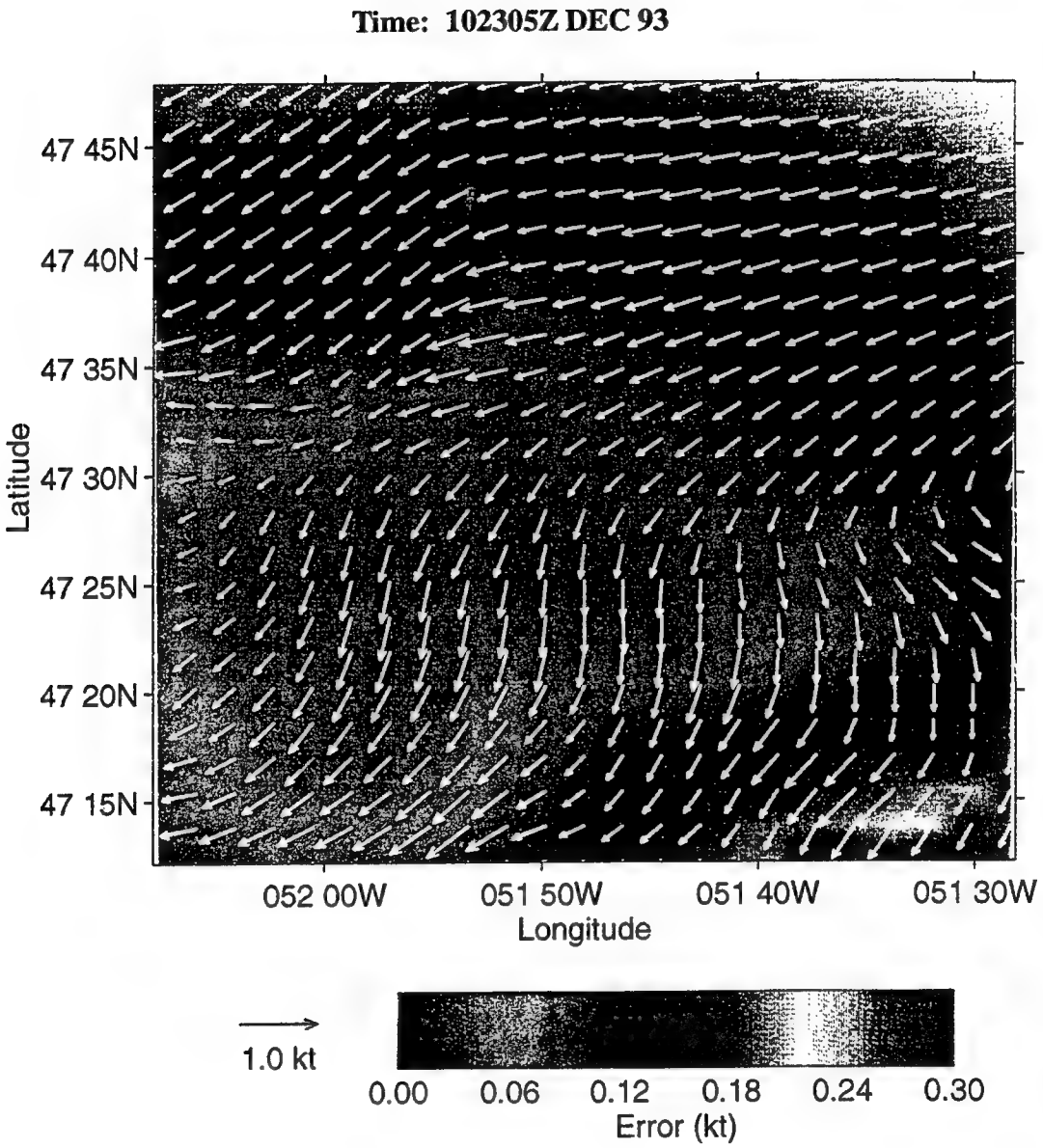

Figure 6-11. OA Velocity Field and Error Field Using a 2 Day Influential Time Window

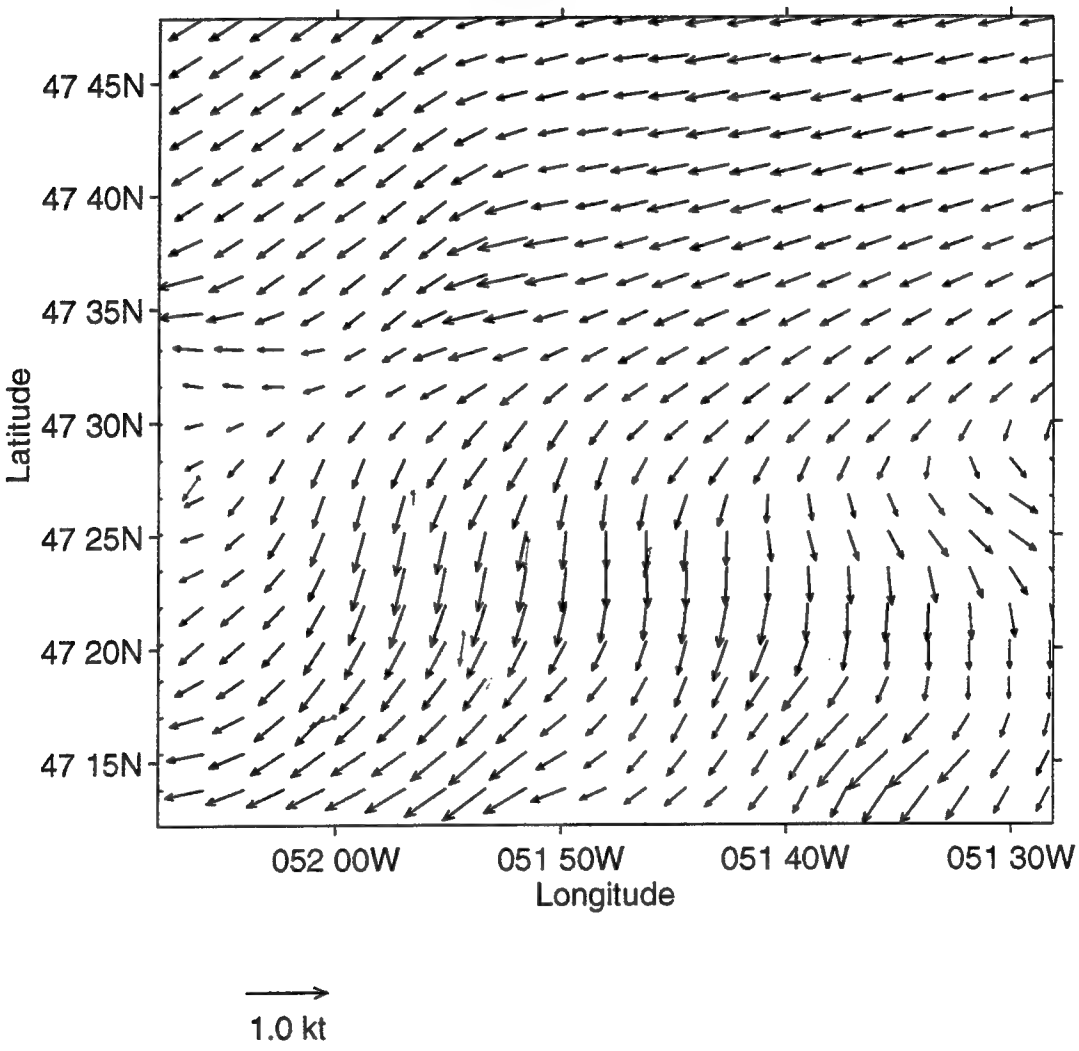

Figure 6-12. OA Velocity Field Using a 2 Day Influential Time Window

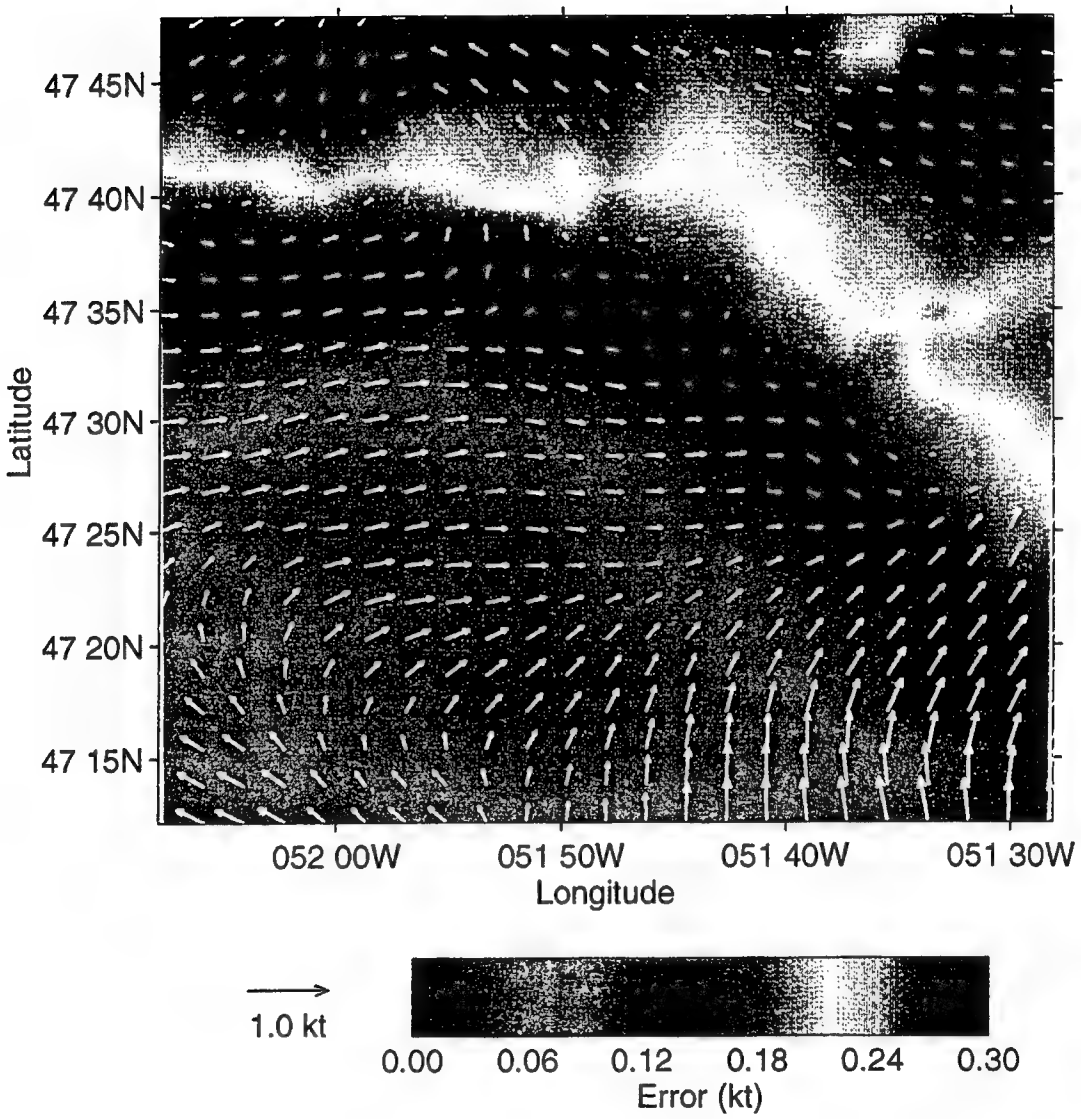

Figure 6-13. OA Velocity Field and Error Field Using a 2 Day Influential Time Window

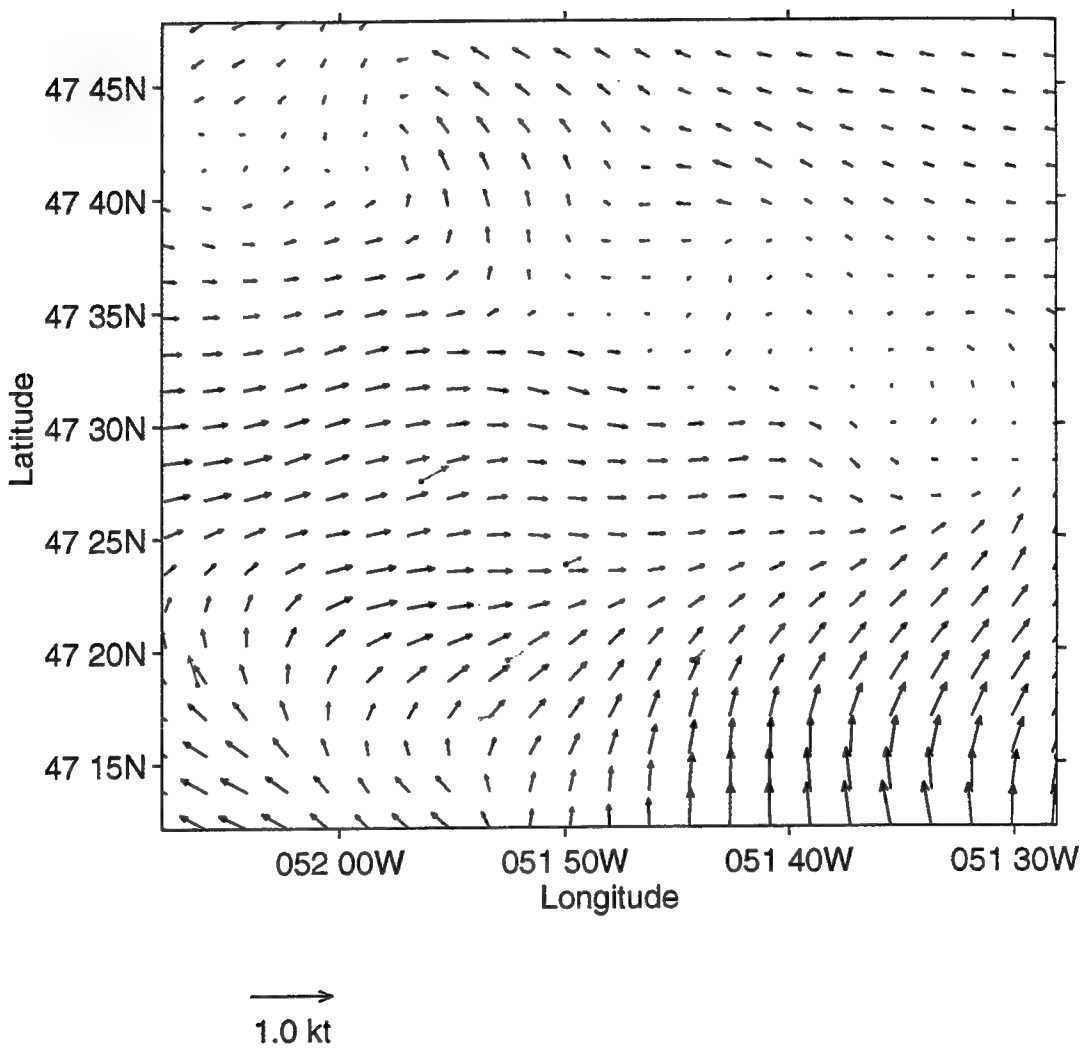

Figure 6-14. OA Velocity Field Using a 2 Day Influential Time Window

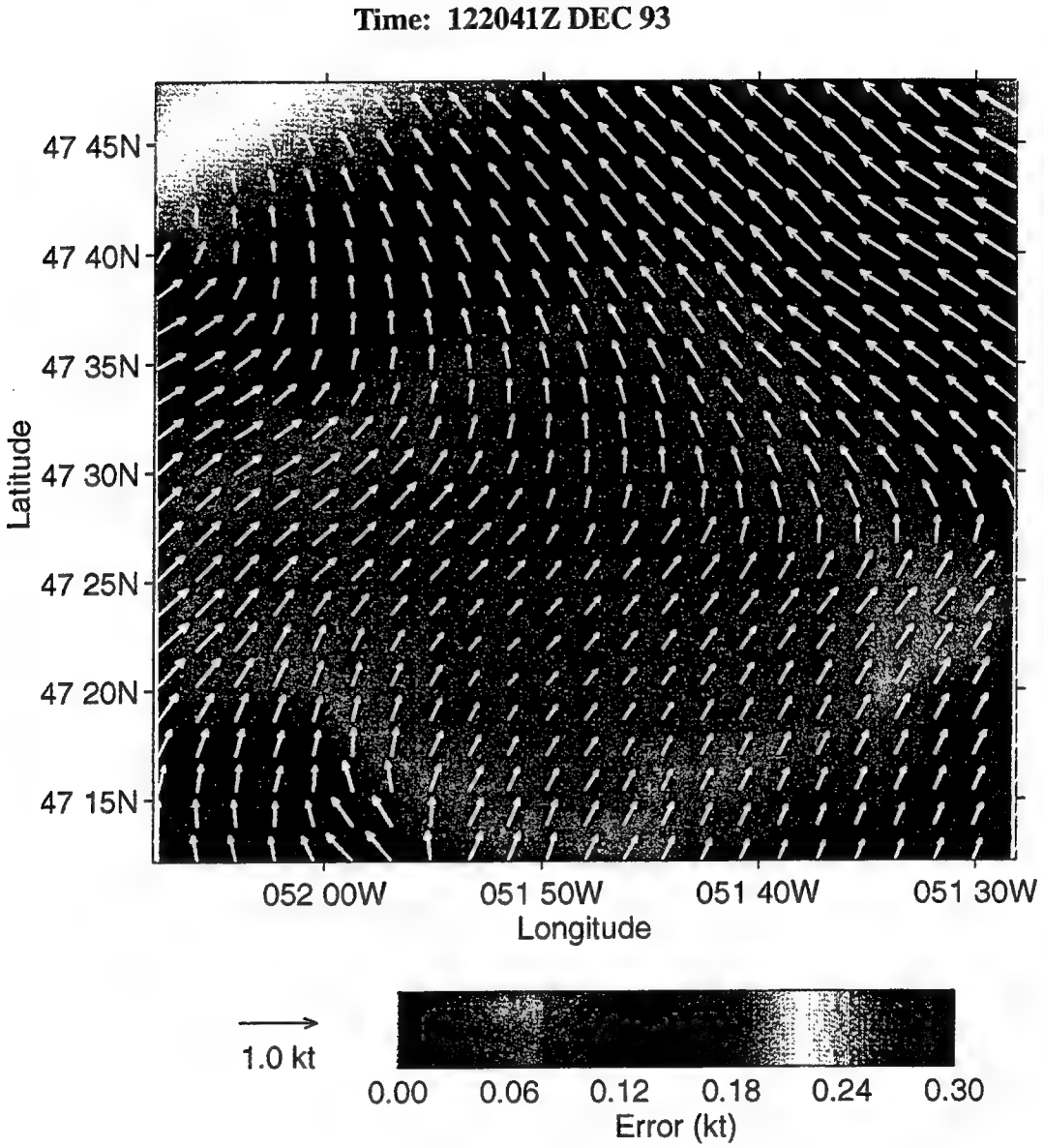

Figure 6-15. OA Velocity Field and Error Field Using a 2 Day Influential Time Window

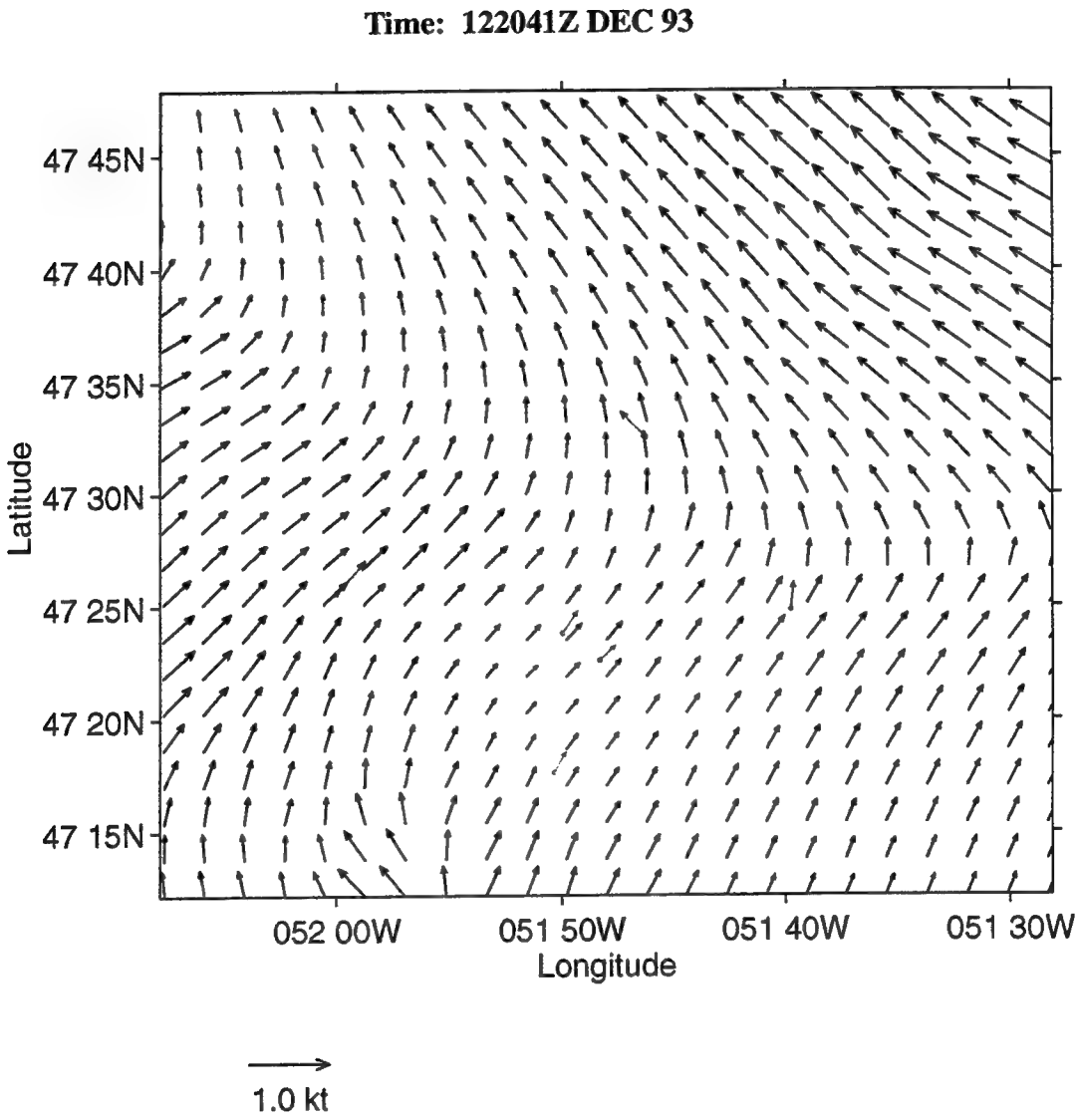

Figure 6-16. OA Velocity Field Using a 2 Day Influential Time Window

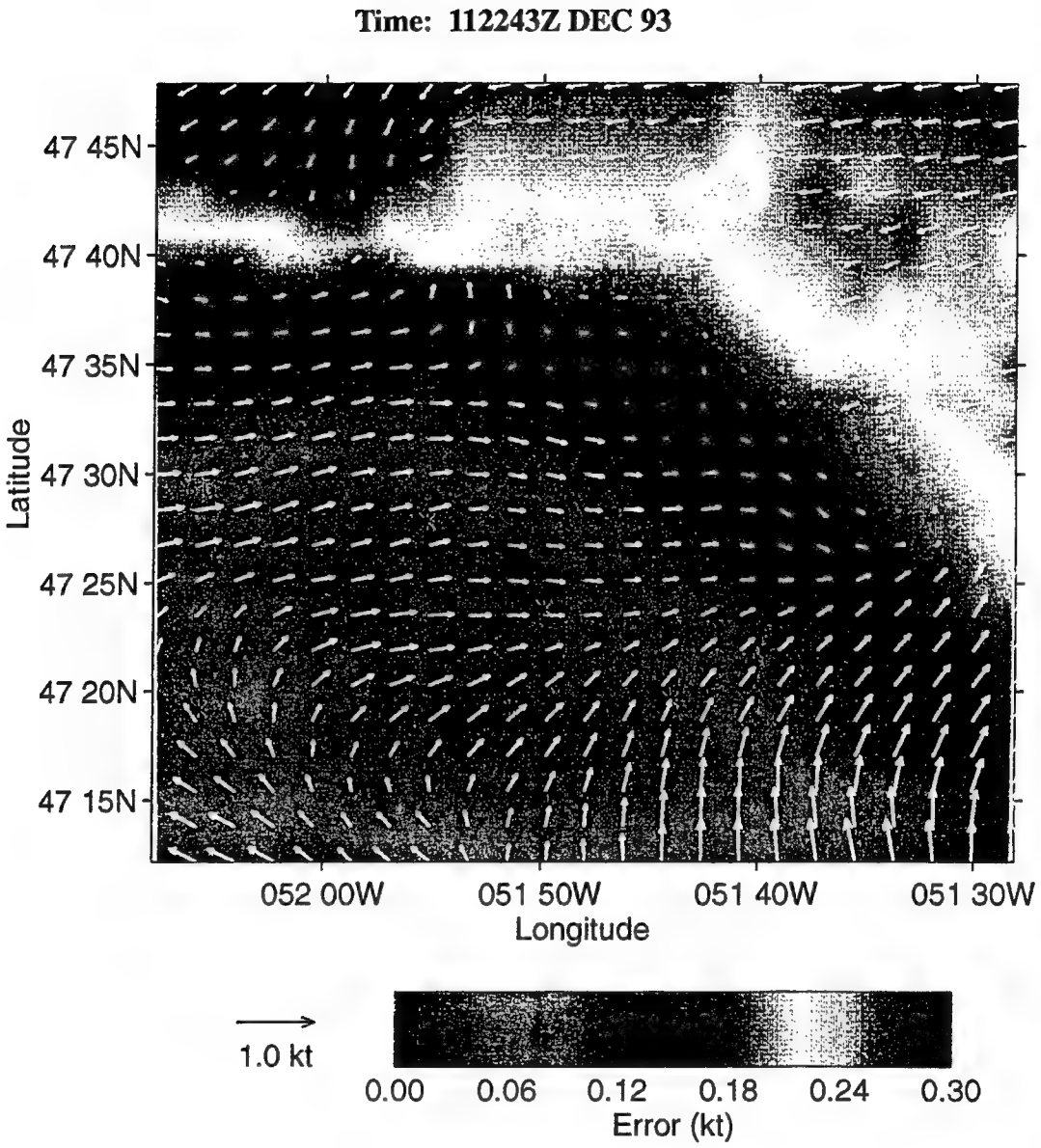

Figure 6-17. OA Velocity Field and Error Field Using a 3 Day Influential Time Window

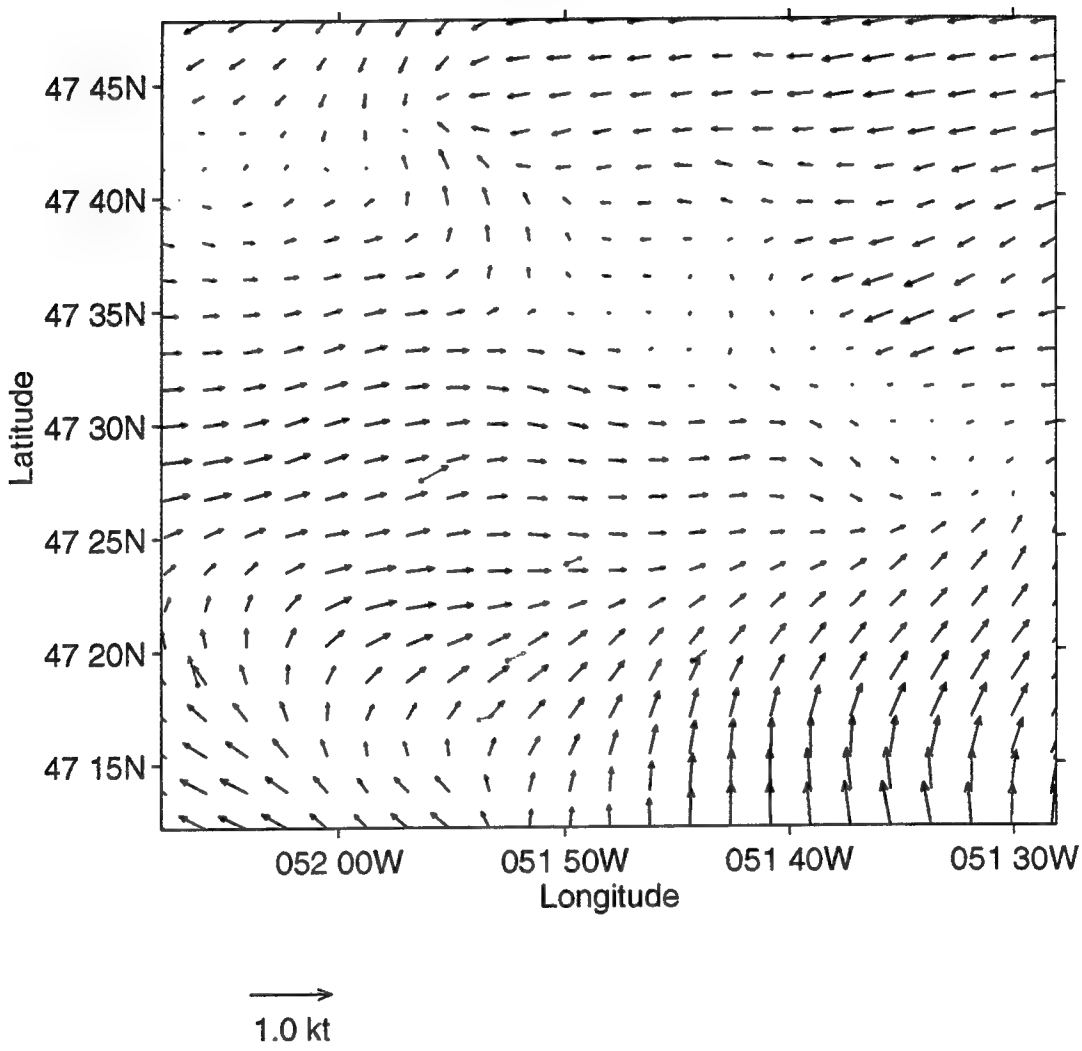

Figure 6-18. OA Velocity Field Using a 3 Day Influential Time Window

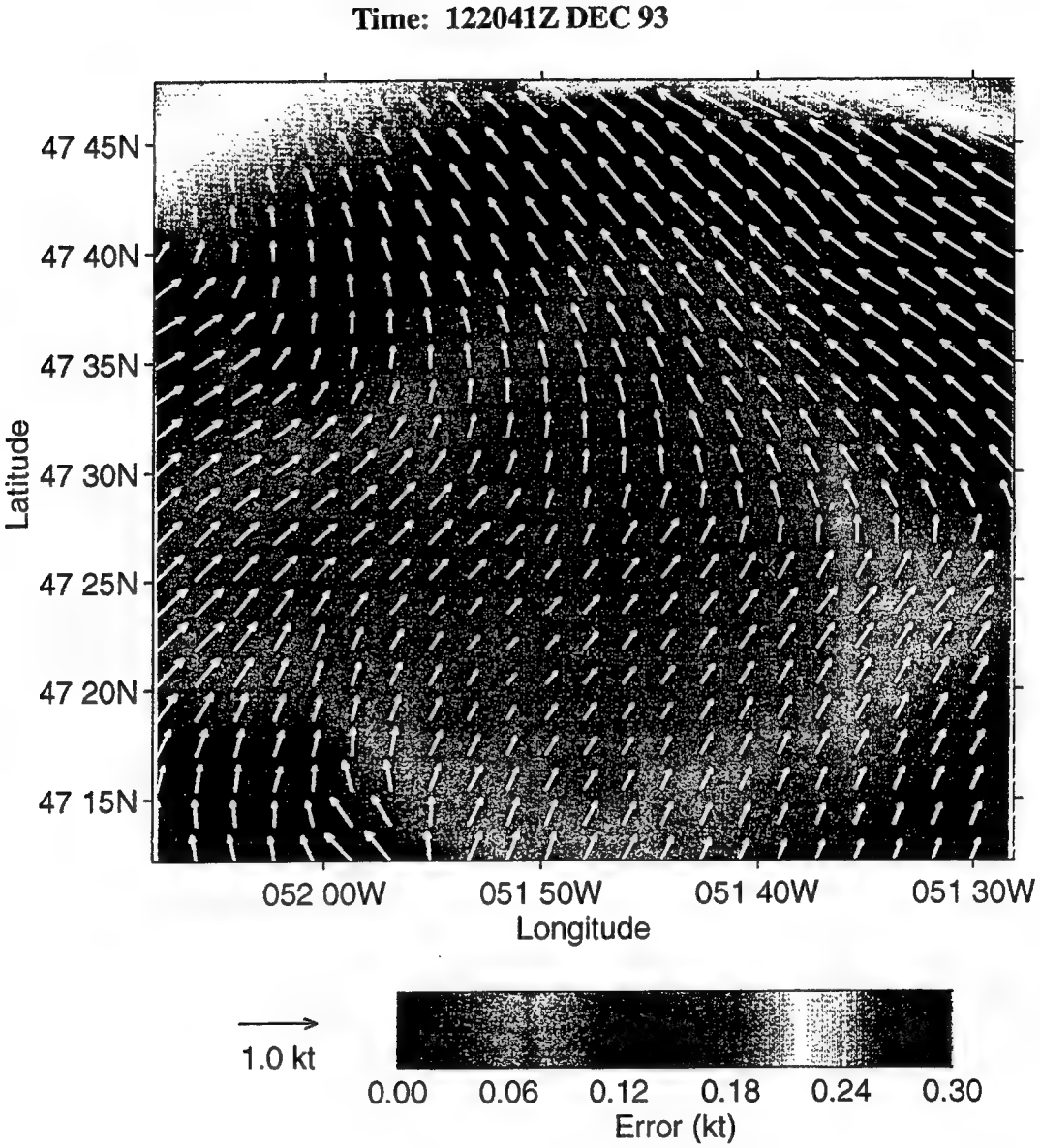

Figure 6-19. OA Velocity Field and Error Field Using a 3 Day Influential Time Window

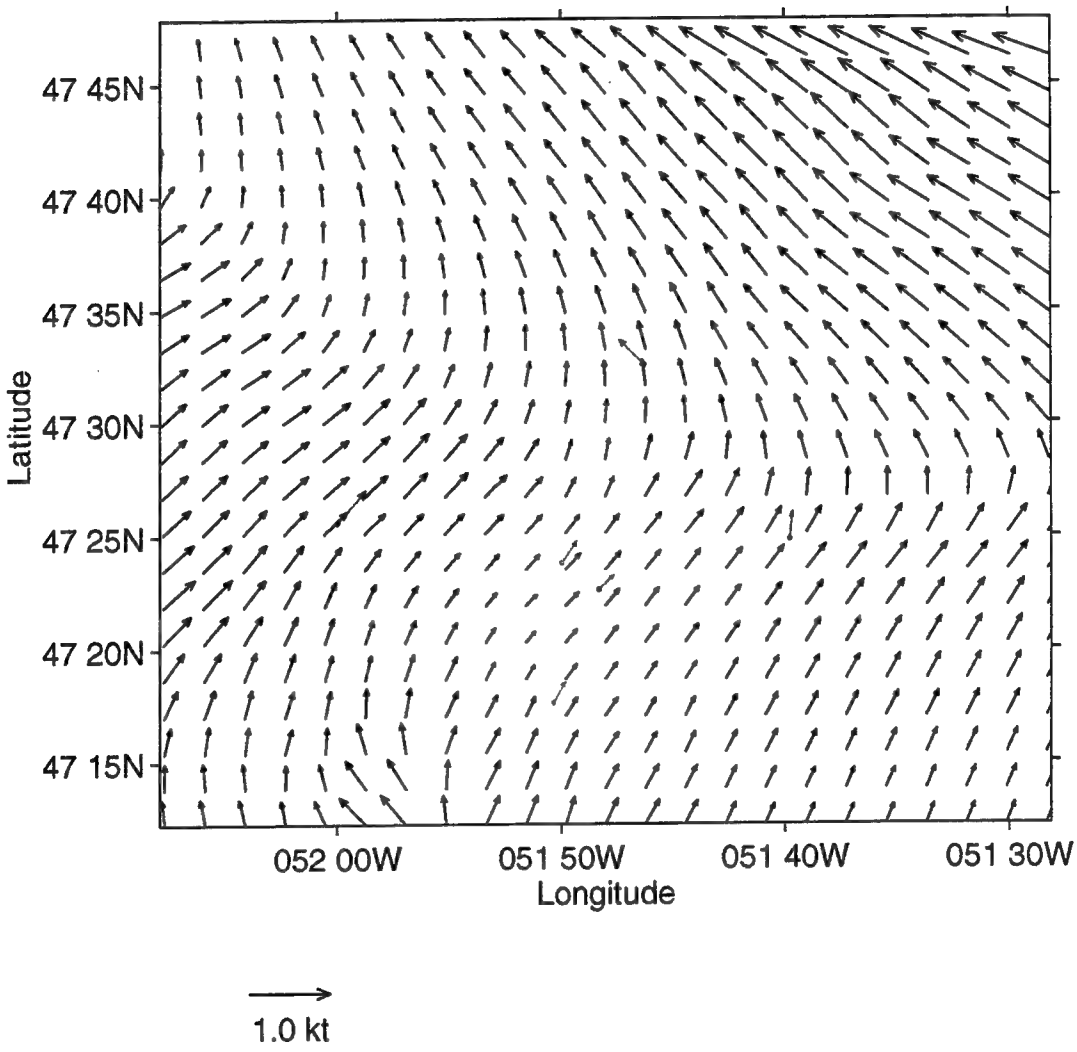

Figure 6-20. OA Velocity Field Using a 3 Day Influential Time Window

variations between the latest buoy velocity prior to the solution time and the estimated velocity field should be expected.

The flow in this region changes significantly from day to day. The predominate flow in the region on 09 DEC is eastward and changes direction to southwestward on 10 DEC. This flow then changes to northeastward on 11 DEC, and is northward on 12 DEC. The one day influential time window plots are shown in Figures 6-3 through 6-10. The two day plots are shown in Figures 6-11 through 6-16, and the three day plots are shown in Figures 6-17 and 6-20. The sensitivity to the influential time window can be seen in the two and three day plots on days 10 DEC and 11 DEC. These velocity estimates contain converging and diverging regions of flow. Such regions are not part of the flow field but are irregularities due to the inclusion of conflicting data in the OA estimate. However, on 12 DEC the two and three day estimates show more realistic fields than the one day estimate.

This analysis demonstrates that the choice of influential time window is an important parameter for this region where the flow field is evolving on scales from one to three days. It is important to note that this is particularly an issue when data is extrapolated from the region containing buoy data. The one, two and three day plots show small differences in the vicinity of the buoys. However, as data is extrapolated from this area, the estimated velocity fields exhibit greater differences.

6.2 SUBSAMPLING EXPERIMENT

A subsampling experiment, using objective analysis, was conducted in order to examine the number of measurements required to represent the prevalent flow field in a typical SAR domain.

A test case domain was selected which is 110 km by 110 km and centered at 69.5°W, 38.5°N. With a resolution of 5 km this domain has 23×23 grid points. The location of this domain is shown in Figure 6-21 with respect to the Harvard Forecast domain (GULFCAST) and Coast Guard District 1.

The BioSynop experiment was carried out during Oct - Nov 1988 in a somewhat larger domain (600×300 km). The BioSynop domain is marked as B and the test domain is marked as T in Figure 6-21. From the hydrographic dataset of temperature and salinity, the dynamic height field is obtained, which is then objectively analyzed for the test domain. The geostrophic velocity components are then obtained as the spatial gradients of the streamfunction field (which is proportional to the dynamic height). The temperature and salinity OAs are shown in Figures 6-22a and 6-22b. The dynamic height OA is shown in Figure 6-22c. The OA input values are shown in Table 6-3. The u and v components are shown as contour plots in Figures 6-23a and 6-23b. The derived vector velocity field is shown in Figure 6-23c.

The major oceanographic feature in this domain is a cold cyclonic patch of water in the mid-eastern region of the domain. This domain is situated just north of the Gulf Stream, in the surrounding recirculation region, generally known as the Slopewater Gyre. The circulation in this region

is a mesoscale eddy field interacting transportationwise with the Gulf Stream through sub-basin scale interactions (Reference [g]).

A subsampling experiment was carried out using this dataset in the test domain starting from the objectively analyzed field shown in Figure 6-23c. This 23 × 23 5 km resolution field is subsampled at varying resolutions from 10 to 50 km. The resulting fields at these different resolutions are objectively analyzed on the original 5 km, 23 × 23 grid.

The vector OA fields for resolutions 10, 20, 35, and 50 km are shown in Figures 6-24a, 6-25a, 6-26a, and 6-27a, respectively. The difference vector fields, shown in Figures 6-24b, 6-25b, 6-26b, and 6-27b, present their respective differences from the original vector field (Figure 6-23c). Note that the difference vectors increase with increasing grid resolution.

The root mean square (rms) difference error vs. resolution is shown in Figure 6-28. The rms error is seen to be only 1 cm/sec for this field which has a range of velocity magnitude between ±30 cm/sec up to the resolution of 35 km, beyond which the rms error rises to 5 - 10% of the maximum velocity magnitudes.

These subsampling results are encouraging. Even with just sixteen (4 × 4) data points for the 35 km resolution in the SAR domain (110 × 110 km), the OA field (Figure 6-26a) depicts most of the oceanographic features as seen by very high resolution sampling (Figure 6-23c). This analysis suggest a buoy deployment of (4 × 4) or even a strategically placed (3 × 3) array for a 110 × 110 km SAR region with a 35 km resolution would suffice to map this region using objective analysis.

Table 6-3. OA Input Values for Subsampling Experiment

Values	Description
69.5 W	Domain center longitude (dd.dd)
38.5 E	Domain center latitude (dd.dd)
5	Zonal grid spacing (km)
5	Meridional grid spacing (km)
80.0	Correlation, zonal zero crossing (km)
80.0	Correlation, meridional zero crossing (km)
40.0	Zonal decorrelation (decay) scale (km)
40.0	Meridional decorrelation (decay) scale (km)
7	Temporal decorrelation (decay) scale (days)
10	Number of influential points
200	Radius of influence (km)
7	Influential time window (days)
266	Solution day

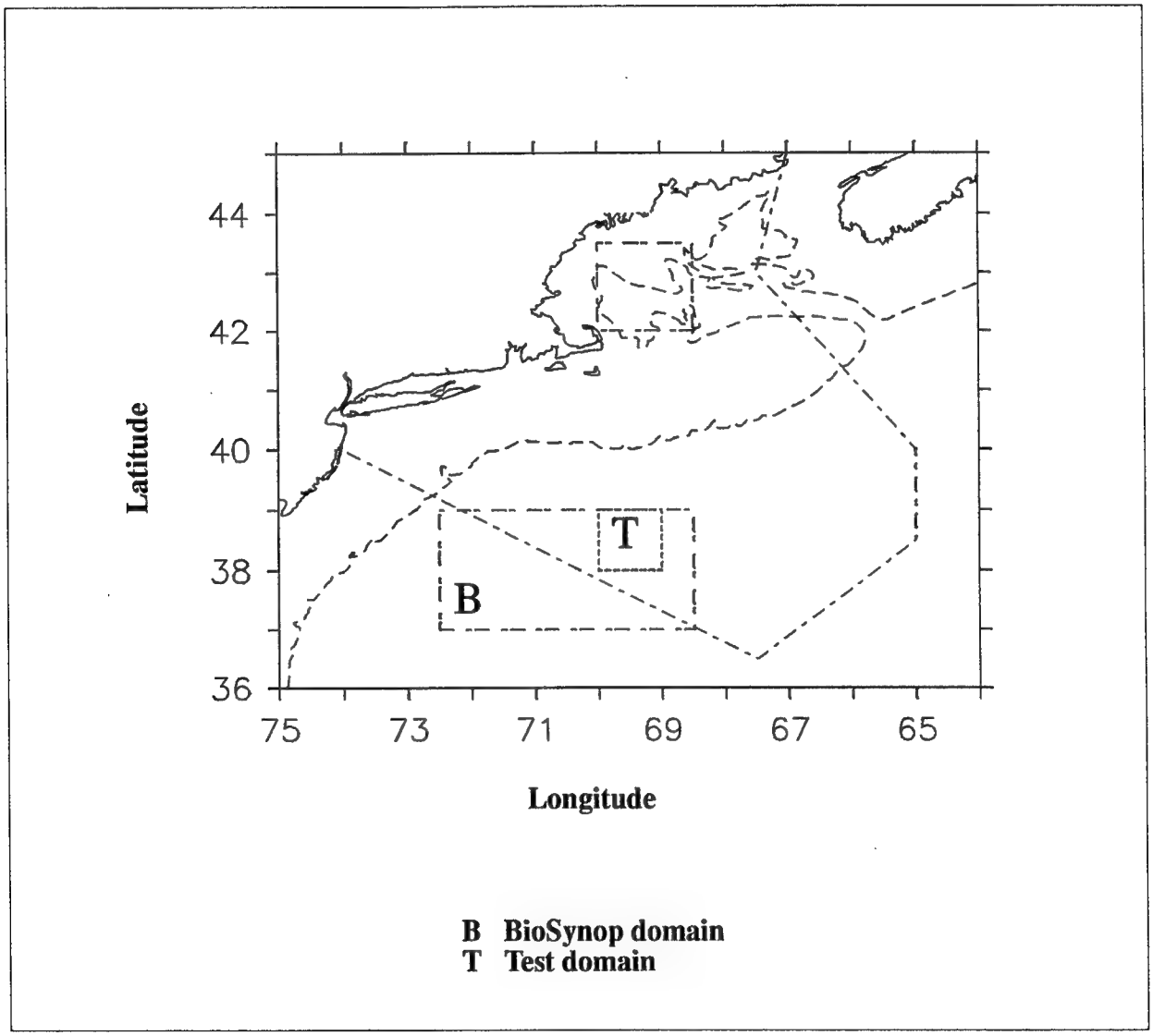

Figure 6-21. BioSynop and Subsampling Test Domain

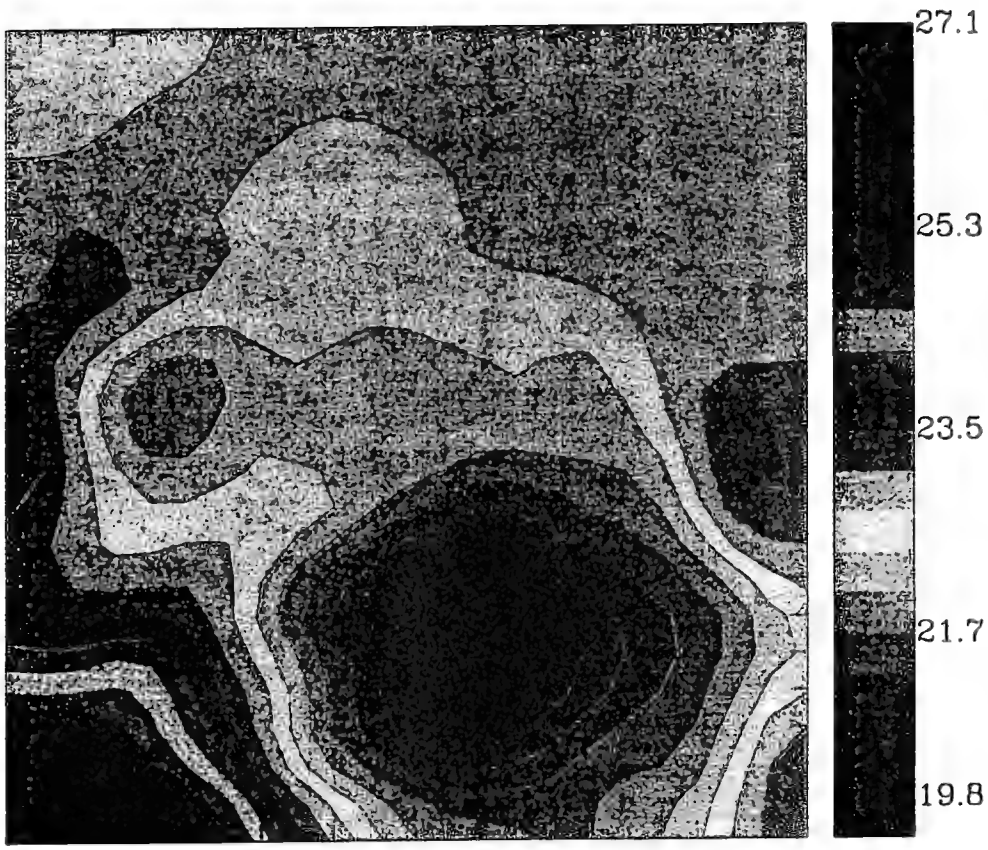

Figure 6-22a. Temperature OA Map

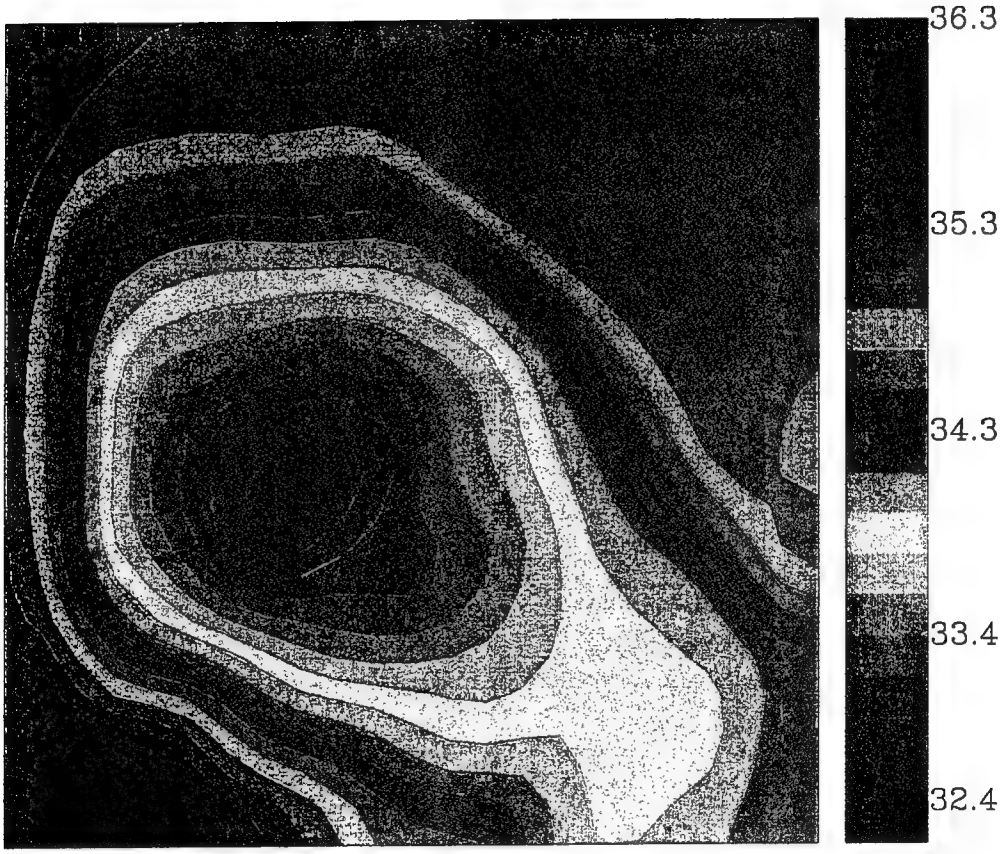

Figure 6-22b. Salinity OA Map

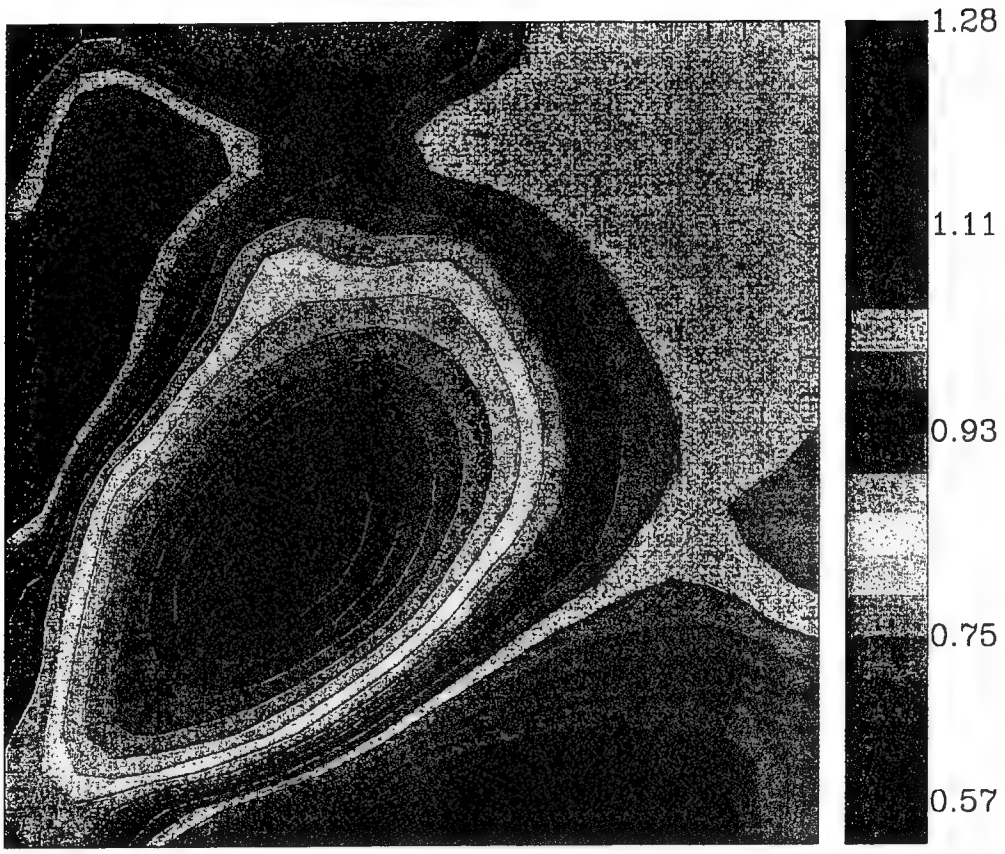

Figure 6-22c. Dynamic Height OA Map

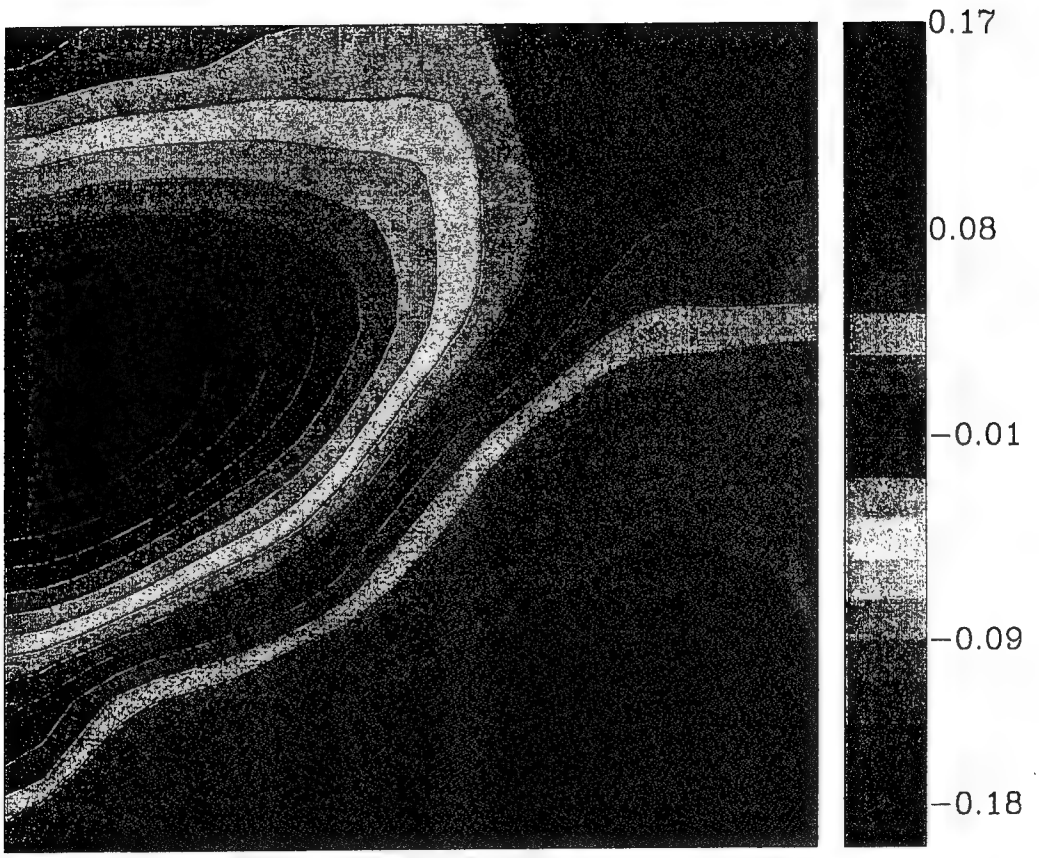

Figure 6-23a. U Component OA Map

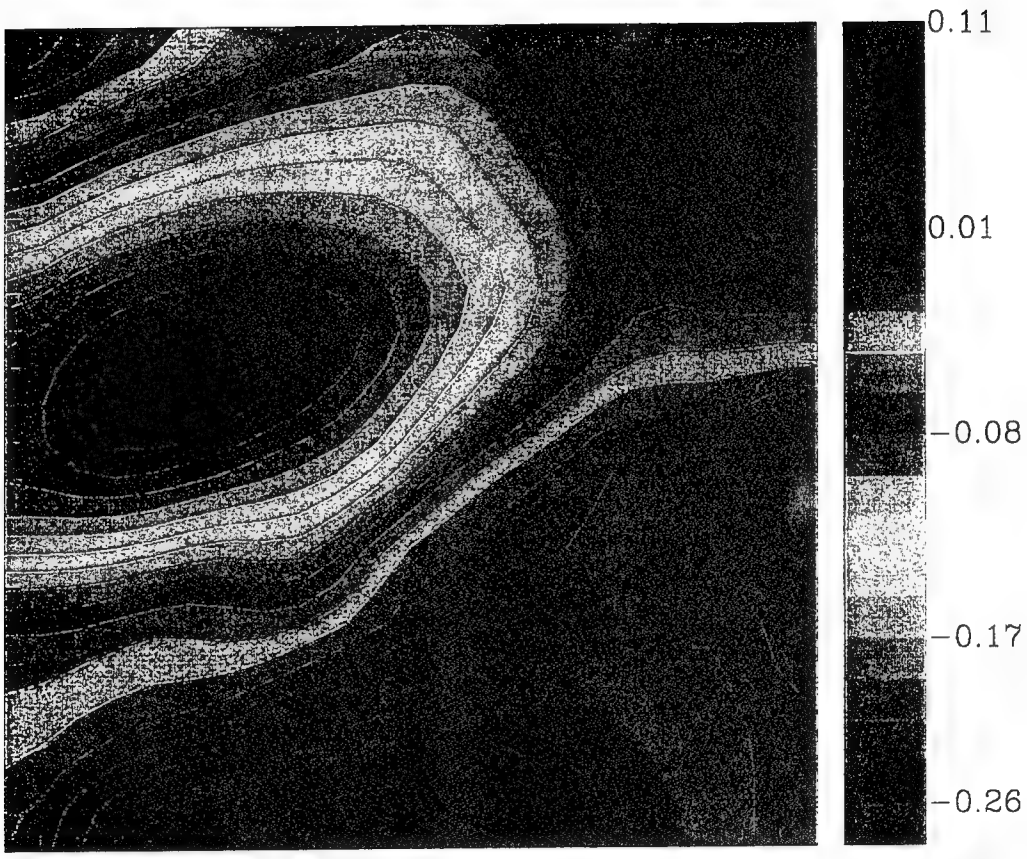

Figure 6-23b. V Component OA Map

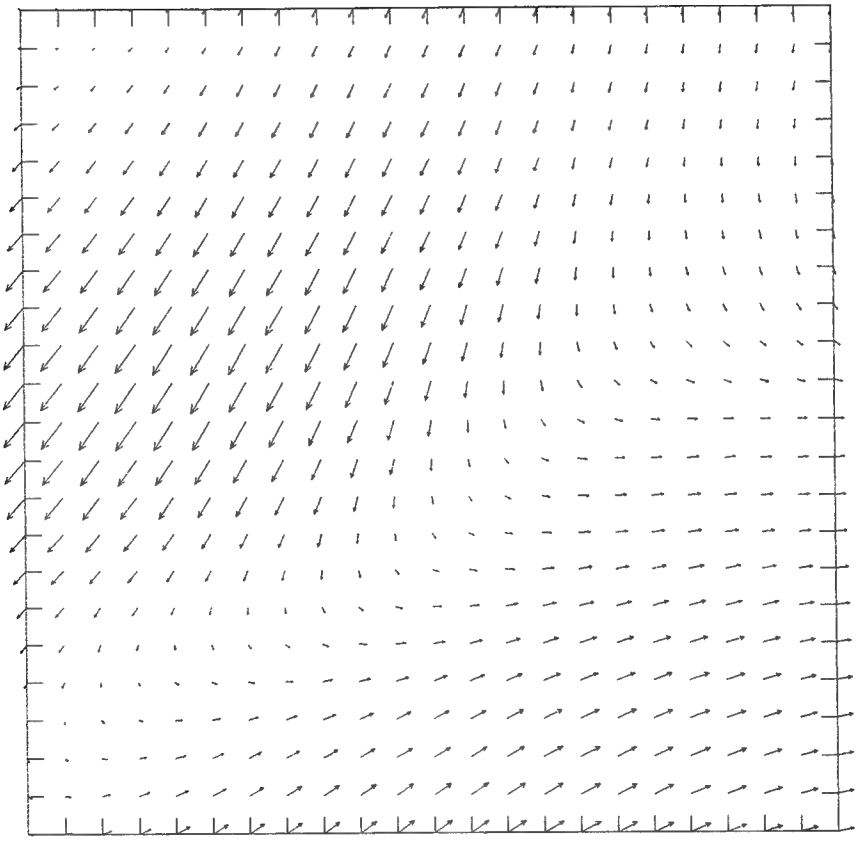

Figure 6-23c. Vector OA Field: 5 km Resolution

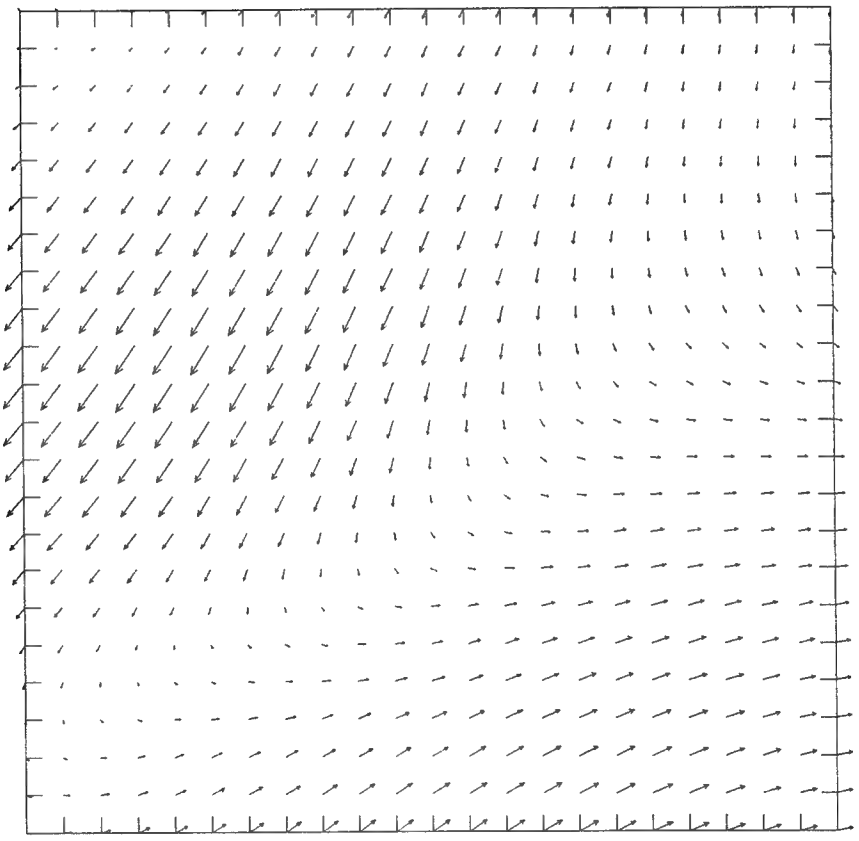

Figure 6-24a. Vector OA Field: 10 km Resolution

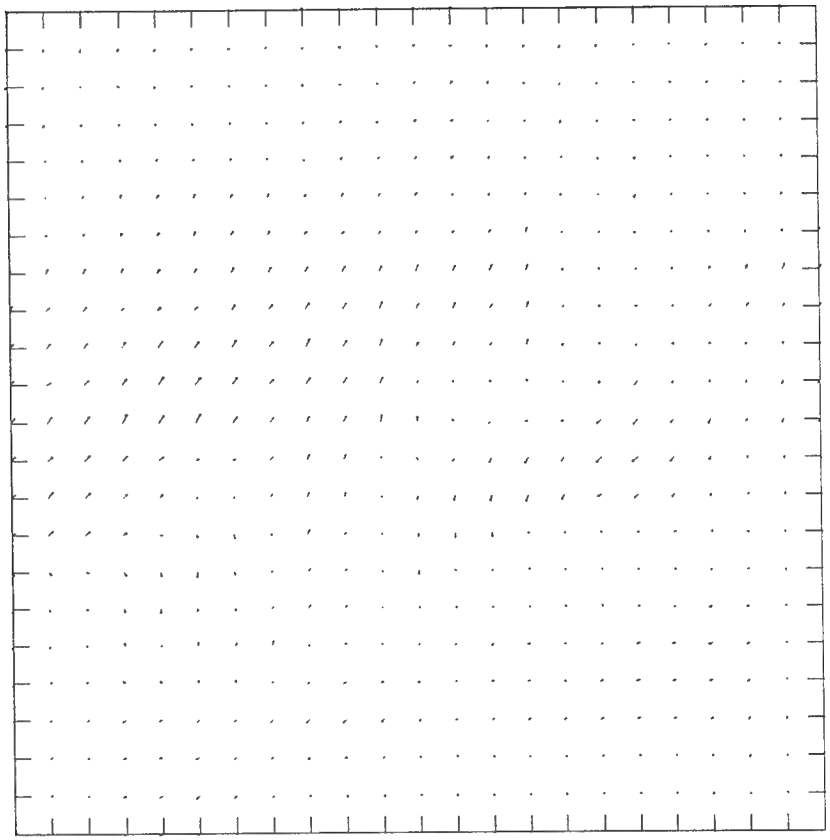

Figure 6-24b. Difference Field between 5 km and 10 km Resolution

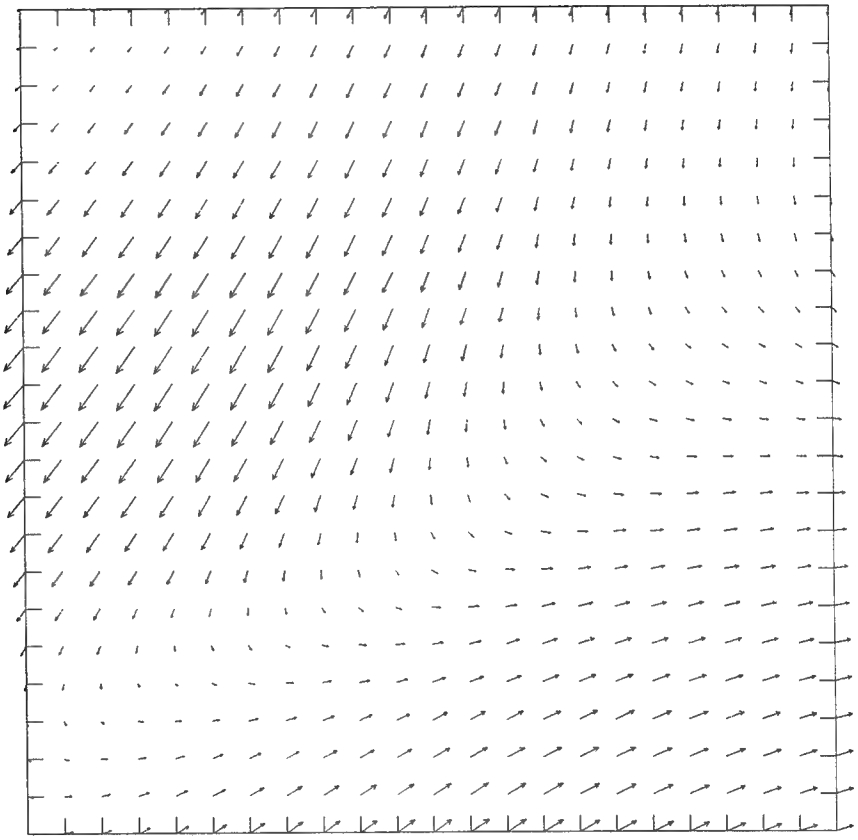

Figure 6-25a. Vector OA Field: 20 km Resolution

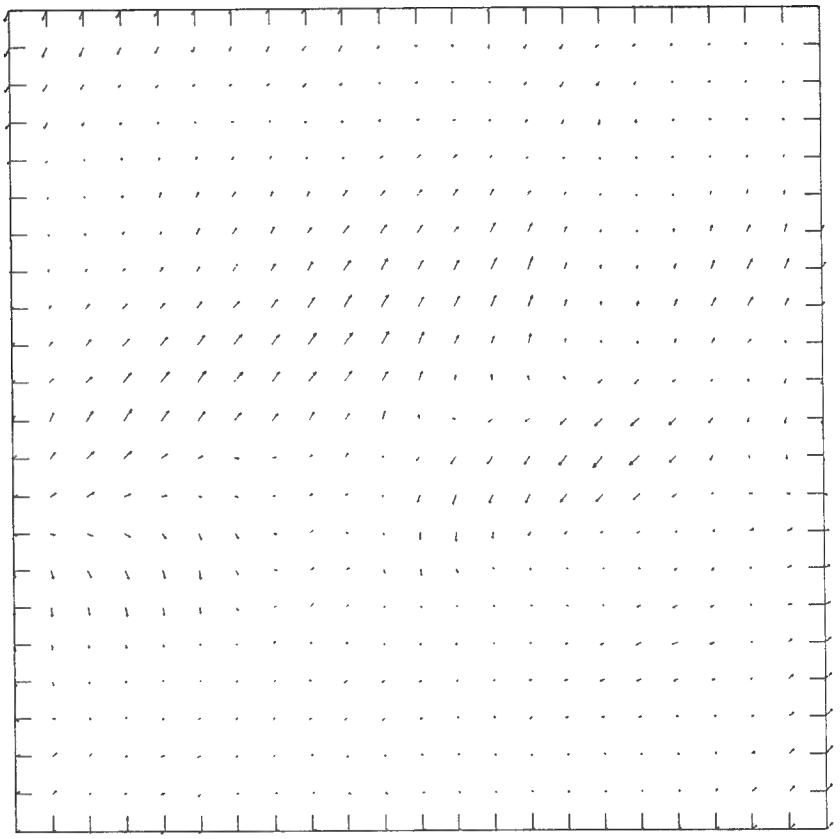

Figure 6-25b. Difference Field Between 5 km and 20 km Resolution

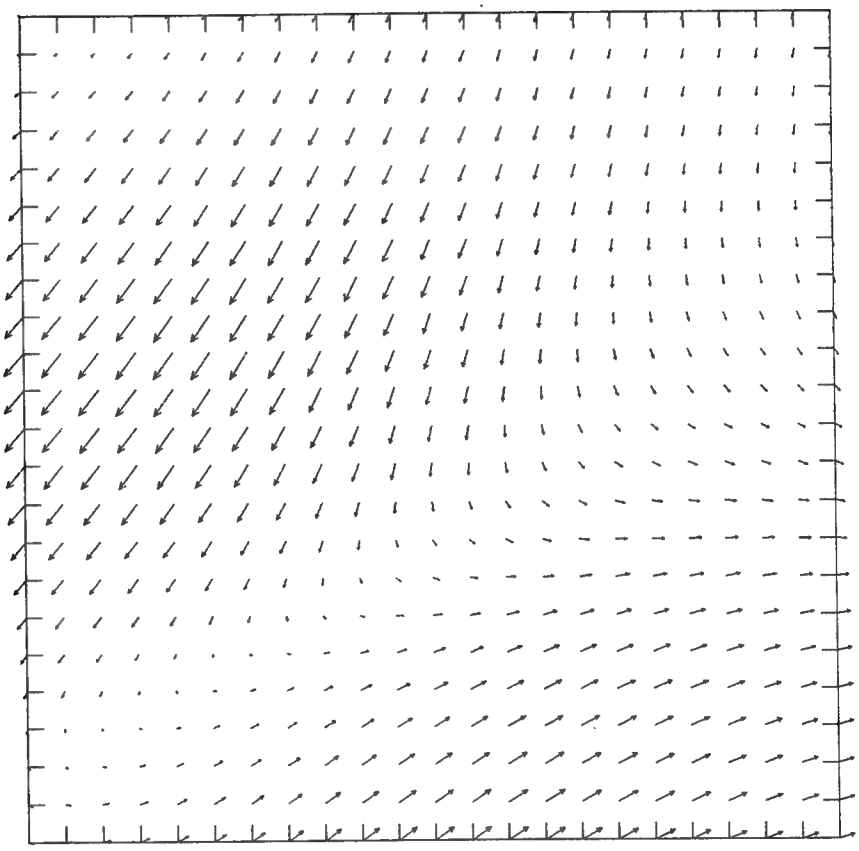

Figure 6-26a. Vector OA Field: 35 km Resolution

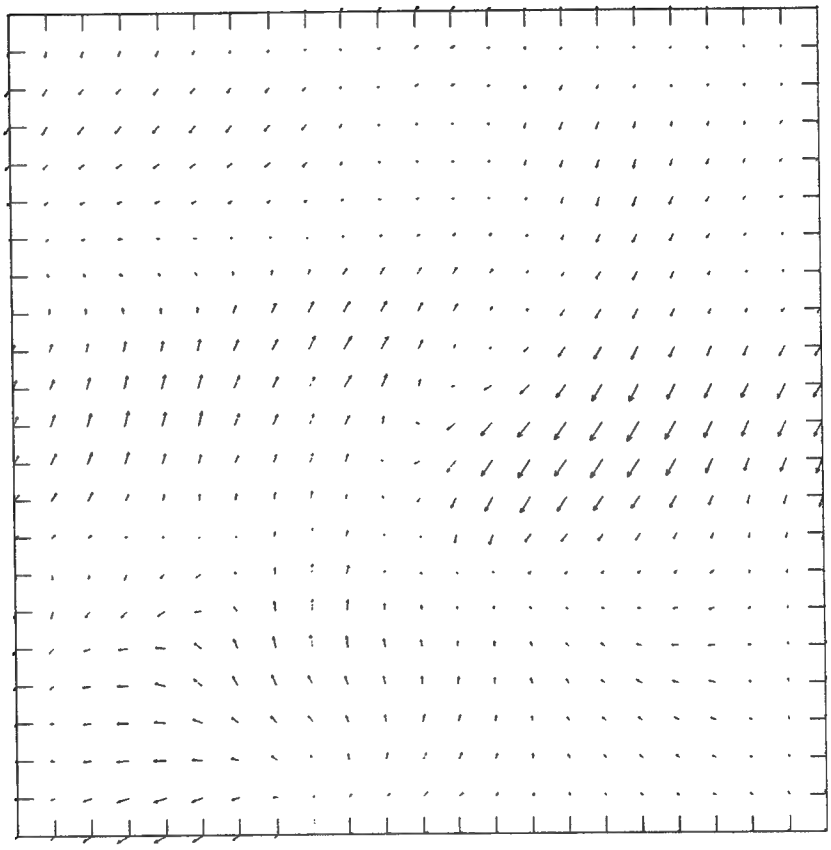

Figure 6-26b. Difference Field Between 5 km and 35 km Resolution

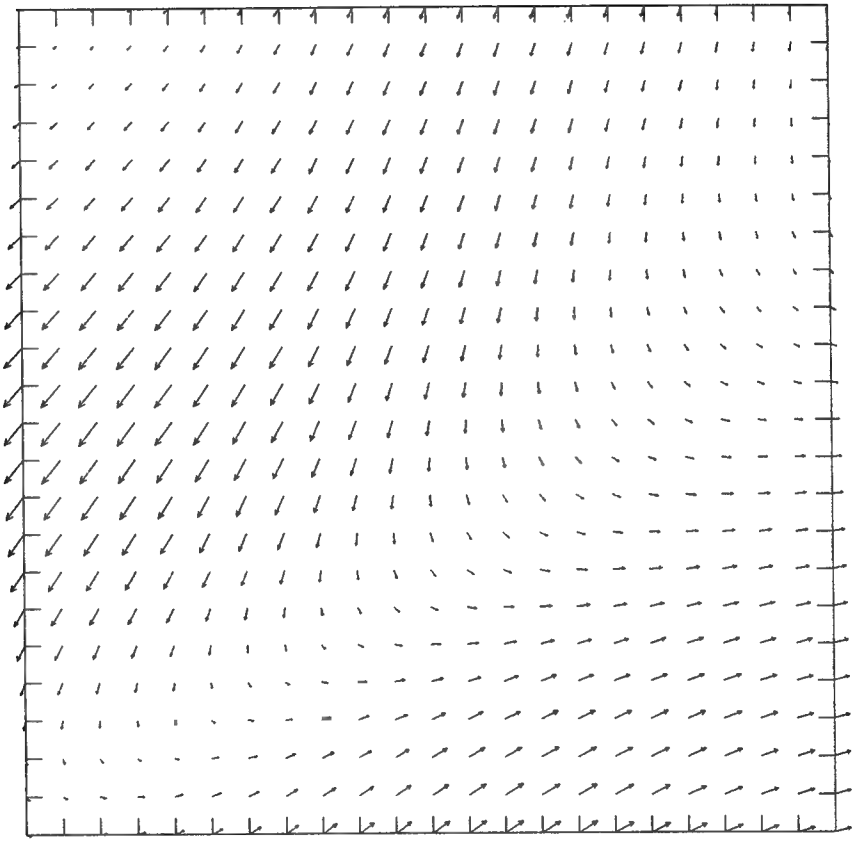

Figure 6-27a. Vector OA Field: 50 km Resolution

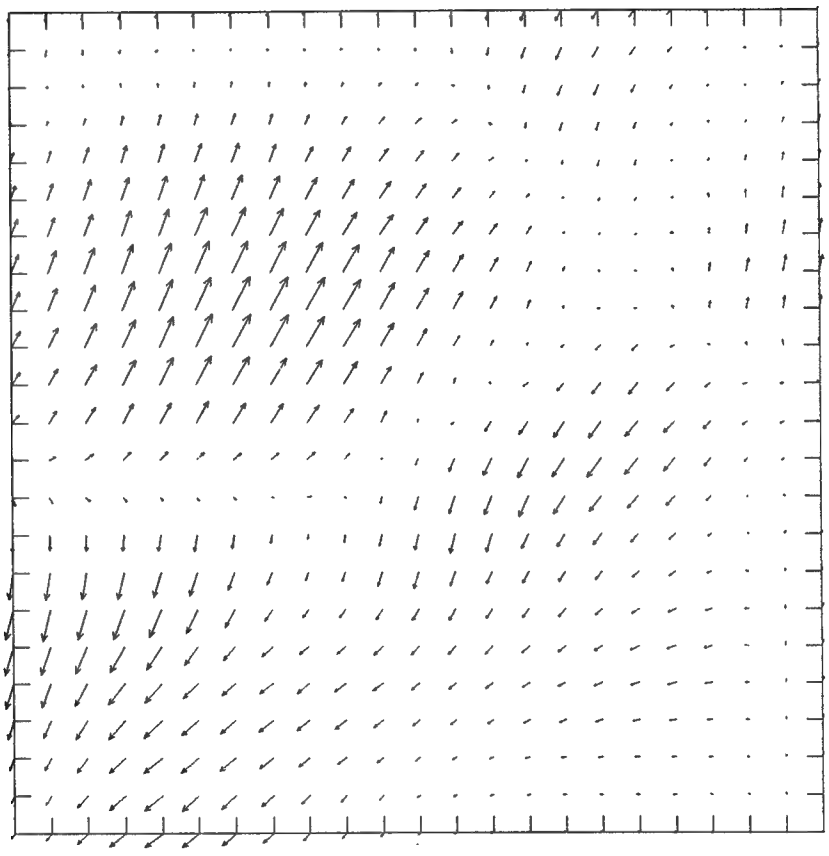

Figure 6-27b. Difference Field Between 5 km and 50 km Resolution

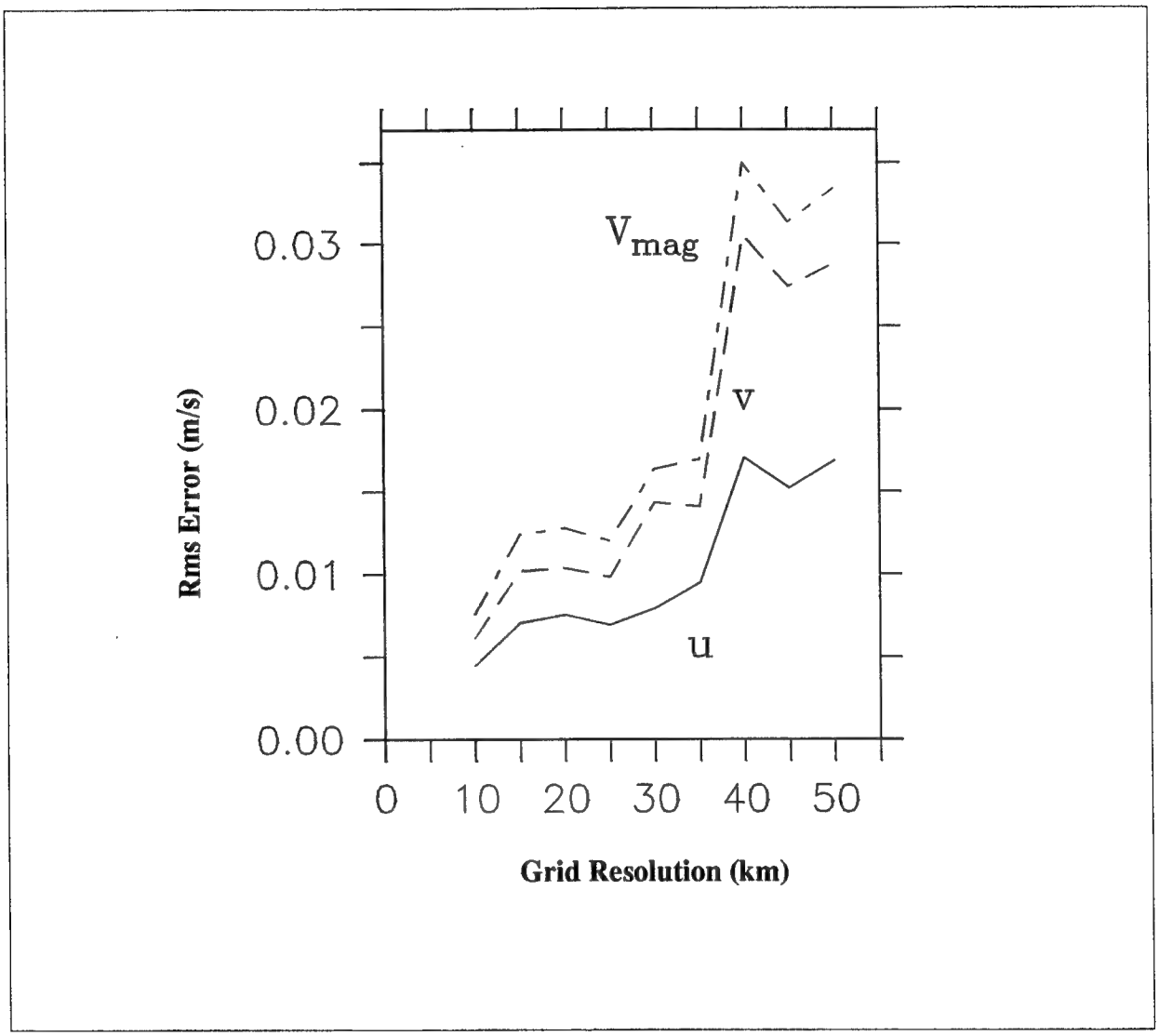

Figure 6-28. RMS Error vs. Grid Resolution

7.0 COMBINING VELOCITY FIELDS

In this section, we describe two approaches for combining or melding regularly gridded velocity data output from two or more ocean circulation models in order to obtain a single optimally estimated velocity field.

In order to demonstrate the two methodologies, we begin with a parent domain P and a subdomain A as shown in Figure 7-1. The OA is used as the full field of the meridional velocity component, described in the Subsampling Experiment in Section 6.2. Figure 7-2a shows the OA field and Figure 7-2b shows the associated error when domain P is sampled with 5 km resolution.

Subdomain A is sampled at 5 km resolution yielding a (14×12) dataset. This can be considered to be the representative dataset for a fine-grid regional numerical model output. These data points are indicated in Figure 7-1 as small x's.

Similarly, domain P is subsampled at 35 km resolution yielding a (4×4) dataset. This data set is representative of a coarse-grid general circulation numerical model output. These data points are marked in Figure 7-1 as asterisks.

If we use objective analysis on the individual datasets separately to obtain information on the parent grid, P, for a resolution of 5 km, we will have fields with large error values where there is missing data for the whole domain. Figure 7-3a shows the 5 km OA on the parent domain, P, using the data in domain A. The associated error field, shown in Figure 7-3b, contains large error values in the region containing no data points. Similarly, Figures 7-4a and 7-4b show the 5 km OA on the parent domain, P, using the coarse-grid dataset and its associated error field, respectively.

Our goal is to reconstruct the OA field for the whole region P so that it matches as closely as possible the original field shown in Figure 7-2a.

Method 1. Objective Analysis. One method is to pool all the observations from both datasets, and carry out an objective analysis via a standard weighting procedure. This method of using both the observations of domain A (at 5 km resolution) and of domain P (at 35 km resolution) results in a field where jagged "seams" are formed along the boundary between the two regions. This is seen in the resulting OA field shown in Figure 7-5a. The seams reflect the irregular, non-smooth behavior of the combined field, which in turn is due to the inconsistency between the fine gridded and coarse-gridded observations in the boundary region. The development of seams is consistent with the high error regions along the boundary between the regions shown in the associated error map (Figure 7-5b).

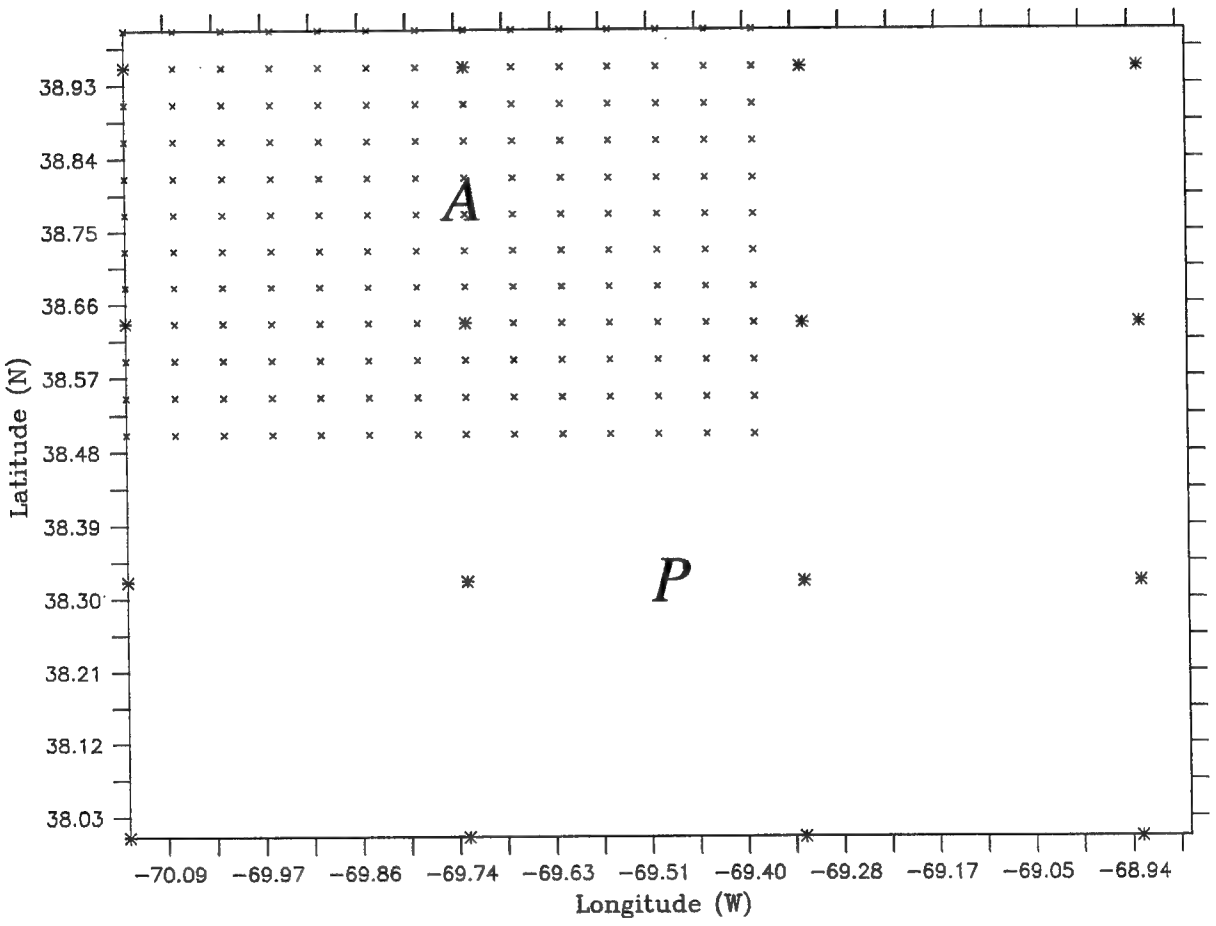

Figure 7-1. Grid Resolution

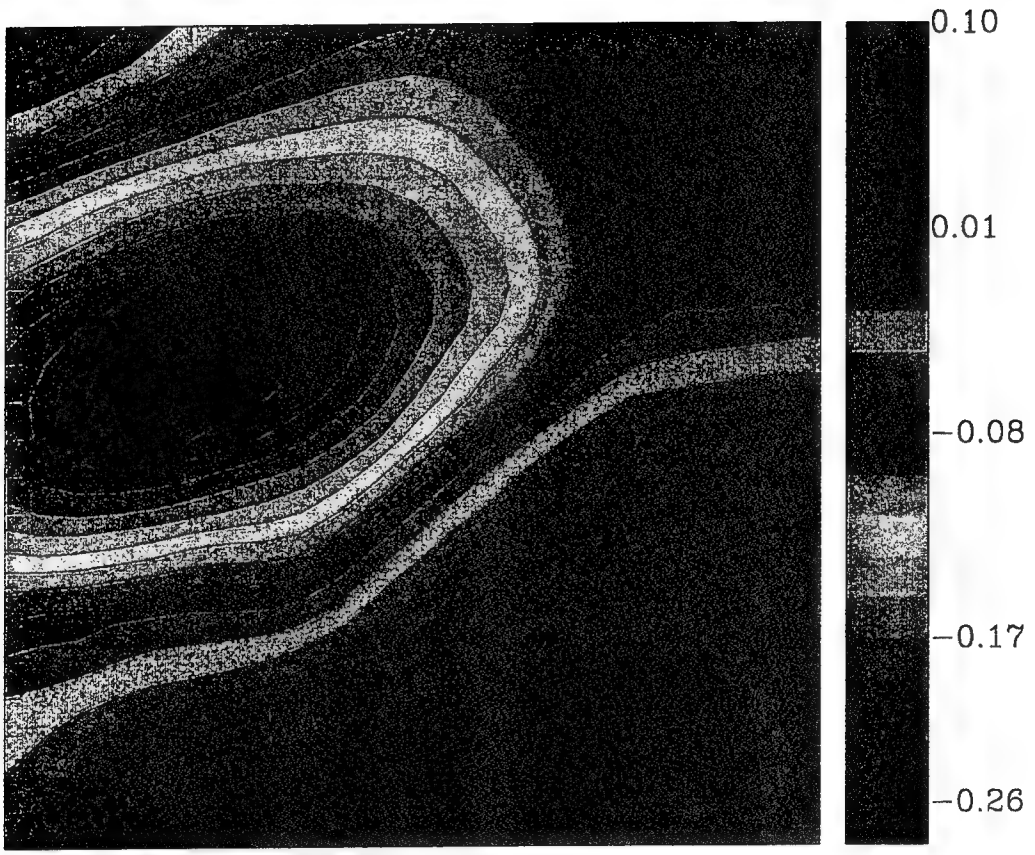

Figure 7-2a. True Field

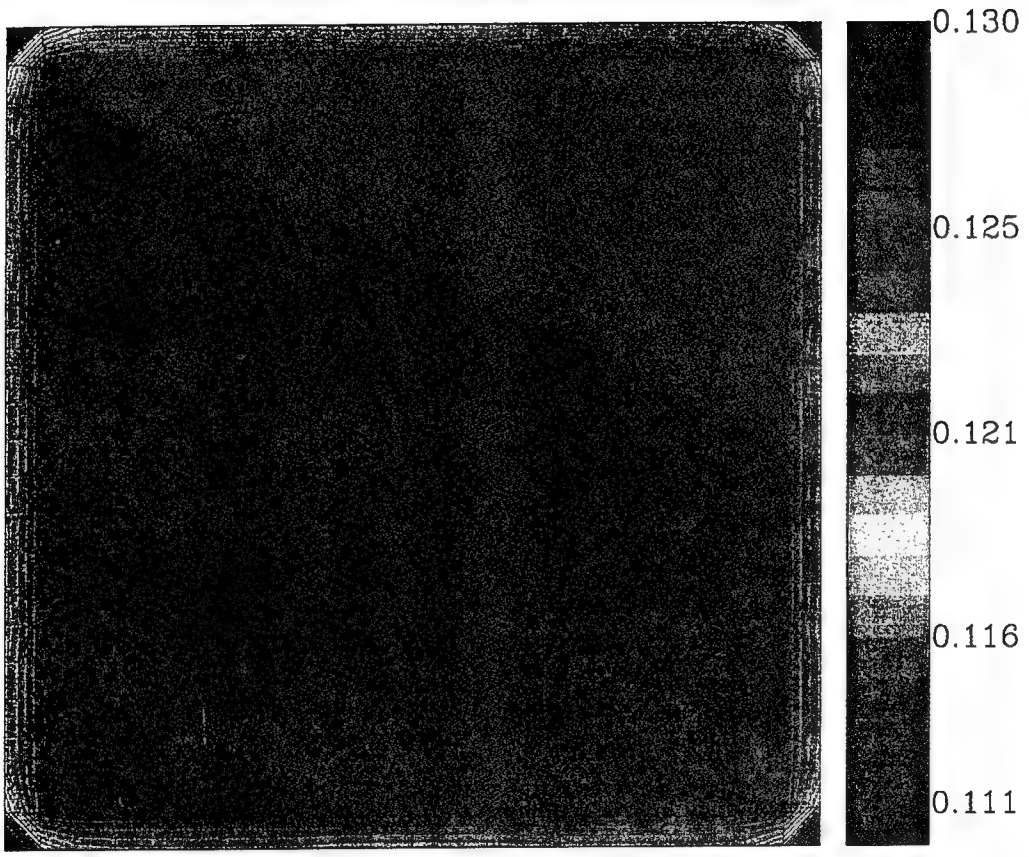

Figure 7-2b. Error Field Corresponding to Figure 7-2a with 5 km Sampling Resolution

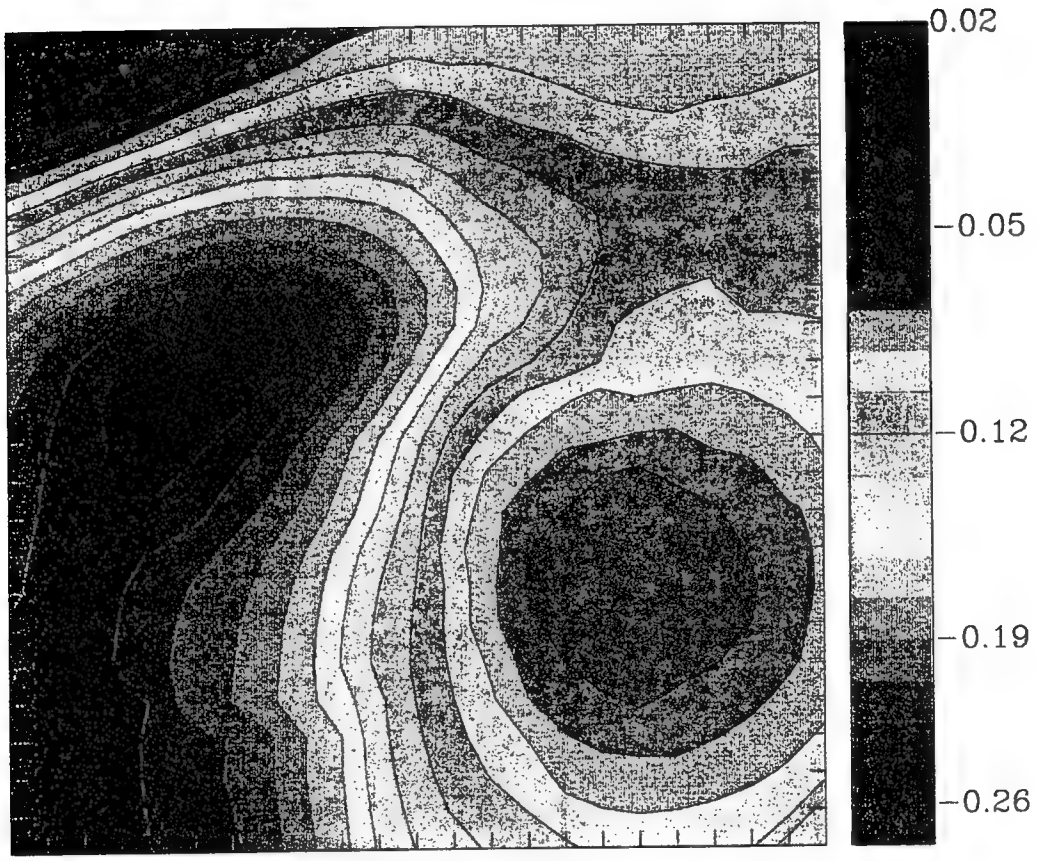

Figure 7-3a. OA for *P* Domain Using Observations from Domain *A* Only

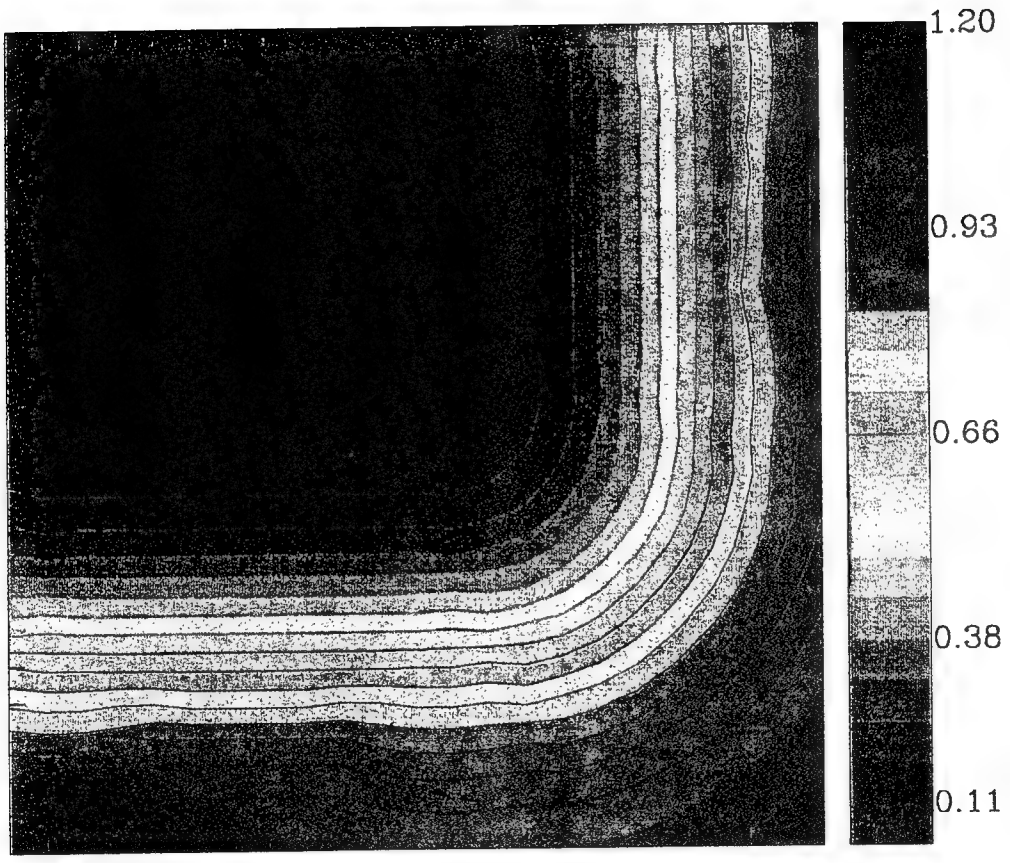

Figure 7-3b. Error Field (*P/A*), Corresponding to Field Shown in Figure 7-3a

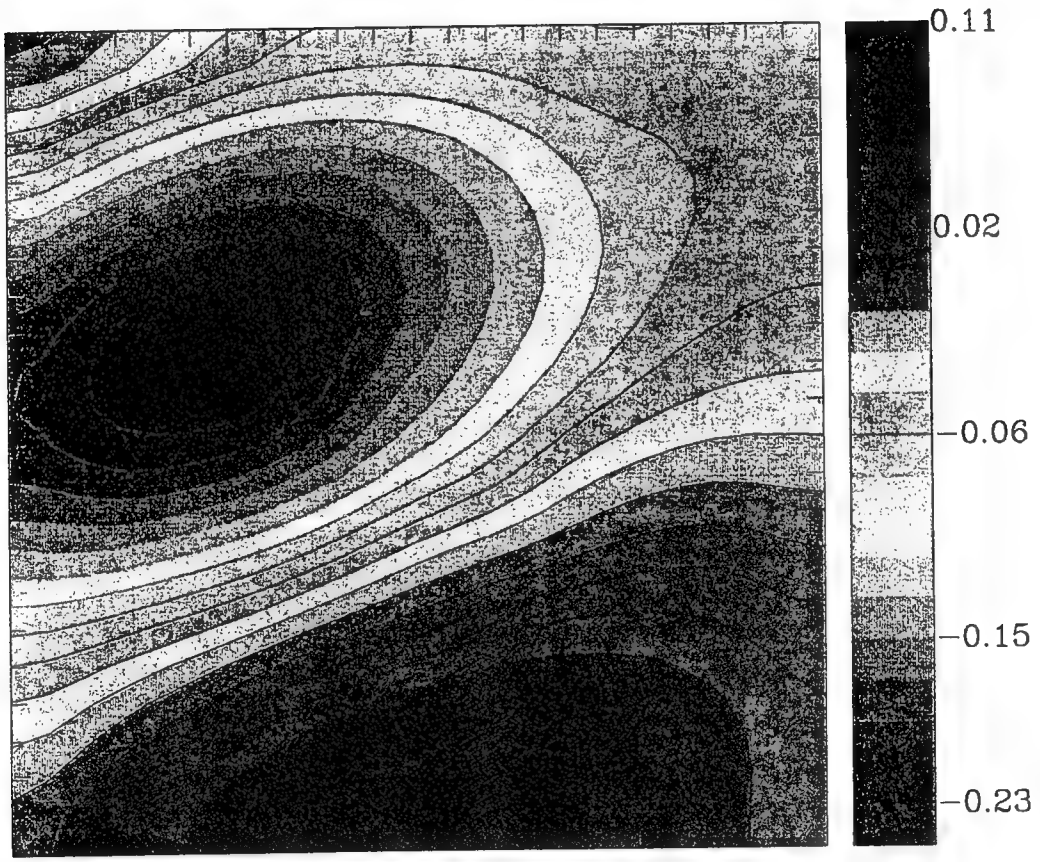

Figure 7-4a. ***P*** **Domain OA Using Coarse Grid (35 km) Observations**

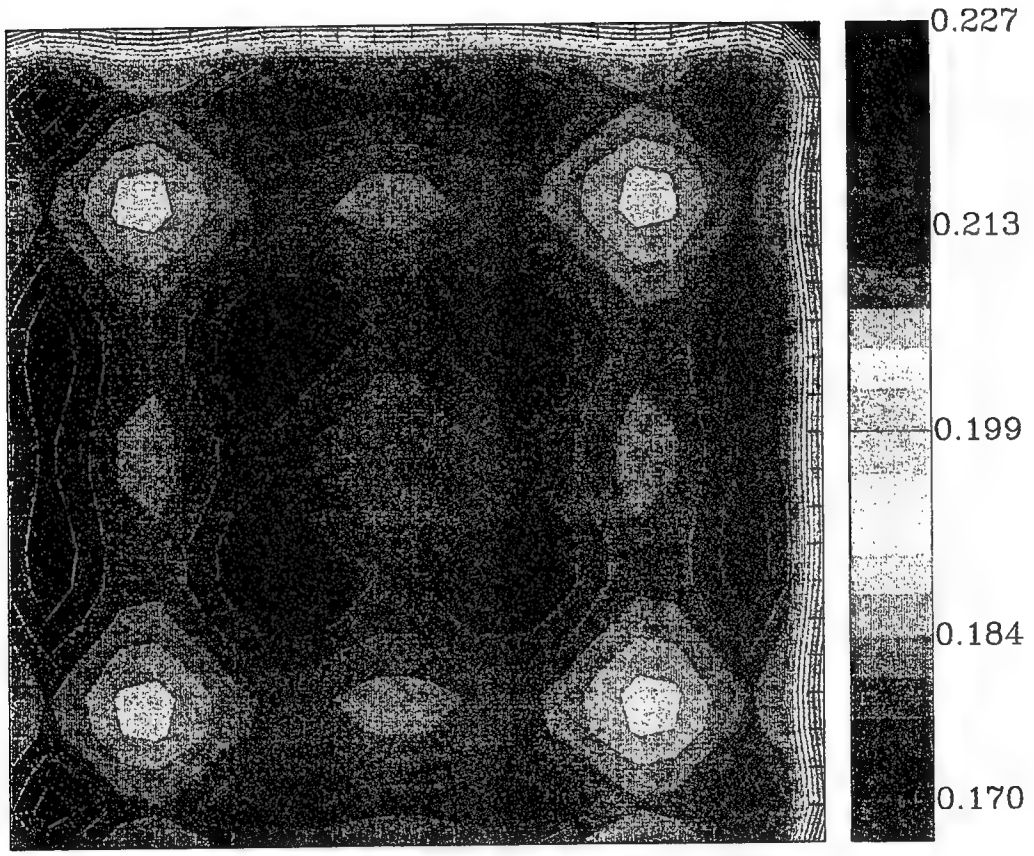

Figure 7-4b. Error Field Corresponding to OA Field Shown in Figure 7-4a

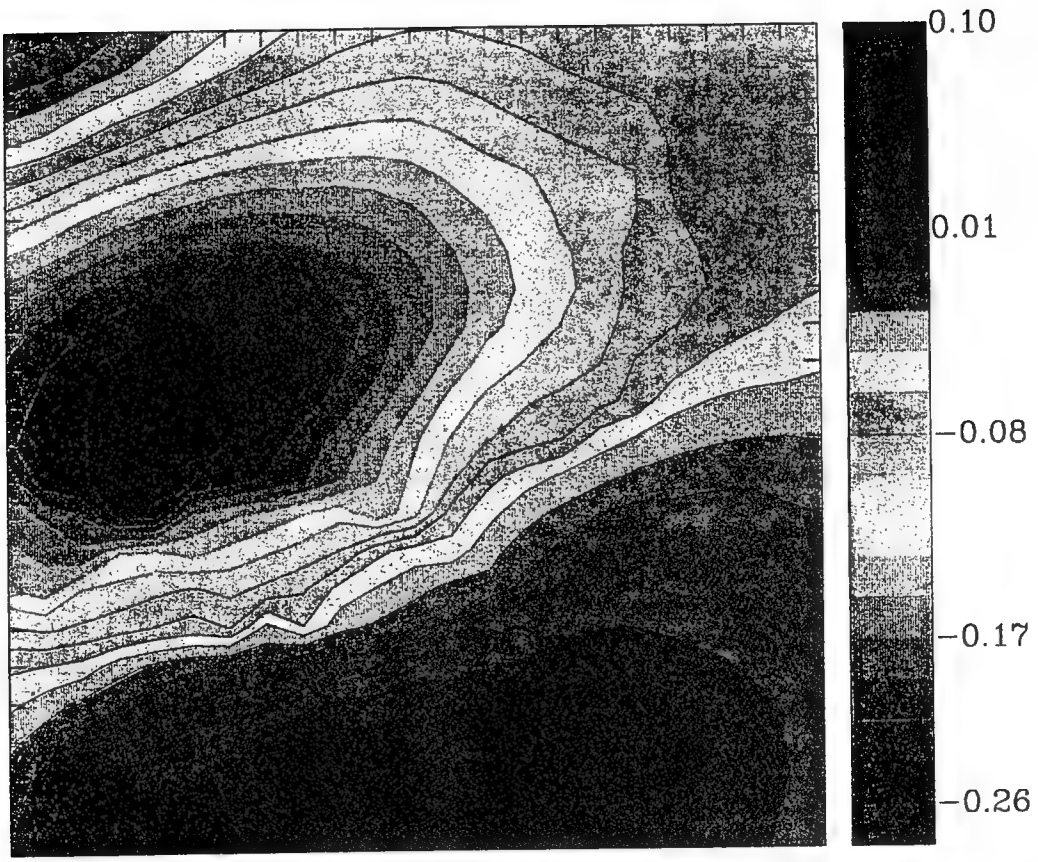

Figure 7-5a. OA Field Using Data From Domains *A* and *P*

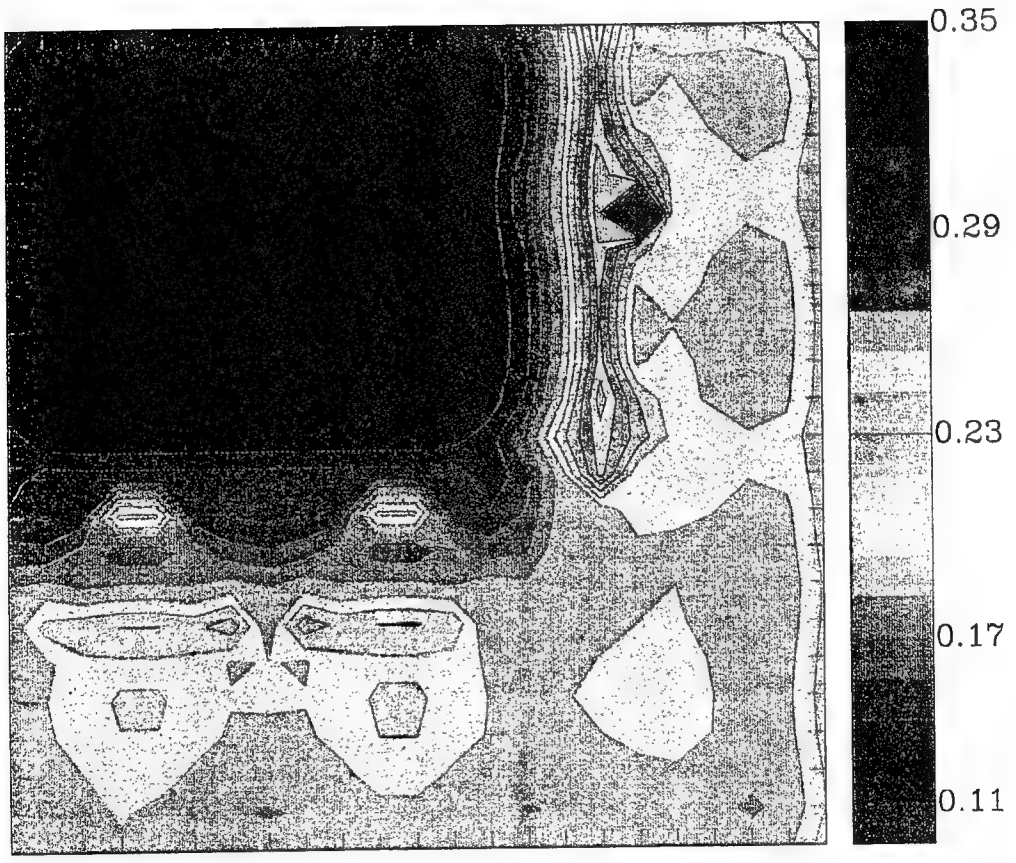

Figure 7-5b. Error Field Corresponding to Field Shown in Figure 7-5a

Method 2. Weighted Combination. The second method of combining the model outputs is to use objective analysis to separately extend each model estimate to the entire domain P. At each point of the extended grid, take a weighted combination of the two resulting field values. The weights are determined by the variances: that is, if models 1 and 2 give field estimates $\hat{f}_{i1}$ and $\hat{f}_{i2}$ at grid point i with attached variances σ_{i1}^2, σ_{i2}^2, respectively, then the melded field estimate at grid point i is

$$\hat{f}_i = \frac{\sigma_{i2}^2 \hat{f}_{i1}}{\sigma_{i1}^2 + \sigma_{i2}^2} + \frac{\sigma_{i1}^2 \hat{f}_{i2}}{\sigma_{i1}^2 + \sigma_{i2}^2}. \tag{40}$$

Under the assumption that $\hat{f}_{i1}$ and $\hat{f}_{i2}$ are independent, the estimate $\hat{f}_i$ has variance

$$\frac{\sigma_{i1}^2 \sigma_{i2}^2}{\sigma_{i1}^2 + \sigma_{i2}^2}. \tag{41}$$

The melded OA estimate given by Equation (40) is shown in Figure 7-6a. The modified error field as given by Equation (41) is shown in Figure 7-6b. The field shown in Figure 7-6a agrees with the field in Figure 7-2a, and does not have any unphysical characteristics like the seam along the boundary between the two regions.

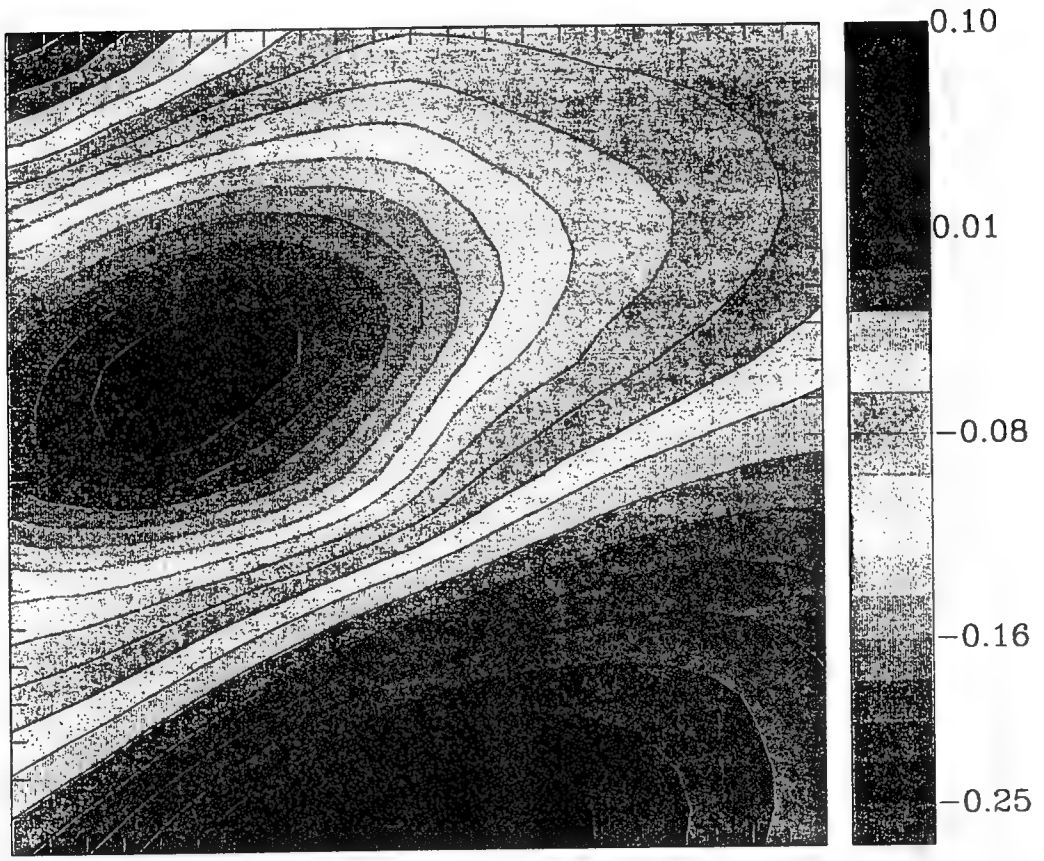

Figure 7-6a. Weighted Combination Field

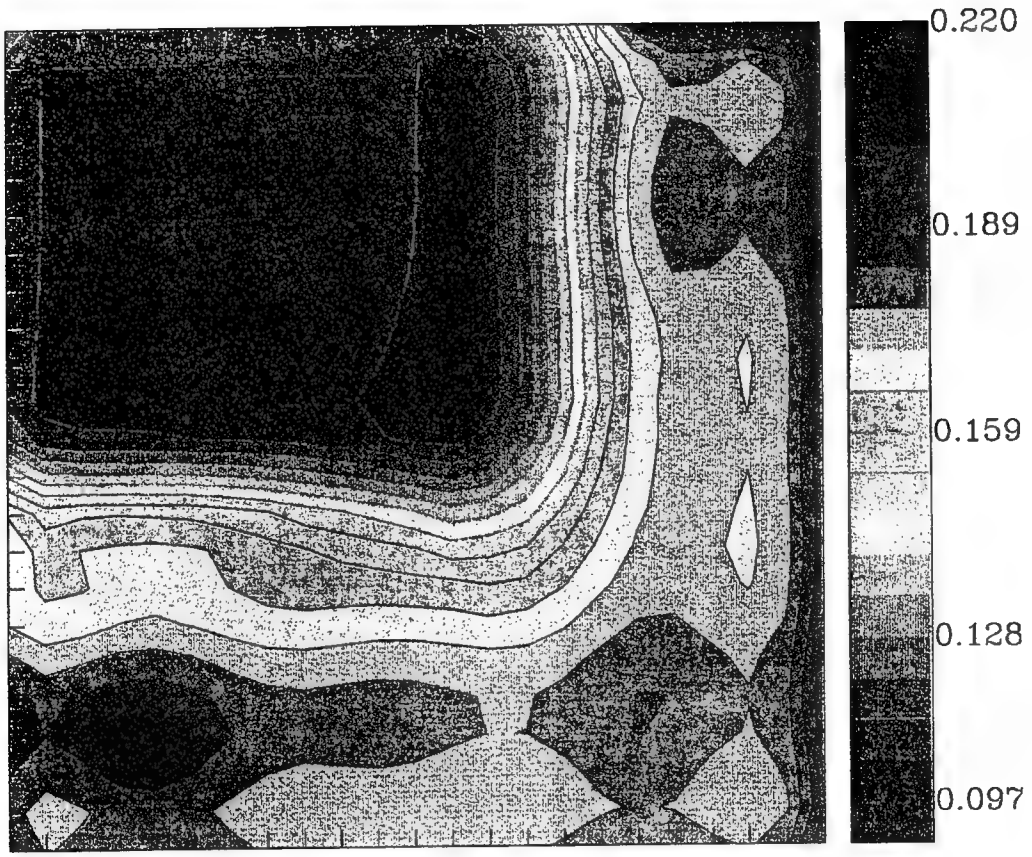

Figure 7-6b. Error Field Estimate Corresponding to Field Shown in Figure 7-6a

8.0 AREA OF UNCERTAINTY PROJECTION USING OA VELOCITY FIELD

The velocity field and its associated error field can be used to project forward in time an area of uncertainty (AOU). This projected AOU can be used, for example, to help determine where to conduct a SAR mission.

In this section, we present a methodology for calculating the AOU projection based on an OA generated velocity and error field.

Goal. Project an AOU forward in time, given a velocity field which has uncertainty at each point in space.

Method. Choose (x_0, y_0) by Monte Carlo from the original AOU. Project forward to time T to get the trajectory. Repeat the process N times, to get an AOU at time T.

Algorithm. The time projection also uses Monte Carlo, because of the uncertainty in velocities. We make the following definitions:

Δt ≡ time step used in projection;

(x_j, y_j) ≡ projected position at time $j\Delta t$;

(u_j, v_j) ≡ OA velocity estimate at position (x_j, y_j);

$(\sigma_{u_j}, \sigma_{v_j})$ ≡ OA velocity variances at position (x_j, y_j); and

(c_{u_j}, c_{v_j}) ≡ correlations between velocities at positions (x_j, y_j) and (x_{j+1}, y_{j+1}) (u and v velocities are assumed to have no cross-correlation).

According to the OA model described in Section 3.0, c_u and c_v have the form

$$c = (1 - a_2)\, e^{b_2},$$

where

$$a_2 = \left(\frac{x_j - x_{j+1}}{x_0}\right)^2 + \left(\frac{y_j - y_{j+1}}{y_0}\right)^2, \text{ and}$$

$$b_2 = -\frac{1}{2}\left[\left(\frac{x_j - x_{j+1}}{x_d}\right)^2 + \left(\frac{y_j - y_{j+1}}{y_d}\right)^2 + \left(\frac{\Delta t}{t_d}\right)^2\right].$$

$\varepsilon_{u_j}, \varepsilon_{v_j}, \delta_{u_j}, \delta_{v_j}$ ≡ random variables to be defined below.

We use the following iterative procedure for determining a Monte Carlo trajectory:

$$(x_1, y_1) = (x_0, y_0) + \Delta t\,(u_0, v_0) + \Delta t\,(\varepsilon_{u_0}, \varepsilon_{v_0}),$$

where $\varepsilon_{u_0} \sim N(0, \sigma_{u_0})$; $\varepsilon_{v_0} \sim N(0, \sigma_{v_0})$.

$$(x_2, y_2) = (x_1, y_1) + \Delta t(u_1, v_1) + \Delta t(\varepsilon_{u_1}, \varepsilon_{v_1}),$$

where

$$\varepsilon_{u_1} = c_{u_0}\varepsilon_{u_0} + \delta_{u_1};\ \delta_{u_1} \sim N(0, \sqrt{\sigma_{u_1}^2 - c_{u_0}^2\sigma_{u_0}^2}), \text{ and}$$

$$\varepsilon_{v_1} = c_{v_0}\varepsilon_{v_0} + \delta_{v_1};\ \delta_{v_1} \sim N(0, \sqrt{\sigma_{v_1}^2 - c_{v_0}^2\sigma_{v_0}^2}).$$

In general,

$$(x_{j+1}, y_{j+1}) = (x_j, y_j) + \Delta t(u_j, v_j) + \Delta t(\varepsilon_{u_j}, \varepsilon_{v_j})$$

where

$$\varepsilon_{u_j} = c_{u_{j-1}}\varepsilon_{u_{j-1}} + \delta_{u_j};\ \delta_{u_j} \sim N(0, \sqrt{\sigma_{u_j}^2 - c_{u_{j-1}}^2\sigma_{u_{j-1}}^2}), \text{ and}$$

$$\varepsilon_{v_j} = c_{v_{j-1}}\varepsilon_{v_{j-1}} + \delta_{v_j};\ \delta_{v_j} \sim N(0, \sqrt{\sigma_{v_j}^2 - c_{v_{j-1}}^2\sigma_{v_{j-1}}^2}).$$

Note that ε_{u_j} is defined so that

$$\sigma(\varepsilon_{u_j}) = \sigma_{u_j};\ \frac{\langle \varepsilon_{u_j}\varepsilon_{u_{j+1}} \rangle}{\sigma_{u_j}\sigma_{u_{j+1}}} = c_{u_j},$$

and similar equations hold for ε_{v_j}; thus, velocity deviation variances and covariances have an appropriate form.

Note that if $\sigma^2_{u_j} - c^2_{u_{j-1}}\sigma^2_{u_{j-1}} < 0$, we may simply take $\delta_{u_j} = 0$; and similarly for δ_{v_j}.

Example. Figure 8-1 shows a velocity field and associated error field. Figure 8-2 illustrates a 12 hour time projection of 3 circular AOUs of radius 2 nm for the field shown in Figure 8-1. The green region denotes the initial AOU; the red region the projected AOU. A total of 288 points were used in the Monte Carlo for this display.

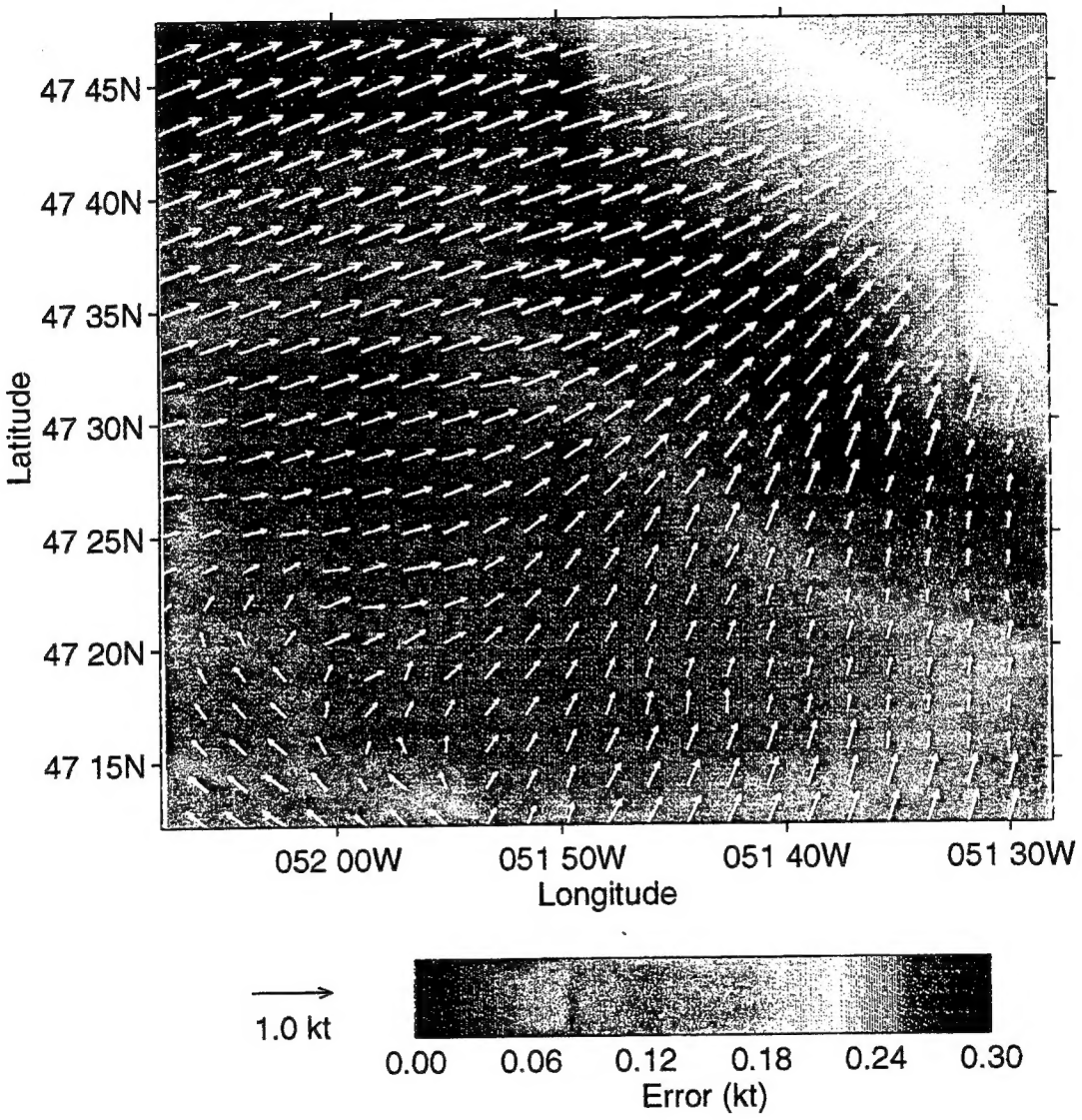

Figure 8-1. Velocity and Error Field Used for AOU Projection

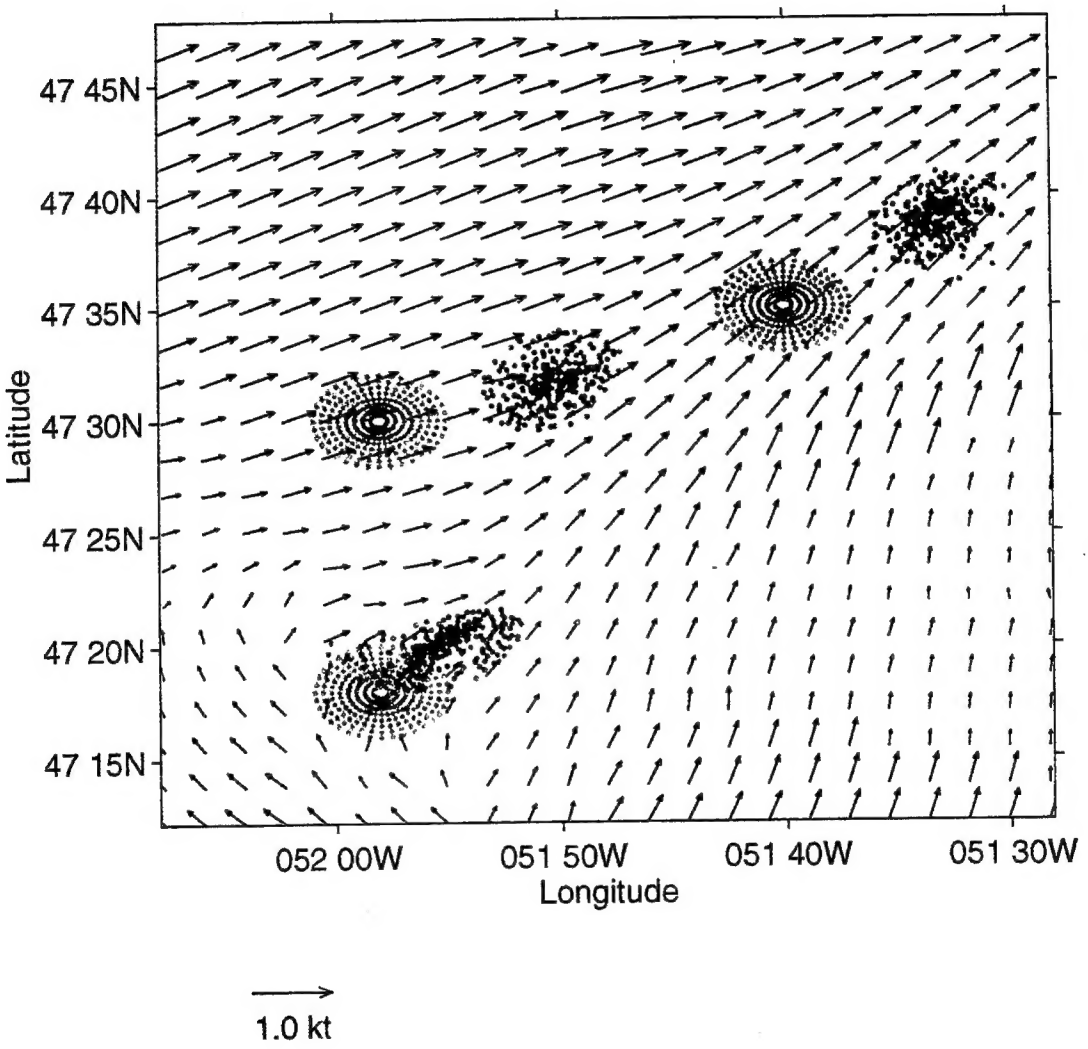

Figure 8-2. 12 Hour Time Projection of 3 Circular AOUs of Radius 2 nm

9.0 CONCLUSIONS

In this section, we present the conclusions of the Phase I effort.

- **Objective analysis numerical techniques can be applied to Coast Guard observational data to provide good estimates of ocean surface velocity field and associated error.**
- **Using a TAC-3 (HP 700 series) computer system, the time required to calculate and display ocean surface velocity fields for typical SAR regions is less than 10 seconds.** (Note: Code has not been optimized. Run time will be considerably reduced with optimized code.)
- **It is technically feasible to develop a system for use in real time by the Coast Guard to provide continuously updated ocean surface velocity estimates as observed data are received.**

REFERENCES

a. "A Review of Methods for Objective Analysis", Nils Gustafsson, in Dynamic Meteorology: Data Assimilation Methods, L. Bengtsson, M. Ghil, E. Källén, editors, Springer-Verlag, New York, 1981.

b. "Objective Analysis: Theory and Code", A. J. Mariano, E. F. Carter, unpublished manuscript, June 1988.

c. "Smoothing, Filling and Boundary Effects", Shapiro, R., Review of Geophysical and Space Physics, Vol. 8, 1970.

d. "Use of Linear Filtering as a Parameterization for Atmospheric Diffusion", Shapiro, R., J. of Atmospheric Science, Vol. 28, 1971.

e. Coast Guard Buoy Dataset, 10 January 1994.

f. "Analysis Models for the Estimation of Oceanic Fields", E. F. Carter and A. R. Robinson, J. of Atmospheric and Oceanic Technology, Vol. 4, No. 1, March 1987.

g. "Multiscale Feature Models for the Circulation of the Western North Atlantic, I: Structures and Synthesis", A. Gangopadhyay, A. R. Robinson and H. G. Arango, to be submitted to J. of Physical Oceanography.